Physics Lib.
Foxon

THE JOURNAL
OF
CHEMICAL PHYSICS

VOLUME 15, NUMBER 1 JANUARY, 1947

Derivative Crystal Structures

M. J. BUERGER
Massachusetts Institute of Technology, Cambridge, Massachusetts
(Received May 24, 1946)

There exists a class of crystal structures which are derived from others by generalization. These are here designated *derivative structures*. A special case of derivative structure is the popular "superstructure." The symmetry of a derivative structure is a subgroup of the symmetry of the basic structure. Here the term "subgroup" is used in a wider sense than common in mathematical crystallography, and includes subgroups with multiple cells. The methods of finding the derivative symmetries are discussed. There are two important kinds of derivative structures, here designated *substitution structures* and *distortion structures*. Substitution structures result when a set of different atoms is substituted for a set of like atoms in the basic structure. For a given kind of substitution, it is possible to predict the cell dimensions of the crystal resulting from the substitution, as well as all the possible symmetries it could have. Examples are cited of the applications of derivative structure theory to several branches of crystallography.

INTRODUCTION

IN this paper some relations are discussed which obtain between a crystal structure and those crystal structures derived from it by generalization. The original crystal structure will be called the *basic structure* and the structures derived from it by generalization will be called *derivative structures*.

One special case of derivative structures has been given a certain amount of casual attention, namely those structures which are commonly known as *superstructures*. About the only relation which has been recognized between a superstructure and its basic structure is that one or more edges of the superstructure cell are multiples of the corresponding edge or edges of the cell of the basic structure. Apparently no attention has been paid to other geometrical relations between superstructure and basic structure, and consequently the very existence of the more general class of derivative structures has escaped attention.

If the currently recognized relation between superstructure and basic structure is expressed in appropriate language, then the extreme specialization of the concept of superstructure becomes evident, and the extension of the notion becomes obvious. In terms of symmetry theory, a superstructure can be derived from a basic structure by suppression of certain sets of the operations of translation in the space group of the basic structure. Stated this way, it is evident that one particular kind of operation of a group of operations has been singled out for consideration. It is evident that structures can be derived from a basic structure by the suppression of sets of any kind of operations or combination of operations. Consequently, we define as a *derivative structure*

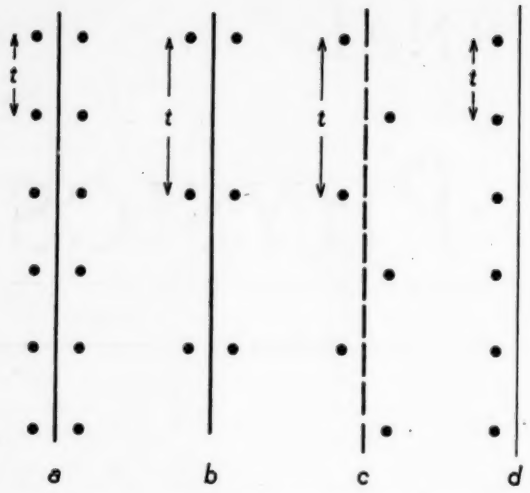

FIG. 1. The repetitions corresponding to a group based on a reflection and a translation, Fig. 1(a). In Figs. 1(b), (c), and (d) are shown the repetitions corresponding with the three types of infinite subgroups. The translation periods are labeled *t*.

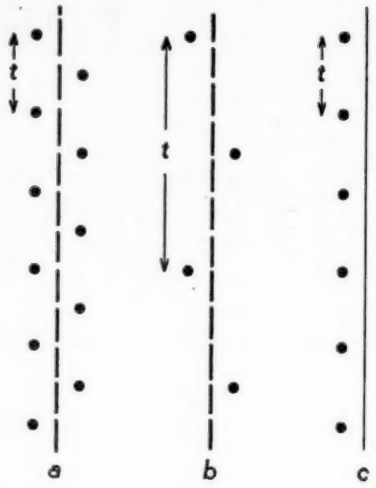

FIG. 2. The repetitions corresponding to a group of glide reflections, Fig. 2(a). In Figs. 2(b) and 2(c) are shown the repetitions corresponding with the two types of infinite subgroups. The translation periods are labeled *t*.

any structure derived from a basic structure by the suppression of one or more sets of operations of the space group of the basic structure (due account being given to the requirements of group theory). Obviously, derivative structures include the class of superstructures.

The reason for the recognition of superstructures and the non-recognition of derivative structures lies in the comparative ease with which the operation of translation can be detected experimentally. Superstructures are commonly recognized in the field of metallography in connection with the formation of ordered phases. In such cases, if a set of translations is suppressed by the ordering process, it is easily detected by the change in dimensions of the cell edges. On the other hand, the suppression of certain other sets of symmetry operations leaves no diffraction record in a powder photograph. Suppose, for example, that the space group of the basic structure is $P2/m$, and suppose the set of all twofold rotations is suppressed. The derivative structure has the space group Pm, and its powder photograph is qualitatively no different from that of the original basic structure. The existence of the derivative structure may consequently escape detection unless its crystal structure has been worked out in detail.

CHARACTERISTICS OF DERIVATIVE STRUCTURES

Symmetries of Derivative Structures

It is important to know how the symmetry of a derivative structure is related to that of its basic structure. The derivative symmetry is composed of some, but not all, the operations of the basic structure group, the missing operations being suppressed. The remaining operations must, of course, also form a group, and since this group is composed of operations contained in the original basic-structure group, it must be a subgroup of it. Thus, it is evident that the symmetry of a derivative structure is a subgroup of the space group of the basic structure. From this it immediately follows that the totality of possible derivative structure symmetries is composed of all the possible subgroups of the space group of the basic structure.

These conclusions are subject to possible misinterpretation. It does not follow from what has been said that the subgroups necessarily have the same cell dimensions as the cell of the basic group. The primitive cell of the subgroup is bound to be different from that of the basic group if any operations of lattice translation are among the suppressed set of operations. When the unit cell of the basic structure is non-primitive, and the suppressed group of operations includes

primitive translations, then the unit cell of the derivative structure may still be the same as the conventional unit cell of the basic structure, or it may have multiple edges. In the latter case, the derivative structure is the particular variety currently recognized as a superstructure.

Furthermore, it does not necessarily follow that the total number of possible derivative structures is equal to the total number of subgroup symmetries of the basic group. This is because for each derivative symmetry there may correspond more than one derivative structure. This matter will be discussed further.

Derivatives of Symmetry Planes Combined with One Translation

Some of the principles implied in the foregoing section can be simply illustrated by certain one-dimensional space groups which amount to certain symmetry elements with one-dimensional translations. In Fig. 1(a) is shown a diagrammatic representation of such a group containing a reflection plane and a parallel translation. The fundamental operations are a reflection, S, and a translation, τ. The operations of the group are

$$\begin{array}{cccccccc} 1 & \tau & \tau^2 & \tau^3 & \tau^4 & \cdot & \cdot \\ S & S\tau & S\tau^2 & S\tau^3 & S\tau^4 & \cdot & \cdot \end{array} \tag{1}$$

and their inverses. This group has an infinite number of proper subgroups, but, provided that all translations are not suppressed, they all fall into three categories. Only the simplest representatives of the three categories are diagrammed in Figs. 1(b), (c), and (d). These simplest representatives have the following operations and their inverses:

$$\begin{array}{lcccccccc} \text{I:} & 1 & & \tau^2 & & \tau^4 & & \tau^6 & \cdot \\ \text{(Fig. 1(b))} & S & & S\tau^2 & & S\tau^4 & & S\tau^6 & \cdot \end{array} \tag{2}$$

$$\begin{array}{lcccccccc} \text{II:} & 1 & & \tau^2 & & \tau^4 & & \tau^6 & \cdot \\ \text{(Fig. 1(c))} & & S\tau & & S\tau^3 & & S\tau^5 & & \cdot \\ & & (=g) & & (=g^3) & & (=g^5) & & \end{array} \tag{3}$$

$$\begin{array}{lcccccccccc} \text{III:} & 1 & \tau & \tau^2 & \tau^3 & \tau^4 & \tau^5 & \tau^6 & \cdot & \cdot & , \\ \text{(Fig. 1(d))} & & & & & & & & & & \end{array} \tag{4}$$

where g represents the operation of glide reflection with translation component τ.

The operations of the general groups of which the above three are the simplest proper representatives are:

$$\begin{array}{lcccccc} \text{I:} & 1 & \tau^{1+n} & \tau^{2(1+n)} & \tau^{3(1+n)} & \tau^{4(1+n)} & \cdot \\ & S & S\tau^{1+n} & S\tau^{2(1+n)} & S\tau^{3(1+n)} & S\tau^{4(1+n)} & \cdot \end{array} \tag{5}$$

$$\begin{array}{lcccccc} \text{II:} & 1 & & \tau^{2(1+n)} & & \tau^{4(1+n)} & \\ & & S\tau^{1+n} & & S\tau^{3(1+n)} & & \cdot \end{array} \tag{6}$$

$$\text{III:}\quad 1 \qquad \tau^{1+n} \qquad \tau^{2(1+n)} \qquad \tau^{3(1+n)} \qquad \tau^{4(1+n)} \qquad \cdot \tag{7}$$

where n is a non-negative integer.

Fewer categories occur for the derivatives of the group of operations representing glide symmetry, Fig. 2(a). The operations of this group are:

$$\begin{array}{ccccccccccc} 1 & S\tau & \tau^2 & S\tau^3 & \tau^4 & S\tau^5 & \tau^6 & S\tau^7 & \tau^8 & S\tau^9 & \cdot \\ & (=g) & & (=g^3) & & (=g^5) & & (=g^7) & & (=g^9) & \end{array} \tag{8}$$

The subgroup categories are represented by the following simplest examples:

$$\begin{array}{lcccccccc} \text{I:} & 1 & & S\tau^3 & & \tau^6 & & S\tau^9 & \cdot \\ \text{(Fig. 2(b))} & & & (=g^3) & & & & (=g^9) & \end{array} \tag{9}$$

$$\begin{array}{lcccccccc} \text{II:} & 1 & \tau^2 & & \tau^4 & & \tau^6 & & \tau^8 & \cdot \\ \text{(Fig. 2(c))} & & & & & & & & & \end{array} \tag{10}$$

These examples are the simplest proper representatives of the two general categories of subgroups which have the following operations:

$$\text{I:}\quad 1 \qquad S\tau^{1+2n}\ (=g^{1+2n}) \qquad \tau^{2(1+2n)} \qquad S\tau^{3(1+2n)}\ (=g^{3(1+2n)}) \quad \cdot \tag{11}$$

$$\text{II:}\quad 1 \qquad \tau^{2+2n} \qquad \tau^{2(2+2n)} \quad \cdot \tag{12}$$

From this it is possible to draw the following conclusions with regard to the derivatives of these symmetry elements combined with a single parallel translation: The derivative of a reflection plane can be

either: (1) a reflection plane parallel to which the translation is multiplied (Fig. 1(b)),

or: (2) a glide plane with component parallel to the translation, the translation period being $2+2n$ ($=2, 4, 6, \cdots$) times that of the basic translation (Fig. 1(c)),

or: (3) a translation of 1, 2, 3, $\cdots$ times that of the basic translation, without reflection (Fig. 1(d)).

On the other hand, the derivative of a glide plane combined with a single parallel translation is

either: (1) a glide plane with component parallel to the translation, the new translation being $2+4n$ basic glides, or $1+2n$ ($=1, 3, 5, \cdots$) times that of the basic translation (Fig. 2(b)).

or: (2) a translation of 1, 2, 3, $\cdots$ times that of the basic translation, without reflection (Fig. 2(c)).

Thus, a reflection plane can have as derivative a reflection plane, a glide plane, or a parallel translation, while a glide plane can have as derivative only a glide plane or a parallel translation. A glide plane cannot have a reflection plane as derivative.

These derivatives of simplified groups illustrate some of the fundamental features of the derivatives of space groups. Two general features to be observed are:

(1) Each symmetry has a limited number of derivative types. Certain derivatives can be expected from a given basic symmetry while others cannot.

(2) Certain derivative symmetries permit, among others, the same translation as the basic symmetry; other derivative symmetries permit only translations which are particular multiples of the basic translation. Those permitting the same translation are the standard subgroups listed in tables of space group characteristics.

Derivatives of Symmetry Planes

The information about the derivatives of symmetry planes is not yet in very useful form, for in crystals a reflection is always normal to a possible lattice net. Consequently, it is important to know the derivatives of reflections combined with the two translations of the net. As a preliminary to this, the derivatives of the net will first be discussed. (The derivatives of lattices will be discussed in another paper since lattice derivatives are not specifically required for the understanding of what follows.)

Derivatives of Nets

To simplify the discussion a primitive cell of the net is chosen and all translation operations are referred to the primitive translations, τ_1 and τ_2. The general translation of the net, in vectorial form, is then $e\tau_1+f\tau_2$, where e and f are any integers. The product form of this is $\tau_1{}^e\tau_2{}^f$. These operations form a group whose table is represented by the following origin portion of the quadrant with positive powers:

$$\begin{array}{cccccc}
1 & \tau_1 & \tau_1^2 & \tau_1^3 & \tau_1^4 & \cdot \\
\tau_2 & \tau_1\tau_2 & \tau_1^2\tau_2 & \tau_1^3\tau_2 & \tau_1^4\tau_2 & \cdot \\
\tau_2^2 & \tau_1\tau_2^2 & \tau_1^2\tau_2^2 & \tau_1^3\tau_2^2 & \tau_1^4\tau_2^2 & \cdot \\
\tau_2^3 & \tau_1\tau_2^3 & \tau_1^2\tau_2^3 & \tau_1^3\tau_2^3 & \tau_1^4\tau_2^3 & \cdot \\
\tau_2^4 & \tau_1\tau_2^4 & \tau_1^2\tau_2^4 & \tau_1^3\tau_2^4 & \tau_1^4\tau_2^4 & \cdot \\
\cdot & \cdot & \cdot & \cdot & \cdot & \cdot
\end{array} \tag{13}$$

Two kinds of subgroups involving both τ_1 and τ_2 can be selected from (13). These are represented by the following two simple examples:

$$P: \quad \begin{array}{ccccc} 1 & & \tau_1^2 & & \tau_1^4 \\ \tau_2^2 & & \tau_1^2\tau_2^2 & & \tau_1^4\tau_2^2 \\ \tau_2^4 & & \tau_1^2\tau_2^4 & & \tau_1^4\tau_2^4 \end{array} \tag{14}$$

$$C: \quad \begin{array}{ccccc} 1 & & \tau_1^2 & & \tau_1^4 \\ & \tau_1\tau_2 & & \tau_1^3\tau_2 & \\ \tau_2^2 & & \tau_1^2\tau_2^2 & & \tau_1^4\tau_2^2 \\ & \tau_1\tau_2^3 & & \tau_1^3\tau_2^3 & \\ \tau_2^4 & & \tau_1^2\tau_2^4 & & \tau_1^4\tau_2^4 \end{array} \tag{15}$$

The first example represents the operations of a primitive net while the second represents the operations of a centered net. Thus, a primitive net can have as derivatives both primitive nets and centered nets. It can easily be shown that the primitive derivatives can have any translation multiplicities, while the centered derivatives can only have translation multiplicities which are even. (This assumes that the cell edges of basic and derivative cells are taken in the same direction. If they are not taken in the same direction, then the edges of the derivative cell in terms of the edges of the basic cell are given by

$$\mathbf{A}=e_1\mathbf{a}+f_1\mathbf{b}, \quad \mathbf{B}=e_2\mathbf{a}+f_2\mathbf{b}.$$

The condition that the derivative cell can be a centered cell is that e_1+e_2 must be even and that f_1+f_2 must be even.)

Derivatives of Mirrors

To investigate the derivatives of a mirror, the translations of the net, (13), must be combined with the reflection S^q, where q has the values 0 or 1. The general operation is then $\tau^e\tau'^fS^q$. These operations form a group represented by the following origin portion of the quadrant with positive powers (in this table, the terms containing S can be thought of as constituting an upper level in the third dimension):

$$\begin{array}{ccccc} 1 & \tau_1 & \tau_1^2 & \tau_1^3 & \tau_1^4 \\ S & S\tau_1 & S\tau_1^2 & S\tau_1^3 & S\tau_1^4 \\ \tau_2 & \tau_1\tau_2 & \tau_1^2\tau_2 & \tau_1^3\tau_2 & \tau_1^4\tau_2 \\ S\tau_2 & S\tau_1\tau_2 & S\tau_1^2\tau_2 & S\tau_1^3\tau_2 & S\tau_1^4\tau_2 \\ \tau_2^2 & \tau_1\tau_2^2 & \tau_1^2\tau_2^2 & \tau_1^3\tau_2^2 & \tau_1^4\tau_2^2 \\ S\tau_2^2 & S\tau_1\tau_2^2 & S\tau_1^2\tau_2^2 & S\tau_1^3\tau_2^2 & S\tau_1^4\tau_2^2 \\ \tau_2^3 & \tau_1\tau_2^3 & \tau_1^2\tau_2^3 & \tau_1^3\tau_2^3 & \tau_1^4\tau_2^3 \\ S\tau_2^3 & S\tau_1\tau_2^3 & S\tau_1^2\tau_2^3 & S\tau_1^3\tau_2^3 & S\tau_1^4\tau_2^3 \\ \tau_2^4 & \tau_1\tau_2^4 & \tau_1^2\tau_2^4 & \tau_1^3\tau_2^4 & \tau_1^4\tau_2^4 \\ S\tau_2^4 & S\tau_1\tau_2^4 & S\tau_1^2\tau_2^4 & S\tau_1^3\tau_2^4 & S\tau_1^4\tau_2^4 \\ \cdot & \cdot & \cdot & \cdot & \cdot \\ \cdot & \cdot & \cdot & \cdot & \cdot \end{array} \tag{16}$$

The subgroups of (16) are restricted by the requirements that (a), they must all be based upon translation subgroups P, (14), or C, (15), and that (b), all radial lines of operations containing the identical operation at the origin must conform to subgroups of types I, II, or III, (2), (3), (4) and (5), (6), (7). Thus the borders and main diagonal of the subgroups of (16) must be of types I, II, or III. To find the subgroups of (16), therefore, one assumes translation subgroup

TABLE I. Derivatives of symmetry planes (referred to a single translation)

Basic symmetry element	Derivative symmetry element	Translation multiplicity of derivative (n is a non-negative integer)
m	m	$1+n$
	g (glide)	$(1+n)2=$ $2+2n$
	$\bar{1}$	$1+n$
g	g	$(\frac{1}{2}+n)2=$ $1+2n$
	$\bar{1}$	$1+n$

TABLE II. Derivatives of symmetry planes, and their translation multiplicities (referred to the axes of the primative net parallel to the symmetry plane).

Basic symmetry	Derivative symmetry	Translation multiplicity of derivative (n_1 and n_2 are non-negative integers) $\parallel \tau_a$	$\parallel \tau_b$
Pm	Pm	$1+n_1$	$1+n_2$
	Pa	$2+2n_1$	$1+n_2$
	Pb	$1+n_1$	$2+2n_2$
	Pn	$2+2n_1$	$2+2n_2$
	$P1$	$1+n_1$	$1+n_2$
	Cm	$2+2n_1$	$2+2n_2$
	$Ca=Cb$	$2+2n_1$	$2+2n_2$
	Cd	$4+4n_1$	$4+4n_2$
	$C1$	$2+2n_1$	$2+2n_2$
Pa	Pa	$1+2n_1$	$1+n_2$
	Pn	$1+2n_1$	$2+2n_2$
	$P1$	$1+n_1$	$1+n_2$
	Cd	$2+4n_1$	$4+4n_2$
	$C1$	$2+2n_1$	$2+2n_2$
Pb	Pb	$1+n_1$	$1+2n_2$
	Pn	$2+2n_1$	$1+2n_2$
	$P1$	$1+n_1$	$1+n_2$
	Cd	$4+4n_1$	$2+4n_2$
	$C1$	$2+2n_1$	$2+2n_2$
Pn	Pn	$1+2n_1$	$1+2n_2$
	$P1$	$1+n_1$	$1+n_2$
	Cd	$2+4n_1$	$2+4n_2$
	$C1$	$2+2n_1$	$2+2n_2$

either P or C and then assumes that the left border, upper border, and diagonal each have one of the forms of I, II, or III. Not all such combinations form groups. The ones which do are the following:

Combination				Designation
	τ_1	τ_2	$\tau_1\tau_2$	
P	I	I	I	Pm
P	II	III	III	Pa
P	III	II	III	Pb
P	III	III	II	Pn
P	III	III	III	$P1$
C	I	I	I	Cm
C	II	II	III	$Ca=Cb$
C	III	III	II	Cd
C	III	III	III	$C1$

TABLE III. Derivatives of axial symmetry elements and their translation multiplicity

Basic symmetry element	Derivative symmetry elements	Translation multiplicity of derivative (n is a non-negative integer)
$\bar{1}$	$\bar{1}$	$1+n$
	1	$1+n$
2	2	$1+n$
	2_1	$(1+n)2$ $=2+2n$
	1	$1+n$
2_1	2_1	$(\frac{1}{2}+n)2$ $=1+2n$
	1	$1+n$
3	3	$1+n$
	$3_1, 3_2$	$(1+n)3$ $=3+3n$
	1	$1+n$
$3_1(3_2)$	$3_1(3_2)$	$(\frac{1}{3}+n)3$ $=1+3n$
	$3_2(3_1)$	$(\frac{2}{3}+n)3$ $=2+3n$
	1(1)	$1+n$
$\bar{4}$	$\bar{4}$	$1+n$
	2	$1+n$
	2_1	$(1+n)2$ $=2+2n$
	1	$1+n$
4	4	$1+n$
	$4_1, 4_3$	$(1+n)4$ $=4+4n$
	4_2	$(1+n)2$ $=2+2n$
	2	$1+n$
	2_1	$(1+n)2$ $=2+2n$
	1	$1+n$
$4_1(4_3)$	$4_1(4_3)$	$(\frac{1}{4}+n)4$ $=1+4n$
	$4_3(4_1)$	$(\frac{3}{4}+n)4$ $=3+4n$
	$2_1(2_1)$	$(\frac{1}{2}+n)2$ $=1+2n$
	1(1)	$1+n$
4_2	4_2	$1+n$
	$4_1, 4_3$	$(\frac{1}{4}+n)4$ $=2+4n$
	2	$1+n$
	2_1	$(1+n)2$ $2+2n$
	1	$1+n$
6	6	$1+n$
	$6_1, 6_5$	$(1+n)6$ $=6+6n$
	$6_2, 6_4$	$(1+n)3$ $=3+3n$
	6_3	$(1+n)2$ $=2+2n$
	3	$1+n$
	$3_1, 3_2$	$(1+n)3$ $=3+3n$
	2	$1+n$
	2_1	$(1+n)2$ $=2+2n$
	1	$1+n$
$6_1(6_5)$	$6_1(6_5)$	$(\frac{1}{6}+n)6$ $=1+6n$
	$6_5(6_1)$	$(\frac{5}{6}+n)6$ $=5+6n$
	$3_1(3_2)$	$(\frac{1}{3}+n)3$ $=1+3n$
	$3_2(3_1)$	$(\frac{2}{3}+n)3$ $=2+3n$
	$2_1(2_1)$	$(\frac{1}{2}+n)2$ $=1+2n$
	1(1)	$1+n$
$6_2(6_4)$	$6_2(6_4)$	$(\frac{1}{3}+n)3$ $1+3n$
	$6_4(6_2)$	$(\frac{2}{3}+n)3$ $2+3n$
	2(2)	$1+n$
	$2_1(2_1)$	$(1+n)2$ $2+2n$
	1(1)	$1+n$
6_3	6_3	$(\frac{1}{2}+n)2$ $1+2n$
	3	$1+n$
	$3_1, 3_2$	$(1+n)3$ $3+3n$
	2_1	$(\frac{1}{2}+n)2$ $1+2n$
	1	$1+n$

Since the borders define the translations of the group, the translations multiplicities of the subgroups can be found from the individual translation multiplicities of the borders, which are listed in Table I. Centered derivatives occur only for even multiplicities, as mentioned in the last section. The two translation multiplicities of all derivatives of mirrors are found listed in Table II.

Derivatives of Glide Planes

The derivatives of glide planes combined with nets can be investigated in the same way as the derivatives of mirrors. The derivations will not be given in detail. The kinds of derivatives of each kind of glide can be predicted from the following considerations: In the case of the axial glide, a, the translation vector associated with the elementary glide operation is $\frac{1}{2}\tau_1$. The other glide operations of the group consist of this glide plus, vectorially, the translations of the net, giving $(\frac{1}{2}+e)\tau_1+f\tau_2$, where e and f are integers. All these glides are candidates for the elementary glide of the derivative symmetry. Thus the translation component of the derivative glide has the form $(\frac{1}{2}+e)\tau_1+f\tau_2$. Note that this derivative glide can have components along both a and b axes, showing that diagonal glides are among the derivatives. Similarly, when f is zero, the derivative has a translation component along a only, showing that parallel axial glides are among the derivatives. On the other hand, no derivative can have zero component along a. Hence the derivatives of the axial glide, a, include the glides n, d, and a, but not b.

In the case of the diagonal glide, the translation component of the elementary glide is $\frac{1}{2}\tau_1+\frac{1}{2}\tau_2$. When this is combined with the translations of the net there results $(\frac{1}{2}+e)\tau_1+(\frac{1}{2}+f)\tau_2$. This is the translation of the general glide operation of the group and is a candidate for the elementary glide of the derivative symmetry. Note that neither coefficient can ever be zero. Therefore, the derivatives of the diagonal glide include n and d but not a or b.

The derivatives of all types of reflection planes and their translation multiplicities are listed in Table II.

Derivatives of Rotation Axes with a Parallel Translation

The derivatives of the rotation axes may be found in the manner illustrated by the following example: In the screw 3_1, the group is composed of operations $(R\tau)^f$, where f is any integer. The rotational components, R^f, have the following identities:

$$\begin{array}{cccc} \cdot & \cdot & R^{-3}=R^0=R^3=R^6 & \cdot \quad \cdot \\ \cdot & \cdot & R^{-2}=R^1=R^4=R^7 & \cdot \quad \cdot \\ \cdot & \cdot & R^{-1}=R^2=R^5=R^8 & \cdot \quad \cdot \end{array}$$

The operations of the group may therefore be written

$$1 \qquad R\tau \qquad R^2\tau^2 \qquad \tau^3 \qquad R\tau^4 \qquad R^2\tau^5 \qquad \tau^6 \qquad \cdot \qquad \cdot \tag{17}$$

By selecting some operation, $(R\tau)^f$, as a primitive operation, a new set of operations $((R\tau)^f)^g$ may be arranged in a group table, for example:

$$1 \qquad R^2\tau^2 \qquad R\tau^4 \qquad \tau^6 \qquad \cdot \qquad \cdot \tag{18}$$

By virtue of the above identities, and by substituting τ_1 for τ^2, this may be rewritten

$$1 \qquad R^{-1}\tau_1 \qquad R^{-2}\tau_1^2 \qquad \tau_1^3 \qquad \cdot \qquad \cdot \tag{19}$$

The subgroup is now recognized as defining the group of operations of a screw 3_2. Other subgroups of the same symmetry can be formed from (17) by taking as the primitive operation of the subgroup any term separated from $R^2\tau^2$ by n basic translations. The first term of this new group thus represents $(\frac{2}{3}+n)$ basic translations. Since this is the primitive operation of 3_2, it is only $\frac{1}{3}$ of the derivative translation. The derivative translation is thus $3(\frac{2}{3}+n)=2+3n$ basic translations. The numeral, 2, indicates that the smallest translation period a derivative can have is 2 basic primitive translations.

The derivatives of the several rotation axes and their translation multiplicities are given in Table III. Table IV is another arrangement of this material of use in quickly determining the possible derivatives of a rotation axis for a given translation multiplicity.

TABLE IV. Derivatives of axial symmetry elements for particular parallel translations (excluding trivial derivative, 1).

Basic symmetry element	Translation Multiplicity 1	2	3	4	5	6	7	8	9	10	11	12	13	14	15	16	17	18	19	20
$\bar{1}$	$\bar{1}$	$\bar{1}$	$\bar{1}$	$\bar{1}$	$\bar{1}$	$\bar{1}$	$\bar{1}$	$\bar{1}$	$\bar{1}$	$\bar{1}$	$\bar{1}$	$\bar{1}$	$\bar{1}$	$\bar{1}$	$\bar{1}$	$\bar{1}$	$\bar{1}$	$\bar{1}$	$\bar{1}$	$\bar{1}$
2	2	2 2_1	2	2 2_1	2	2 2_1	2	2 2_1	2	2 2_1	2	2 2_1	2	2 2_1	2	2 2_1	2	2 2_1	2	2 2_1
2_1	2_1		2_1		2_1		2_1		2_1		2_1		2_1		2_1		2_1		2_1	
3	3	3	3 $3_{1,2}$	3	3	3 $3_{1,2}$	3	3	3 $3_{1,2}$	3	3	3 $3_{1,2}$	3	3	3 $3_{1,2}$	3	3	3 $3_{1,2}$	3	3
3_1 (For basic 3_2, interchange 3_1 and 3_2 in derivatives)	3_1	3_2		3_1	3_2		3_1	3_2		3_1	3_2		3_1	3_2		3_1	3_2		3_1	3_2
$\bar{4}$	$\bar{4}$ 2	$\bar{4}$ 2 2_1	$\bar{4}$ 2	$\bar{4}$ 2 2_1	$\bar{4}$ 2	$\bar{4}$ 2 2_1	$\bar{4}$ 2	$\bar{4}$ 2 2_1	$\bar{4}$ 2	$\bar{4}$ 2 2_1	$\bar{4}$ 2	$\bar{4}$ 2 2_1	$\bar{4}$ 2	$\bar{4}$ 2 2_1	$\bar{4}$ 2	$\bar{4}$ 2 2_1	$\bar{4}$ 2	$\bar{4}$ 2 2_1	$\bar{4}$ 2	$\bar{4}$ 2 2_1
4	4 2	4 4_2 2 2_1	4 2	4 $4_{1,3}$ 4_2 2 2_1	4 2	4 4_2 2 2_1	4 2	4 $4_{1,3}$ 4_2 2 2_1	4 2	4 4_2 2 2_1	4 2	4 $4_{1,3}$ 4_2 2 2_1	4 2	4 4_2 2 2_1	4 2	4 $4_{1,3}$ 4_2 2 2_1	4 2	4 4_2 2 2_1	4 2	4 $4_{1,3}$ 4_2 2 2_1
4_1 (For basic 4_3, interchange 4_1 and 4_3 in derivatives)	4_1 2_1		4_3 2_1		4_1 2_1		4_3 2_1		4_1 2_1		4_3 2_1		4_1 2_1		4_3 2_1		4_1 2_1		4_3 2_1	
4_2	4_2	4_2 $4_{1,3}$	4_2	4_2	4_2	4_2 $4_{1,3}$	4_2	4_2	4_2	4_2 $4_{1,3}$	4_2	4_2	4_2	4_2 $4_{1,3}$	4_2	4_2	4_2	4_2 $4_{1,3}$	4_2	4_2
	2	2 2_1	2	2 2_1	2	2 2_1	2	2 2_1	2	2 2_1	2	2 2_1	2	2 2_1	2	2 2_1	2	2 2_1	2	2 2_1
6	6	6	6 $6_{2,4}$	6	6	6 $6_{1,5}$ $6_{2,4}$ 6_3	6	6 6_3	6 $6_{2,4}$	6 6_3	6	6 $6_{1,5}$ $6_{2,4}$ 6_3	6	6 6_3	6 $6_{2,4}$	6 6_3	6	6 $6_{1,5}$ $6_{2,4}$ 6_3	6	6 6_3
	3	3	3 $3_{1,2}$	3	3	3 $3_{1,2}$	3	3	3 $3_{1,2}$	3	3	3 $3_{1,2}$	3	3	3 $3_{1,2}$	3	3	3 $3_{1,2}$	3	3
	2	2 2_1	2	2 2_1	2	2 2_1	2	2 2_1	2	2 2_1	2	2 2_1	2	2 2_1	2	2 2_1	2	2 2_1	2	2 2_1
6_1 (For basic 6_5, interchange 6_1 and 6_5, also 3_1 and 3_2 in derivative)	6_1 3_1 2_1	3_2	2_1	3_1	6_5 3_2 2_1		6_1 3_1 2_1	3_2	2_1	6_5 3_1	3_2 2_1		6_1 3_1 2_1	3_2	2_1	3_1	6_5 3_2 2_1		6_1 3_1 2_1	3_2
6_2 (For basic 6_4, interchange 6_2 and 6_4 in derivative)	6_2 2	6_4 2 2_1	2	6_2 2 2_1	6_4 2	2 2_1	6_2 2	6_4 2 2_1	2	6_2 2 2_1	6_4 2	2 2_1	6_2 2	6_4 2 2_1	2	6_2 2 2_1	6_4 2	2 2_1	6_2 2	6_4 2 2_1
6_3	6_3 3	3	6_3 3 $3_{1,2}$	3	6_3 3	3 $3_{1,2}$	6_3 3	3	6_3 3 $3_{1,2}$	3	6_3 3	3 $3_{1,2}$	6_3 3	3	6_3 3 $3_{1,2}$	3	6_3 3	3 $3_{1,2}$	6_3 3	3
	2_1		2_1		2_1		2_1		2_1		2_1		2_1		2_1		2_1		2_1	

Derivatives of Groups of Operations in a Plane

An interesting aspect of derivative structures may be illustrated by the simplified cases of operations confined to a plane. Fig. 3(a) shows a basic structure for a simple group consisting of rotations and perpendicular one-dimensional translations. The group is based on operation $A(\pi)$, i.e., a

rotation about the axis A through the angle π, and translation t. The group contains the following operations and their inverses:

$$\begin{array}{cccccccccc} 1 & t & t^2 & t^3 & t^4 & t^5 & t^6 & \cdot & \cdot \\ A(\pi) & A(\pi)t & A(\pi)t^2 & A(\pi)t^3 & A(\pi)t^4 & A(\pi)t^5 & A(\pi)t^6 & \cdot & \cdot \end{array} \tag{20}$$

Each of the operations which are the result of combining t^n with $A(\pi)$ is equivalent to a rotation of π about an axis half a translation away from A. The axes fall into two classes, A and A', which are shown with different orientations in Fig. 3(a). The A's are translation-equivalent and the A''s are translation-equivalent, but the A's and A''s are non-equivalent.

The following two kinds of subgroups can be formed from the operations of (20) by suppressing half the operations:

$$\text{I:} \quad \begin{array}{cccccccc} 1 & & t^2 & & t^4 & & t^6 & \cdot \quad \cdot \\ A(\pi) & & A(\pi)t^2 & & A(\pi)t^4 & & A(\pi)t^6 & \cdot \quad \cdot \end{array} \tag{21}$$

$$\text{II:} \quad 1 \quad t \quad t^2 \quad t^3 \quad t^4 \quad t^5 \quad t^6 \quad \cdot \quad \cdot \tag{22}$$

Consider, now, the first kind of subgroup, (21), in relation to the structure itself. The operation at the bottom of the first column of the basic group, (20), can be either $A(\pi)$, or $A'(\pi)$, depending on choice of origin. The subgroup (21) has the same form in both cases, but in one case all axes are of type A, in the other they are all A'. This amounts to saying that, in the derivative structure, Figs. 3(b) and 3(c), either axes of A' or A are entirely suppressed. The resulting two derivative structures have the same symmetry but have structures which are quite different, as shown in Figs. 3(b) and 3(c).

In (20) the even columns were retained to form subgroup (21). If columns divisible by 3 are retained, the subgroup becomes

$$\begin{array}{cccc} 1 & t^3 & t^6 & t^9 \quad \cdot \\ A(\pi) & A(\pi)t^3 & A(\pi)t^6 & A(\pi)t^9 \quad \cdot \\ (=A) & (=A') & (=A_2) & (=A_2') \end{array} \tag{23}$$

This subgroup contains both A and A' varieties of original axes, and its origin can be chosen in any one of three places, namely A, A', or A_2. The three resulting structures, Fig. 3(d), are identical with change of origin.

In a corresponding way, subgroups may be chosen in several ways from the other combinations of permissible operations with translations in a plane. In general, if the subgroup is composed of operations originally equivalent, several derivative structures are possible and these are found by placing the origin of the group at the several similar but non-equivalent points of the basic group. On the other hand, if the subgroup contains a sampling of all the elements of the original basic group, only one kind of derivative structure results.

In a diagrammatic way, Fig. 4 illustrates some of the derivatives of basic structures for other groups in a plane.

Derivatives of Space Groups

The total number of possible derivatives of a space group consist of all its subgroups in the wide sense. The number of these is infinite. They belong to the following categories:

(1) Subgroups having the same translation group, i.e., having the same lattice mode and cell dimensions as the basic structure. These are the subgroups ordinarily found listed in subgroup tables.[1]

(2) Subgroups having different translation groups, i.e., referable to different cells than the basic structure either with regard to lattice mode or to cell dimensions. The primitive cell of such a subgroup is always a multiple of that of

[1] Paul Niggli, *Geometrische Kristallographie des Diskontinuums* (Gebrüder Borntraeger, Leipzig, 1919) pp. 125–131. The *International Tables for the Determination of Crystal Structures* also list the subgroups of each space group in the description of that group.

the basic group. Unfortunately, lists of such subgroups are not available.

The subgroups consistent with a specific derivative cell can be found by forming the possible groups of the derivatives of the symmetry elements of the basic structure. (Naturally, these derivative space groups will be isomorphous with the possible subgroups of the point groups of the basic structure.) To illustrate how these subgroups may be found, an example is given of the process:

Derivatives for a Particular Cell

To illustrate the finding of the derivatives of a structure for a specific relation between derivative cell and basic cell, the case of finding the derivatives of marcasite consistent with the arsenopyrite cell is offered. This problem has been solved by other methods.[2]

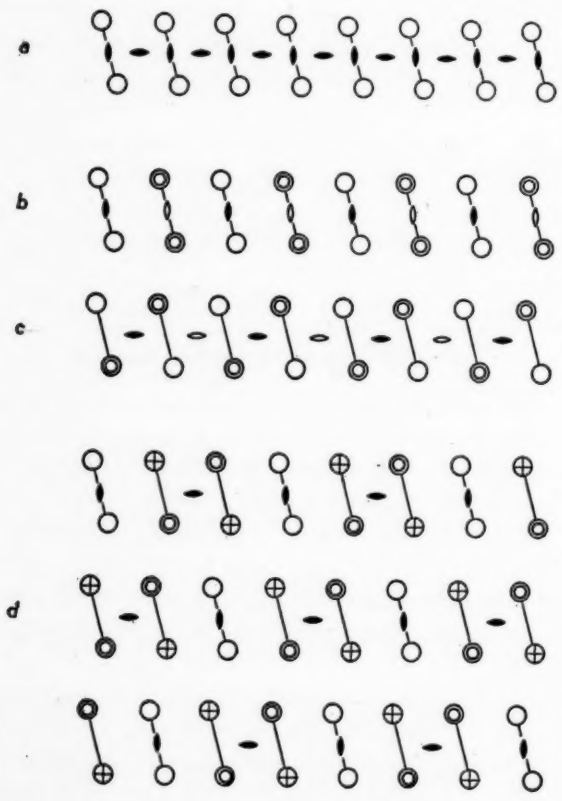

FIG. 3. The kinds of derivative structures based on the ame subgroup. Fig. 3(a) is the basic structure. Figs. 3(b) and 3(c) show two different structures based on the same subgroup. Fig. 3(d) illustrates that such different structures do not arise when the subgroup contains a sampling of the several kinds of symmetry elements in the basic structure.

The basic cell (marcasite, FeS_2) has symmetry *Pmnn*. It is desired to find the derivative symmetries consistent with a *C*-centered cell of multiplicity 2. The derivative cell in terms of the basic cell is represented by the matrix

$$\begin{Vmatrix} 1 & 1 & 0 \\ 1 & \bar{1} & 0 \\ 0 & 0 & 1 \end{Vmatrix}. \tag{24}$$

The upper part of Fig. 5 diagrammatically represents the symmetry *Pmnn* and the shape and dimensions of the derivative cell. Fig. 5 illustrates the following discussion:

Consider first the symmetry axes:

Parallel to a: The basic structure has twofold rotation axes. The derivatives of 2 for $2t$ are 2, 2_1, and 1. Owing to the fact that a face parallel to *a*, namely *C*, is centered, rotations and screws must occur mixed, so that the only possible derivative symmetries are $(2+2_1)$ and 1.

Parallel to b: The basic structure has twofold screws. The derivatives of 2_1 for $2t$ are 2_1 and 1. Since a face parallel to *b*, namely *C*, is centered, rotations and screws must occur mixed. Since 2 is not a derivative of 2_1, the mixture $(2+2_1)$ cannot be a derivative, hence the only derivative symmetry is 1.

Parallel to c: The basic structure has twofold screws. The derivatives of 2_1 for $1t$ are 2_1 and 1.

The axial derivatives are thus

$\|\|a$	$\|\|b$	$\|\|c$
$(2+2_1)$ and 1	1	2_1 and 1.

(25)

These can only be combined into the following groups: $C211$, $C112_1$, $C1$.

Consider next the symmetry planes:

Parallel to (100): The basic structure has a mirror. The derivatives of *m* are *m*, *g* (glide) and 1. The only possible glide for translations $(2t_b; t_c)$ is *b*. Hence the only derivatives of *m* for $(2t_b; t_c)$ are *m*, *b*, and 1. However, since the cell is *C*-centered, glides and mirrors must occur mixed, so the only derivatives are $(m+b)$ and 1.

[2] M. J. Buerger, "A systematic method of investigating superstructures, applied to the arsenopyrite crystal structural type," Zeits. f. Krist. (A)94, 425–438 (1936).

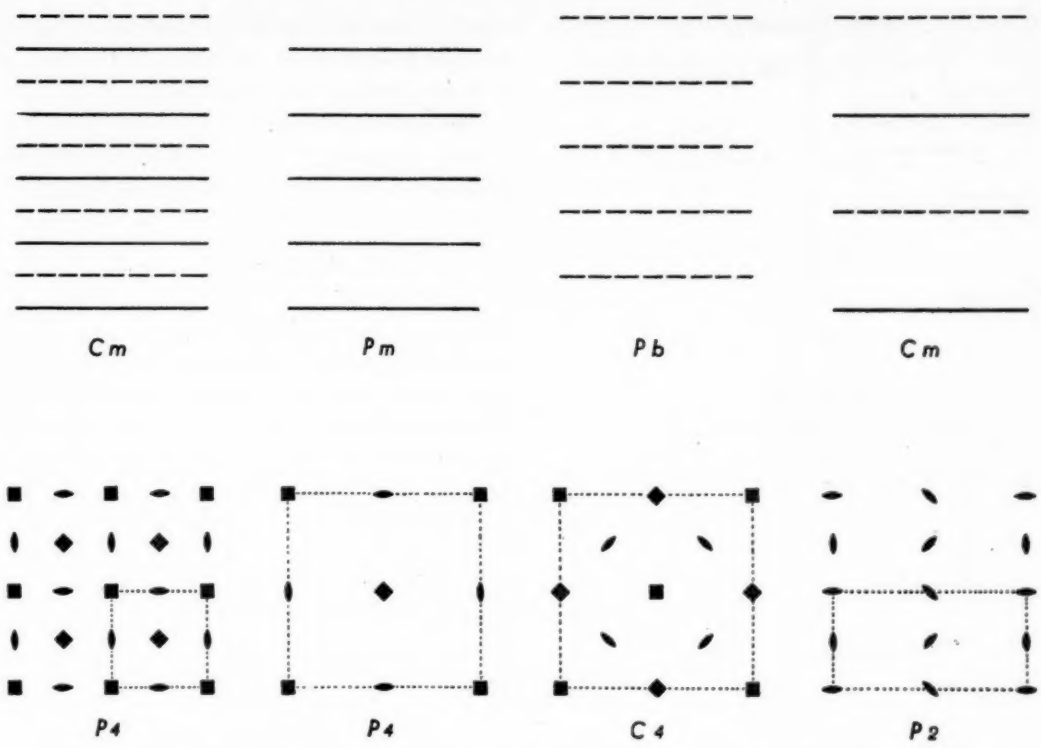

FIG. 4. Examples of derivative symmetries for the two basic symmetries, *Cm* and *P*4. In each case the basic symmetry is shown at the left. To the right of it are three examples of derivative symmetry.

Parallel to (010): The basic structure has a glide ***n***. The only derivatives of a glide for translations $(2t_a; t_c)$ is 1.

Parallel to (001): The basic structure has a glide ***n***. The derivatives of a glide ***n*** for translations $(t_{a+b}; t_{a-b})$ are ***n*** and 1.

The derivatives of the symmetry planes are thus

‖(100)	‖(010)	‖(001)
$(m+b)$		n
and 1	1	and 1.

(26)

By combining the derivatives of plane symmetry, (26), with the derivatives of axial symmetry, (25), there result the following possible derivative symmetries:

$C2/m$ 1 1, and subgroups $C2$ 1 1, Cm 1 1
C 1 1 $2_1/n$ and subgroups C1 1 2, C 1 1 n } and C1.

The symmetry $C1$ is inconsistent with the theory of substitution structures, discussed beyond. The remaining symmetries each determine two derivative structures differing in a manner similar to Figs. 3(b) and 3(c).

KINDS OF DERIVATIVE STRUCTURES

There are two distinct kinds of derivative structures. These are here designated *substitution structures* and *distortion structures*. The distinction between these can be illustrated by one-dimensional examples. Suppose the basic structure is a linear array of equally spaced atoms, A, thus:

$$\underset{\leftarrow t\rightarrow}{A}\quad A\quad A\quad A\quad A\quad A. \tag{27}$$

If another kind of atom, B, is substituted for every alternate atom A, there results:

$$\underset{\longleftarrow t\longrightarrow}{A}\quad B\quad A\quad B\quad A\quad B. \tag{28}$$

The substitution doubles the translation period, t. This is an instance of the suppression of a set of operations, thus leaving only a subgroup of operations, and therefore a derivative symmetry and a derivative structure, (28). The specific case of the operation of translation has been used for illustration, but obviously substitution can occur within any periodic operation, thus giving

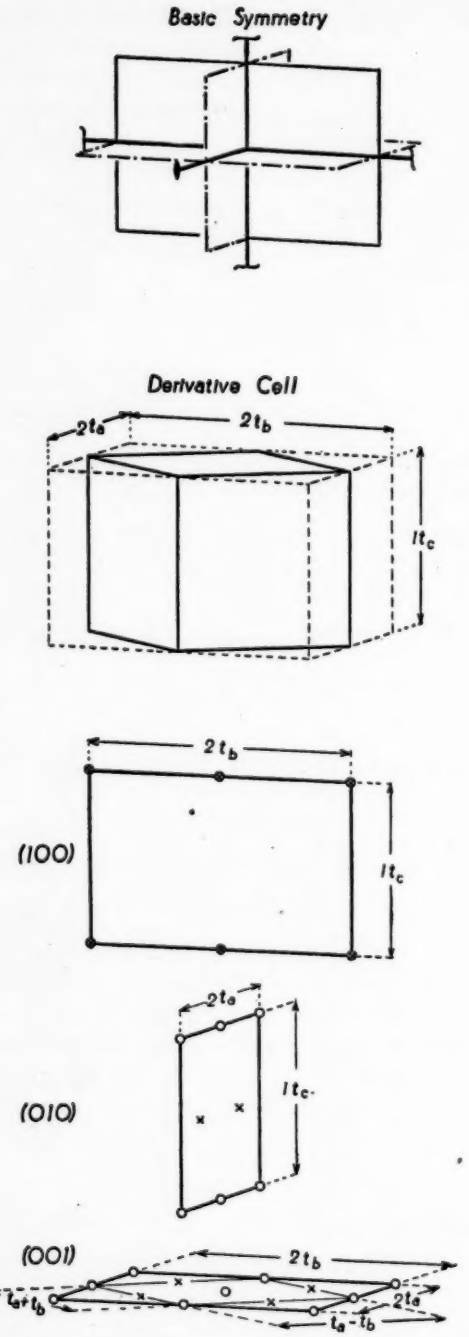

FIG. 5. Diagrams to illustrate the finding of the derivative symmetries of marcasite, FeS_2, for a particular derivative cell. Open circles and x's are reflection-equivalent points.

rise to derivative structures by substitution. Substitution structure may be regarded as formally including the case of structures with regularly arranged holes, by the device of substituting holes for certain atoms A. Similarly the notion may be extended to include substitution of two or more atoms for a single atom, A.

The period of (27) can be multiplied by other means. Suppose alternate atoms A are slightly displaced by identical amount and direction, thus:

$$A\ A \underset{\longleftarrow t \longrightarrow}{\ \ \ } A\ A \ \ \ \ A\ A\ . \quad (29)$$

Then the period of the array is again doubled. This amounts to a distortion of the basic structure, hence the designation *distortion structure.* Evidently such a structure can arise by the suppression of certain coincidence operations present in the basic structure; consequently a distortion structure is a derivative structure.

Substitution and distortion are obviously two different mechanisms for realizing the decreased symmetry of derivative structures. Consideration of these structures is important in many aspects of crystal relations.

SUBSTITUTION STRUCTURES

Kinds of Substitution Structures

If, for every series of like atoms, $M, M, \cdots$ in a crystal structure, there is substituted a sequence of unlike atoms, $P, Q, \cdots$, then there results a new structure whose characteristics depend on the original symmetry relations between the M's and also on how the substitution is effected. Depending upon these, the new structure may be one of several kinds:

I. If the original atoms, M, were related by any symmetry operation in the basic structure, then, depending on how the substitution is effected, two possible kinds of structures may result:

(a) If some regular plan is followed in substituting $P, Q, \cdots$, for $M, M, \cdots$, (Fig. 6(a)) as described in the last section, then some kind of alternation of $P, Q, \cdots$, results. This necessarily suppresses the symmetry elements which carried one M atom into another. Such a structure may be called a *regular substitution structure* merely to distinguish it from the one which follows. Unless otherwise qualified, the term substitution structure will be taken to imply a regular substitution structure.

(b) If the unlike atoms, $P, Q, \cdots$, are substi-

tuted for M, M, $\cdots$ without any plan or regularity, but at random, then the resulting substitution structure is in disorder with respect to the atoms P, Q, $\cdots$. Such a structure is a *random substitution structure.* It has no true symmetry, for it lacks any periodicity in the repetition of P, Q, $\cdots$. Insofar, however, as P, Q, $\cdots$ may together be regarded as statistically equivalent to the original M, M, $\cdots$, the structure has periodicity. In this sense, it statistically has the exact symmetry of the basic structure.

(c) There is a possibility of a combination of the features of (a) and (b). For example, for the sequence of like atoms M, M, $\cdots$ there could be substituted the sequence A, B, B, A, B, B, A, $\cdots$, where the B atoms may be either B' or B'' at random. While this kind of sequence has no true periodicity, it may be regarded as having, statistically, a symmetry controlled by the distribution of the similar A atoms.

II. If the atoms M', M'', $\cdots$ are not equivalent by symmetry in the original structure (Fig. 6(b)), then the substitution of P, Q, $\cdots$, for M', M'', $\cdots$ does not involve the suppression of any symmetry element of the crystal. An example of this is afforded by Fe_3O_4. This crystal contains two structurally distinct kinds of Fe, so that its formula might well be written $FeFe_2O_4$. In this case the replacement of the atoms $FeFe_2$ by $MgAl_2$ does not give rise to any loss of symmetry. $MgAl_2$ is not a "substitution" for $FeFe_2$; rather $FeFe_2$ is a degenerate case of $MgAl_2$. This kind of "substitution" does not give rise to substitution structures in the sense here employed. Rather it gives rise to the non-degenerate case of a structure whose "basic" structure was degenerate.

Regular substitution structures constitute an important category of crystal structures. Recognition of the fact that an otherwise complicated structure is a substitution structure may become the key to its structural analysis. In order to handle such cases intelligently, the theory of regular substitution structures is briefly discussed below. Before entering into the theory, however, some examples will be given:

Examples of Substitution Structures

Mineralogy provides many structures which may be recognized as substitution structures. A number are known which are based upon the sphalerite and wurtzite structures. The mineral chalcopyrite affords an example of a substition structure based upon sphalerite. This may be brought out as follows:

basic structure: (*sphalerite*)	Zn S
substitution structure: (*chalcopyrite*)	$\left\vert \begin{matrix} Cu_{\frac{1}{2}} \\ Fe_{\frac{1}{2}} \end{matrix} \right\vert$ S

In this case the Zn of the basic structure is replaced by half Cu and half Fe. The formula of chalcopyrite is customarily written $CuFeS_2$, a form which tends to conceal the fact that it is a substitution structure based upon sphalerite, ZnS. The formula

$$\left\vert \begin{matrix} Cu_{\frac{1}{2}} \\ Zn_{\frac{1}{2}} \end{matrix} \right\vert S$$

brings out the relation to the basic structure, ZnS.

Substitution is by no means confined to half and half substitution. There are no restrictions on the proportions of the atoms entering into the substitution other than that they must be such as to fit into possible crystal structures. As an example of a more complicated substitu-

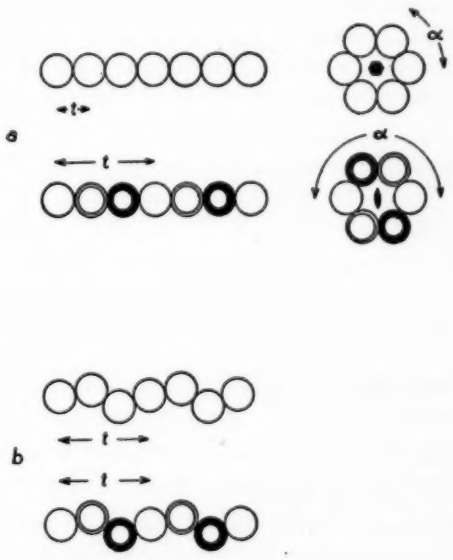

FIG. 6. In Fig. 6(a) is illustrated the increase in repetition period due to the regular substitution of unlike atoms for equivalent atoms. Figure 6(b) shows that this increase does not occur if the atoms in the basic structure are not equivalent. The translation repetition period is t, the angular repetition period is α.

tion there may be cited the structure formed by the substitution of Cu, Cu, Cu, As for Zn, Zn, Zn, Zn, in the basic wurtzite (ZnS) structure. This may be brought out with the following comparison:

basic structure: Zn S
(*wurtzite*)

substitution structure: $\left|\begin{matrix}Cu_{\frac{1}{4}}\\As_{\frac{1}{4}}\end{matrix}\right|$ S $\Rightarrow \frac{1}{4}Cu_3AsS_4$.
(*enargite*)

Furthermore, the substitution is not necessarily confined to substitution by two atoms. For example, stannite is a substitution structure based upon sphalerite in which the sequence Cu, Fe, Cu, Sn, is substituted for Zn, Zn, Zn, Zn, thus:

basic structure: Zn S
(*sphalerite*)

substitution structure: $\left|\begin{matrix}Cu_{\frac{1}{4}}\\Fe_{\frac{1}{4}}\\Sn_{\frac{1}{4}}\end{matrix}\right|$ S $\Rightarrow \frac{1}{4}Cu_2FeSnS_4$.
(*stannite*)

It appears likely that many apparently complex sulfosalt minerals will prove to have substitution structures based upon simple basic sulfide structures.

Many, but not all, double salts and other multiple salts have substitution structures. The double salt dolomite may be taken as an illustration. Its formula can be written as a double salt, $CaCO_3 \cdot MgCO_3$, or as $CaMg(CO_3)_2$. The relation to the calcite structure is brought out as follows:

basic structure: Ca CO_3
(*calcite*)

substitution structure: $\left|\begin{matrix}Ca_{\frac{1}{2}}\\Mg_{\frac{1}{2}}\end{matrix}\right|$ CO_3
(*dolomite*)

Structures resulting from the ordering of disordered crystals (i.e., random substitution structures) are (regular) substitution structures. For example (notation taken from reference 6):

disordered (basic structure)	ordered (regular substitution structure)	
$\left[\begin{matrix}Cu_{\frac{1}{2}}\\Zn_{\frac{1}{2}}\end{matrix}\right]$	$\left\|\begin{matrix}Cu_{\frac{1}{2}}\\Zn_{\frac{1}{2}}\end{matrix}\right\|$	$\Rightarrow \frac{1}{2}CuZn$ (β brass)
$\left[\begin{matrix}Cu_{\frac{1}{4}}\\Pt_{\frac{3}{4}}\end{matrix}\right]$	$\left\|\begin{matrix}Cu_{\frac{1}{4}}\\Pt_{\frac{1}{4}}\end{matrix}\right\|$	$\Rightarrow \frac{1}{4}Cu_3Pt$.

Cell Multiplicity of the Substitution Structure

A simple relation exists between the characteristics of the substitution and the size of the cell of the substitution structure. Let the volume of the cell of the substitution structure be m times the volume of the cell of the basic structure. Let the atom A, for which substitution is made, occupy an R-fold equipoint in the basic structure. Then in m cells there are mR atoms of A. In the substitution structure cell, the A atom occupies an r-fold equipoint. Thus r of the original mR atoms of A must remain if m cells are to be involved in the substitution. If F is the fraction of A remaining, then

$$F = r/mR. \tag{30}$$

It should be observed that since the group of operations carrying the A's of r into each other is a subgroup of the operations carrying the A's of R into each other, r cannot exceed R, nor can r be less than 1.

A useful form of (30) is

$$m = \frac{1}{F}\frac{r}{R} \quad \left\{\begin{matrix} 1 \leqslant r \leqslant R \\ \text{or, } 1 > \frac{r}{R} > \frac{1}{R} \end{matrix}\right\}. \tag{31}$$

The maximum multiplicity, m, occurs when r/R is a maximum, namely 1. Therefore

$$m_{max} = 1/F. \tag{32}$$

The minimum multiplicity, m, is 1. For this situation (30) becomes

$$F_{m=1} = r/R. \tag{33}$$

(In the above argument, it was assumed that the atoms A occupy one R-fold equipoint in the basic structure and that those remaining after substitution occupy one r-fold equipoint in the substitution structure. The argument remains valid if the atoms A occupy several R-fold equipoints in the basic structure and those remaining occupy several r-fold equipoints in the substitution structure, provided that in the above relations R is replaced by ΣR and r by Σr.)

These simple relations impose restrictions on substitution structures. To illustrate their use, suppose one wishes to know what maximum size cell could possibly come up for consideration in

a substitution structure of arsenopyrite,

$$\mathrm{Fe}\left|\begin{matrix}\mathrm{As}\\ \mathrm{S}\end{matrix}\right|,$$

derived from the basic structure FeS, marcasite. In this case half the S atoms are replaced by As atoms. Thus the fraction, F, of S atoms remaining is $\frac{1}{2}$. According to (32), $m_{\max}=2$. Thus only cells having a multiplicity of 2 or less could exist having composition FeAsS and based upon the marcasite packing. Another characteristic of the substitution structure is the symmetry number, r, of the resulting space group. For this purpose, (30) may be solved for r. In this example, F was ascertained to be $\frac{1}{2}$. For marcasite, $R=4$ sulfur atoms per cell. For these values and $m=1$, (30) shows that $r=2$, and for $m=2$, $r=4$. Hence the derivative symmetries must have 2-fold equipoints if referred to a single cell or 4-fold equipoints if referred to a double cell. (This analysis eliminates the derivative symmetry $C1$ as determined above, since this space group has only 1-fold equipoints for a single (P) cell or 2-fold equipoints for a C-centered double cell.)

Thus for this substitution, only the following structure characteristics are possible

$$\mathrm{I}\begin{cases}m=1\\ r=2\end{cases}\qquad\qquad \mathrm{II}\begin{cases}m=2\\ r=4.\end{cases}$$

With the cell multiplicities, m, limited in this fashion, it is possible to write quickly the translation multiplicities of all possible substitutions structures. For each of these, it is possible to pursue a derivative structure analysis of the type illustrated above under the heading "Derivatives for a Particular Cell." Therefore for a given substitution, all possible structures can be predicted. This procedure is an aid in the crystal analysis of structures which can be recognized as substitution structures.

DISTORTION STRUCTURES

The relation of distortion to basic structure is known to occur in two different ways:

(1) The atoms in two different kinds of crystals may be arranged in essentially the same way, yet differ in some slight detail. The result may be that one is the distortion equivalent of the other. An example of this is afforded by the pair:

	basic structure	distortion structure
	PtS	CuO
	(*Cooperite*)	(*Tenorite*)
Symmetry:	$P4_2/m\ 2/m\ 2/c$	$C2/c$.

Both of these structures have square coordinated metals, tetrahedrally coordinated non-metals, and the structures are similarly linked. The CuO structure is, in effect, a slumped PtS structure. The derivative relation of the CuO structure to the PtS structure would be suspected by the comparable formulae, comparable cells and cell content, and derivative symmetry.

(2) Many rapid (*high-low*) inversions are polymorphic transformations from basic structure (high temperature, low pressure) to distortion structure (low temperature, high pressure). Good examples are afforded by the high-low inversions of quartz and cristobalite (in these examples, $m=1$):

	basic structure (high-T form)	distortion structure (low-T form)
quartz	$H6_2\ 2$	$H3_1\ 2$
cristobalite	$F4_1/d\ \bar{3}\ 2/m$	$P4_1\ 2_1$.

The derivative natures of the low temperature structures are evident from the symmetries.

Distortion structures may be formally treated as substitution structures by the device of substituting distorted structure complexes for the undistorted complexes.

APPLICATIONS OF DERIVATIVE STRUCTURE THEORY

In this paper the elements of derivative structure theory and substitution structure theory have been presented. These relations are useful in several branches of crystallography. A few instances where they have been applied by the writer are mentioned below:

It is not generally possible to determine the space group symmetry of a crystal by qualitative x-ray means, although the crystal can be assigned to a diffraction group[3] usually embracing several space groups. Between the space groups of this set one cannot decide by the methods of ordinary

[3] M. J. Buerger, *X-Ray Crystallography* (John Wiley and Sons, New York, 1942), pp. 510–511.

qualitative x-ray crystallography. If, however, the crystal has a high-low inversion, the symmetries of the high form and low form are connected by derivative structure theory which restricts the symmetry possibilities for both forms. With the aid of this additional relation, it has been possible to determine the space groups of both[4] high-Cu_2S and low-Cu_2S.

Derivative structure theory provides a basis for understanding certain varieties of twinning,[5] particularly twinning which is the result of inversion. The number and orientation of the twins which descend by inversion from the high temperature form are readily provided[5] by derivative structure theory. The results are applicable to high-low inversions as well as to inversions due to ordering[6] of a disordered structure.

For the special case of derivative structures which are substitution structures, the theory outlined under "Substitution Structures" permits one to predict, within a comparatively small group, the structures to be expected as the result of any given kind of substitution in any desired structure. In popular language, this enables one to predict the kinds of "superstructures" which could conceivably result from a selected substitution.

Dr. A. L. Patterson was kind enough to read the manuscript of this paper. The writer is indebted to him for a number of valuable suggestions.

[4] M. J. Buerger and Newton W. Buerger, "Low-chalcocite and high-chalcocite," Am. Mineral. **29**, 55–65 (1944).

[5] M. J. Buerger, "The genesis of twin crystals," Am. Mineral. **30**, 469–482 (1945).

[6] M. J. Buerger, "The temperature-structure-composition behavior of certain crystals," Proc. Nat. Acad. Sci. **20**, 444–453 (1934).

THE JOURNAL OF CHEMICAL PHYSICS VOLUME 15, NUMBER 1 JANUARY, 1947

The Effect of Physical Adsorption on the Electrical Resistance of Activated Carbon*

R. McIntosh, R. S. Haines, and G. C. Benson
Division of Chemistry, National Research Laboratories, Ottawa, Canada

(Received October 1, 1946)

The change of electrical resistance of several rods of activated carbon on the adsorption of a variety of vapors has been determined. The direction and extent of the resistance change appear to depend upon the adsorbate. The hypothesis that the changes in resistance are due to the variations in contact resistance between the carbon granules does not appear to be adequate to explain the observations.

INTRODUCTION

THE resistance of carbon conductors has been shown to change when the conductors are exposed to an atmosphere of some gas or vapor.[1–3] For carbon filaments the reduction in conductivity was found by Siebel[1] to increase with increasing pressure in the gas phase and to be larger for ammonia than for air. Sandor[3] exposed rods of coal to the saturated vapors of methanol and of water and obtained an increase of resistance in both cases. Since the compressibility of carbon crystals was too small to account for the observed change of approximately 10 percent in resistance by distortion of the crystals, Sandor attributed the change to a variation in the contact resistances between the granules. Schwab and Karkalos[2] adopted somewhat the same view in explaining the decrease of resistance of charcoal beds exposed to bromine and a variety of other vapors. Since the particles of charcoal were maintained under a constant external load, and since they swelled on adsorption of the vapors, the increased area of contact was presumed to account for the decreased resistance of the bed.

Since resistance changes with direct current were obtained in these cases, either variations in contacts or solution of the adsorbate in the conductor would appear to be the most reasonable causes of the phenomenon.[4] However, where the ratio of surface to volume is very large for the conductor, it is also possible that surface effects, owing to the presence of the adsorbate, might influence the resistance of the conductor. In the case of certain coal samples studied by Maggs,[5] surface areas as large as 200 m^2/g were reported, while for activated charcoals areas as large as 2000 m^2/g have frequently been estimated.[6] For materials possessing surfaces as large as this latter figure, Young[7] has pointed out that about every second carbon atom must be considered as part of the adsorbing surface. With activated charcoal, therefore, the conductance might be altered because the presence of the adsorbate on the surface would alter the electrical properties of both adsorbate and adsorbent. For example Ouellet and Rideal[8] have shown that the photoelectric threshold of gold leaf is reduced when a vapor is adsorbed, and Frost and Hurka[9] have measured the change in potential at an interface caused by the (presumed) adsorption of such substances as ethylacetate.

If, in the case of carbon conductors, the explanation of altered contact resistances were adopted, one might expect that adsorption of all vapors would cause a resistance change in the same direction. It might also be anticipated that for a given conductor the magnitude of the change would be governed primarily by the spreading pressure of the film, and that a rough

* Contribution Number 1445 from the National Research Laboratories, Ottawa, Canada.

[1] K. Siebel, Zeits. f. Physik **4**, 288 (1921).

[2] G. M. Schwab, and B. Karkalos, Zeits. f. Elektrochemie **47**, 345 (1941).

[3] J. Sandor, *The Ultra-Fine Structure of Coals and Cokes* (British Coal Utilization, Research Association, London, 1944), p. 342.

[4] J. W. McBain, *Sorption of Gases and Vapours by Solids* (G. Routledge and Sons, Ltd., London, 1932), p. 399.

[5] F. A. P. Maggs, *The Ultra-Fine Structure of Coals and Cokes* (B. C. U. R. A., London, 1944), p. 95.

[6] S. Brunauer, *The Adsorption of Gases and Vapors, Volume I, Physical Adsorption* (Princeton University Press, 1945) p. 313.

[7] T. F. Young, Chemistry Department, University of Chicago, private communication.

[8] C. Ouellet and E. K. Rideal, J. Chem. Phys. **3**, 150 (1935).

[9] A. A. Frost and V. R. Hurka, J. Am. Chem. Soc. **62**, 3335 (1940).

parallelism would be shown between the dimensional change of the conductor and its resistance variation.

Some preliminary studies of the influence of several vapors on the conductance of rods of zinc chloride activated charcoal showed immediately that both the magnitude and the direction of the resistance change for a given rod depended on the nature of the gaseous adsorbate, and that the phenomenon was more complicated than had been anticipated. In an attempt to determine the factors which were involved, observations have been made of the resistance and length changes of a number of rods as functions of the amount of material adsorbed. The length measurements and the method of determining them are both of some interest, and are reported in detail in a second paper, although some of the length measurements are required in interpreting the resistance data and are therefore discussed here.

EXPERIMENTAL

The activated carbon rods were prepared by the National Carbon Company of Fostoria, Ohio, and supplied to us through the courtesy of the Chemical Warfare Laboratories, Ottawa, Canada. The rods were formed by extrusion when the cellulosic material and the zinc chloride were still in a plastic condition. The zinc chloride was removed by volatilization at a high temperature about 600°C, and the rods were finally leached with water. The ash content determined for several rods by burning at about 800°C was 0.4 percent by weight. The rods used were all approximately 8 mm in diameter and varied from 8 to 13 cm in length.

The experimental assembly may be most easily described by its separate units. These were: (a) the carbon rod and its electrical connections; (b) the resistance measuring circuit; (c) the degassing system; and (d) the adsorption system.

(a) The carbon rod was placed in a glass envelope to form the assembly shown diagrammatically in Fig. 1. Four heavy copper cable leads were attached to the carbon by means of a special type of spring clamp of phosphor-bronze, separated from the carbon by a thin strip of platinum foil. The spring clamp was found to be essential in order to maintain a roughly constant pressure at the carbon, since the rod swelled or shrank with addition or removal of adsorbate. The outside leads at each end of the carbon carried the current, and the inner leads provided a measure of the potential drop along the rod. (As the spring clamps had an appreciable width (about 8 mm) it was not possible to express resistance values as resistivities.)

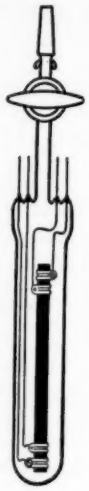

FIG. 1. Carbon rod and containing envelope.

(b) The electrical source of the resistance measuring circuit was a 6v storage battery. From it one lead connected through a switch with a variable resistance, then from the resistance through a Leeds and Northrup Standard Ohm, then through the activated carbon rod, and finally back to the battery. The potential drop across the standard ohm and across the carbon were determined by means of a Leeds and Northrup K_2 potentiometer and a standard cell. The resistance of the carbon between the potential electrodes was therefore the ratio of the voltage across the potential electrodes to that across the standard ohm. Since the current in the potential circuit approached zero as a balance with the bridge system was approached, there was no contact resistance in this part of the circuit and no error in the resistance of the rod was introduced.

The resistance values determined in this way were independent of the current being passed through the rods from 10 milliamperes to 60 milliamperes and showed that the rods obeyed Ohm's law within the precision of the measure-

ments whether a film was on the surface or whether the surface was clean. The resistance values were also independent of the time of passage on the current and of the direction of the current. They did not change with time once adsorption equilibrium had been established except where noted specially below. The resistance value of a clean rod could be repeated to about 3 parts in 10,000, but when the repetition also included the adsorption equilibrium with some vapor, 1 part in 1000 was the order of the reproducibility. (See for example the values for water vapor at 100 percent relative humidity in Table VI.)

In order to insure that the mounting of the rod was not an important factor in the resistance effect, the second extensometer constructed was so arranged that values of the resistance could be measured along with the length of the rod. (A description of the assembly is given in the second paper.) The different arrangement of the rod did not affect the character of the resistance variations, and data obtained with that apparatus are included here without special identification.

(c) In order to free the carbon from physically adsorbed gases a three-stage mercury diffusion pump backed by a Hyvac was provided. The envelope containing the carbon was attached to this system through a standard taper joint, and the envelope was then surrounded by an air oven whose temperature could be raised to 150°C. The carbon was degassed at between 120°C and 130°C until no further change in electrical resistance was observed. The temperature of the air oven was then varied and the resistance of the rod determined as a function of temperature. If no hysteresis was observed in the resistance on heating and cooling the rod, the charcoal was considered to be thoroughly evacuated. This procedure usually took up to seven days when the carbon was first evacuated, but in subsequent evacuations after exposure to the adsorbates, 24 hours pumping sufficed to bring the carbon to its original resistance.

(d) The usual form of gas adsorption apparatus was employed. This consisted of a constant volume manometer, a gas burette with bulbs of different volumes, and several storage bulbs for the purified gases. Vacuum stopcocks were used where the dead space was unimportant, and Apiezon *N* grease was used throughout. An oil thermostat, the temperature of which could be adjusted between 5°C and 30°C and controlled to ±.02°C, was provided for the adsorption cell. The dead space of each carbon cell was determined when in position by expanding helium from the calibrated burette. The effect of helium on the resistance was observed at the same time. No corrections for deviations from the ideal gas law were applied for the adsorbates since the vapors were usually appreciably above their boiling points at the temperature of the burette, and because the pressure at the highest value was below atmospheric. The temperature of the envelope containing the carbon was lower than that of the burette, but the volume of gas in the cell only became appreciable at the higher pressures, and only a small correction would be necessary. That no serious error was introduced by this omission was indicated by the good agreement for the total surface area values obtained for a given rod with the various adsorbates and for the same adsorbate at different temperatures. (See Table III.)

Whenever measurements of the effect of water vapor were desired, the carbon cell was placed in the oil thermostat and connection made with a water reservoir rather than with the adsorption system. The water in the humidifier was freed of dissolved gases by repeated freezing in dry ice-acetone and evacuation. The humidifier contained a glass stirrer actuated by a solenoid, and stirring was maintained during the establishment of equilibrium. The relative pressure of water vapor was controlled through the temperature of the water thermostat surrounding the humidifier. Its temperature was controlled to ±.01°C.

The vapors used were obtained in cylinders and as received were all 99.5 percent pure or better, the main impurities being air and moisture. The materials were distilled under vacuum from a dry ice receiver to a liquid air receiver, the first and final portions being rejected.

The helium was purified by passing it slowly over activated carbon which had been degassed at about 200°C, and which was maintained at liquid-air temperature while the helium was passed over it.

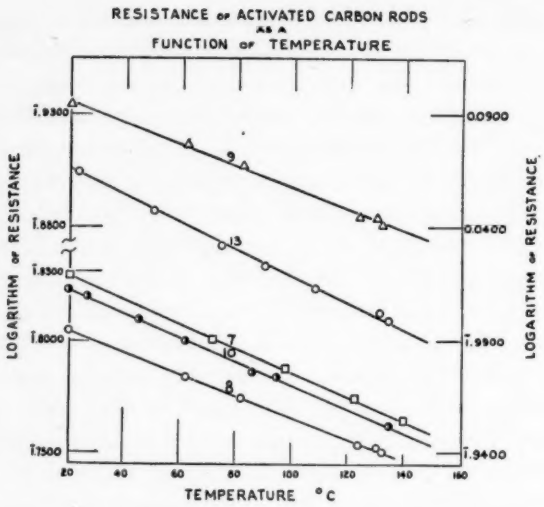

FIG. 2. Relationship between resistance and temperature for several rods. Ordinate is $\log_{10}$ resistance; abscissa is temperature, °C. Rods are indicated by number. Right-hand ordinate for rod No. 13 only.

RESULTS

Resistance Variation with Temperature

The electrical resistance of several rods as a function of temperature is given in Table I, and shown graphically in Fig. 2, where the logarithm of the resistance is plotted against temperature. The relation $\log_{10}R=A-BT$, where R is the resistance in ohms, T the temperature, °C, and A and B are constants, was found to represent the data for all carbons much better than the relationship $\log_{10}R'=A'+B'/T'$, where R' is the resistivity in ohms/cm, T' the absolute temperature, and A' and B' constants. This latter relation was employed by Sandor,[3] who utilized it to obtain from the constant B a value of "some energy barrier opposing the passage of electricity." Since our data do not conform with this relation, a similar calculation of such an energy barrier was not possible. Both Sandor's data and our own show that the resistance decreases with increasing temperature, a behavior typical of semiconductors.

Since the rods were all about 8 mm diameter as closely as could be estimated, the relative resistivities were inversely proportional to the length between the potential electrodes, and were different for the different rods. The temperature coefficient of resistance was also slightly different for the various rods. These differences may have been due to minor variations in the structure created in the preparation. If structural differences did exist in the several rods they did not appear to cause important variations in the effect of the adsorbates. Qualitatively, a given vapor always caused the same general behavior on all rods, although the extent of the change varied somewhat from one carbon to another.

Qualitative Observations of the Resistance Change

The first experiments were designed to determine whether any specific behavior could be attributed to the kind of adsorbate employed. The degassed rods were therefore exposed to varying pressures of a large number of adsorbates and the extent and direction of the resistance change noted as a function of the gas pressure. These results, along with others obtained when the gas adsorption was also measured, are given

TABLE I. The resistance of activated charcoal rods as a function of temperature.

Rod	Temperature °C	Temperature °K	Resistance, ohms
No. 8.	130	403	0.5664
Length between potential	132	405	0.5633
electrodes 7.3 cm	82	355	0.5952
	62	335	0.6081
	134	397	0.5660
	20.2	293	0.6376
No. 9.	130	403	0.7654
Length between potential	132	405	0.7603
electrodes 7.0 cm	82	355	0.8072
	62	335	0.8241
	124	397	0.7662
	20.2	293	0.8577
No. 7.	140	413	0.5818
	123	396	0.5953
	98	371	0.6127
	72	345	0.6316
	20.2	293	0.6733
No. 10.	135	408	0.5787
Length between potential	95	368	0.6085
electrodes 7.5 cm	86	359	0.6113
	62	335	0.6308
	45	318	0.6440
	27	300	0.6593
	20.2	293	0.6642
No. 13.	131	404	1.0054
Length between potential	134	407	0.9966
electrodes 8.3 cm	108	381	1.0296
	90	363	1.0541
	74.5	347	1.0764
	50	323	1.1150
	23	296	1.1596

in Table II. The identity of the rod is given by number. The direction of the resistance change and the maximum value of the resistance change as a percentage of the initial resistance are also recorded. No exact comparison of adsorption conditions is represented here as the relationship between pressure (or volume adsorbed) and resistance change was not a simple one for certain of the adsorbates. The saturated hydrocarbons, water and carbon dioxide always showed a regular decrease in resistance, which appeared to level off as the higher values of amount adsorbed on the rod were approached. Peculiarities were observed with ethylene oxide, dimethyl ether, sulphur dioxide, and ethyl chloride. The first three substances always showed an initial increase in resistance and then a gradual decrease from this value as the pressure of the adsorbate was increased. Of these only sulphur dioxide fell appreciably below the original resistance value as the amount adsorbed was increased. Ethyl chloride showed a marked decrease in resistance which passed through a sharp minimum near the highest adsorption points.

The unsaturated hydrocarbons and ammonia showed further peculiarities which are discussed more fully below. The important finding that a specific behavior exists, depending upon the nature of the adsorbate, is well illustrated, however, as is the reproducibility of results from rod to rod.

TABLE II.

Rod	Temperature of experiment °C	Adsorbate	Direction of resistance change	Maximum resistance change as percent of original resistance
5	20.0	Dimethyl ether	Increase; decreases to value above original at highest pressure	1
13	6.5	Dimethyl ether	Increase; decrease to value above original at highest pressure	0.9
6	20.0	Butane	Decrease	4
8	20.0	Butane	Decrease	3.6
9	20.0	Butane	Decrease	3.1
12	25.0	Butane	Decrease	3.8
5	20.0	Ethane	Decrease	1
5	20.0	Isobutane	Decrease	3.1
5	20.0	Sulphur dioxide	Increases to maximum then falls below original	Maximum increase 1 Maximum decrease 1.9
5	20.0	Water vapor	Decrease	4.4
8	20.0	Water vapor	Decrease	3.7
8	20.2	Ethylene oxide	Increase; very gradual fall at higher pressures	0.9
9	20.2	Ethylene oxide	Increase; very gradual fall at higher pressures	0.8
8	8.0	Butene-1	Decrease; some drift towards higher resistance	1.9
9	8.0	Butene-1	Decrease; some drift towards higher resistance	2.3
8	20.0	Methyl propene	Decrease; marked drift towards higher resistance	—
9	20.0	Methyl propene	Decrease; marked drift towards higher resistance	—
8	20.0	Helium	nil	nil
9	20.0	Helium	nil	nil
13	15.0	Helium	nil	nil
8	20.2	Carbon dioxide	Decrease	0.3
9	20.2	Carbon dioxide	Decrease	0.2
12	25.0	Ethyl chloride	Decrease; not followed to high pressures	1.2
13	20.0	Ethyl chloride	Decrease; not followed to high pressures	1.7
13	10.0	Ethyl chloride	Decrease; sharp minimum at relative pressure of about 0.2	2.6
9	10.0	Ammonia	Increase; decreases to below original on desorbing	3.1

Evidence of Reaction at the Surface

In two separate instances noted above in Table II, the resistance values were not constant with time, and in a third, depended very markedly on the previous adsorption history of the rod. Rods which had adsorbed butene-1 or methyl propene exhibited drifts in resistance, which were fairly slow, that for methyl propene being faster than for butene-1. In both cases the rate of drift was approximately proportional to the quantity adsorbed, which suggested that some reaction was occurring with the surface. These drifts were superimposed on a curve resembling one for the saturated hydrocarbons. No drifts were observed in the pressure of the gas phase, and the adsorption data conformed well with the multi-layer formula of the B.E.T. theory.[10] The possibility of a reaction with the surface is not precluded by the constant pressure values, since the sensitivity of the resistance values to the reaction may be great.

Rods exposed to ammonia showed another type of behavior. When the gas was admitted to the surface a large increase in resistance was observed, and the values appeared quite stable. On desorbing the gas, however, the resistance fell appreciably below that of the clean surface. When ammonia was again added the resistance rose sharply again, but fell below the starting value on the second desorption. Apparently this phenomenon would have continued, although an original hysteresis in the gas adsorption data had been largely eliminated.

[10] S. Brunauer, P. H. Emmett, and E. Teller, J. Am. Chem. Soc. 62, 1723 (1940).

TABLE III. Evaluation of spreading pressures at equivalent fractions of the surface covered.

Adsorbate	Rod	Temperature of experiment °C	B.E.T. constants V_m	C	Density of liquid adsorbate g/cm³	Area covered by adsorbate molecule A²	Total surface atea of rod, m²	Spreading force, erg/cm² $V_m/3$	$V_m/2$	V_m
Butane	8	20.2	336	95	0.575	33.1	3.00×10^3	7.5	13.9	42.8
Methyl propene	8	20.0	321	120	0.596	31.6	2.74×10^3	7.4	13.3	40.5
Butene-1	8	20.0	335	119	0.595	31.6	2.86×10^3	7.5	13.9	42.4
Butene-1	8	8.0	333	139	0.609	31.3	2.88×10^3	6.6	11.8	35.4
Dimethyl ether	8	20.0	421	91	0.661	25.9	2.95×10^3	8.0	14.2	41.5
Ethyl chloride	8	10.0	408	122	0.909	26.0	2.75×10^3	8.2	14.4	42.0
Butane	9	20.0	277	124	0.575	33.1	2.48×10^3	7.1	13.1	39.9
Methyl propene	9	20.0	269	152	0.596	31.6	2.30×10^3	7.3	13.1	39.7
Dimethyl ether	9	20.0	326	70	0.661	25.9	2.28×10^3	7.6	13.2	37.2
Dimethyl ether	9	10.0	294	80	0.676	25.6	2.06×10^3	7.3	12.6	35.6
Ethyl chloride	11	25.0	313	64	0.887	26.6	2.25×10^3	8.0	14.1	40.7
Dimethyl ether	11	20.0	300	67	0.661	25.9	2.10×10^3	7.7	13.6	38.5
Methyl propene	11	20.0	264	138	0.596	31.6	2.26×10^3	7.4	13.4	41.0
Butane	11	20.0	242	126	0.575	33.1	2.16×10^3	7.3	13.4	41.3
Ethyl chloride	12	25.0	448	118	0.887	26.6	3.30×10^3 or 940 m²/gm	7.5	14.2	40.6
Butane	12	20.0	382	105	0.575	33.1	3.30×10^3	7.6	14.1	43.5
Ethyl chloride	13	10.0	450	111	0.909	26.0	3.18×10^3	7.6	13.3	38.2
Dimethyl ether	13	6.5	479	104	0.681	25.3	3.29×10^3	8.4	14.9	43.4

Since the primary purpose of the investigation was to measure the effects of physical adsorption, these three substances were not investigated further. It was noted, however, that the resistances of carbons 8 and 9 after pumping 24 hr. at 130°C had increased about 0.3 percent above the starting value subsequent to the exposure to butene-1. The change after adsorption of methyl propene was not known with certainty as the air furnace reached 160°C during evacuation. With exposure to ammonia and subsequent evacuation the resistance of the clean rod was unchanged within the usual limit of less than 0.1 percent. These observations have not yet been confirmed.

Resistance Change as a Function of Amount Adsorbed

The quantity of gas adsorbed and the concomitant resistance variation were measured for four rods, and particular attention paid to the behavior with butane, ethyl chloride, dimethyl ether, and, to a lesser extent, water vapor. Typical data have been selected to illustrate the chief finding of the investigation, namely, that the resistance changes bear no simple relation to the dimensional changes of the rods or to the calculated film spreading pressures, and cannot apparently be explained from the dimensional changes or contact variations alone. The following general considerations are helpful in discussing the data.

Whenever adsorption occurs the Gibbs surface tension of the system is decreased. Following Bangham,[11] it is customary to consider that the decrease in Gibbs surface tension may be equated to the spreading pressure of the adsorbed film, that is $\sigma_0-\sigma=F$, where σ_0 is the Gibbs surface tension of the solid in vacuum, σ is the Gibbs surface tension of solid plus film, and F is the spreading pressure of the film. Furthermore, Bangham and his associates[12] have shown that the percent linear expansion of the adsorbent is proportional to the calculated spreading force of the adsorbed film, which may be deduced from the relation

$$F=\frac{RT}{\Sigma V_1}\int_0^P \frac{V}{P}dP$$

where Σ is the total surface area of the adsorbent, V_1 is the molecular volume of the gaseous adsorbate at N.T.P., V is the volume of gas adsorbed at pressure P and temperature T reduced to N.T.P., P is the equilibrium pressure in the gas phase.

The proportionality between calculated spread-

[11] D. H. Bangham, and N. Fakhoury, J. Chem. Soc. Pt. 1, 1324 (1931)

[12] D. H. Bangham, N. Fakhoury, and A. F. Mohamed, Proc. Roy. Soc. **A147**, 152 (1934).

ing pressure and percent extension is shown in the second paper, to be valid only in a limited region of the adsorption range for the rods studied here, but it is also shown that the length change of the rods is similar for all organic adsorbates. Further, the calculated spreading pressures for the various adsorbates are nearly equal at equal fractions of the surface covered (see Table III), and the length variations plotted against the calculated spreading pressures lie almost on a common line (see Fig. 3). From these observations it follows that the dimensional changes of a given conductor for different adsorbates may be taken as nearly equal at equal fractions of the surface covered. The resistance change should then be equivalent for the various adsorbates under these conditions, provided that the change is presumed to be due to the variations of the contact resistances between the carbon particles.

That this expectation is not fulfilled may be seen by comparing the data of Table IV or examining the curves of Fig. 4. In that figure curves 1 and 2 represent the resistance changes due to adsorption of butane on rods No. 9 and No. 12 plotted against the fraction of the monolayer volume which has been adsorbed. The similarity of the type of curve for different rods is here illustrated. Curve 3 represents the resistance variation of rod No. 12 with ethyl chloride. From what has been stated above curves 2 and 3 would be identical if the same dimensional change brings about the same contact variations and if these contact variations alone govern the observed alterations of resistance.

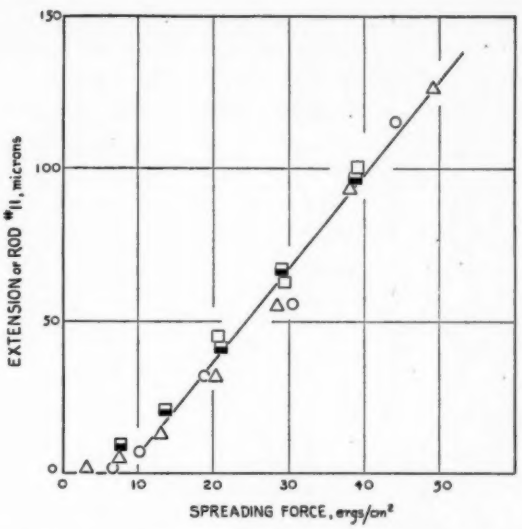

FIG. 3. Extension of rod No. 11 plotted against calculated spreading pressure for several adsorbates. Ordinate is extension in microns; abscissa is calculated spreading force in ergs/cm². ⊙ butane at 20.0°C, △ ethyl chloride at 25.0°C, ⊡ ◪ dimethyl ether at 20.0°C.

TABLE IV. Resistance changes of rods No. 9 and No. 12 with butane and ethyl chloride

Rod and adsorbate	Volume adsorbed cc at N.T.P.	P/P_0	Fraction of V_m adsorbed	Resistance change ohms
No. 9 with butane at 20.0°C	27.0	1.2×10^{-4}	.097	−.0053
P_0 = 1664 mm	60.6	5.4×10^{-4}	.218	−.0101
V_m = 277 cc	117	2.2×10^{-3}	.422	−.0167
	200	1.64×10^{-2}	.724	−.0230
	258	6.13×10^{-2}	.931	−.0250
	295	1.16×10^{-1}	1.065	−.0261
	321	1.65×10^{-1}	1.159	−.0257
	342	2.31×10^{-1}	1.235	−.0258
	233*	3.21×10^{-2}	.841	−.0238
	193*	1.29×10^{-2}	.697	−.0218
	nil*		nil	nil
	117	2.3×10^{-3}	.422	−.0159
	235	3.50×10^{-2}	.848	−.0238
	280	1.14×10^{-1}	1.011	−.0248
	318	1.69×10^{-1}	1.148	−.0257
No. 12 with butane at 20.0°C	39.8	1.32×10^{-4}	.104	−.0068
V_m = 382 cc	82.7	3.00×10^{-4}	.216	−.0148
P_0 = 1664 mm	148	1.23×10^{-3}	.388	−.0237
	229	5.67×10^{-3}	.599	−.0336
	316	2.94×10^{-2}	.827	−.0438
	417	1.24×10^{-1}	1.092	−.0449
	450	1.95×10^{-1}	1.178	−.0461
	470	2.67×10^{-1}	1.230	−.0452
No. 12 with ethyl chloride at 25.0°C	90.4	1.2×10^{-3}	.202	.0000
P_0 = 1195 mm	194	5.0×10^{-3}	.433	−.0028
V_m = 448 cc	298	1.70×10^{-2}	.665	−.0067
	392	4.35×10^{-2}	.875	−.0104
	454	8.00×10^{-2}	1.016	−.0132
	399*	4.65×10^{-2}	.890	−.0100
	334*	2.39×10^{-2}	.745	−.0068

* Desorption values.

It should also be noted, Fig. 4, for the data of butane on carbon No. 9 that no hysteresis is apparent between the adsorption and desorption points, a behavior which is not true for certain other adsorbates.

A further comparison of the same type is given in Table V and Fig. 5, where the behavior of carbon No. 13 is given for dimethyl ether and for ethyl chloride. Several curves for dimethyl ether are shown which were determined at 6.5°C, 20.0°C and 35.0°C. In the three cases an initial increase of resistance is observed, which is followed by a gradual decrease, the resistance value finally falling below the original for the two runs at 20.0°C and 35.0°C, but not for that at 6.5°C. Although the extension of the rod is marked, and may be compared with the length variation for ethyl chloride from the correlation given above, it is clear that the resistance change is appreciably different. It should also be empha-

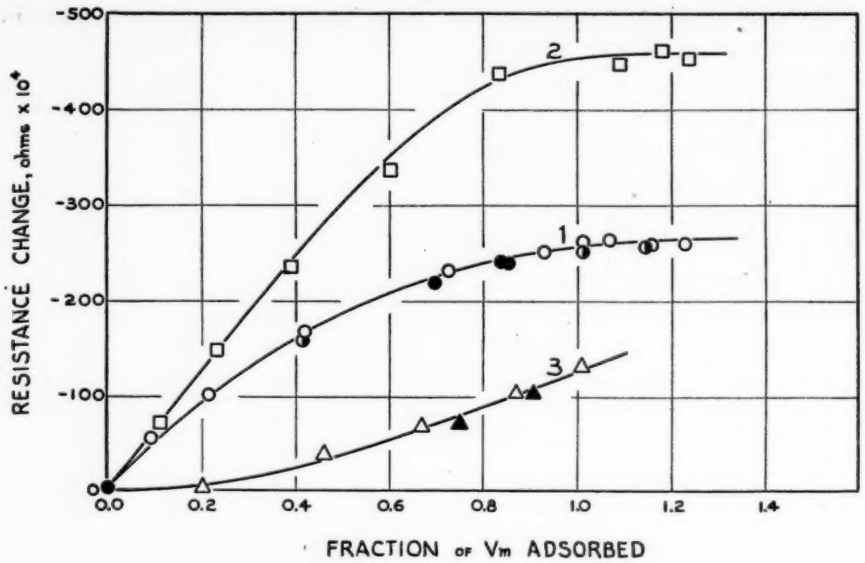

FIG. 4. Comparison of resistance changes for rods No. 9 and No. 12 caused by butane and ethyl chloride. Ordinate is—resistance change in ohms; abscissa is fraction of monolayer volume adsorbed. Curve 1—butane on carbon No. 9. Curve 2—butane on carbon No. 12. Curve 3—ethyl chloride on carbon No. 12. Solid symbols represent desorption values.

sized that a marked hysteresis of the resistance value is normally observed with dimethyl ether, but is not observed for most of the other vapors, as exemplified by carbon No. 9 with butane. No difference in length was found on desorption which was sufficiently greater than experimental error to be significant, and this finding was general for all the vapors studied. The hysteresis also did not appear to be due to chemi-sorption, since the resistance returned to its original value with prolonged pumping at room temperature (72 hr.) or about 24 hours at the standard temperature of 120°C. A third point of interest in dealing with the extensions as the governing factor in the observed resistance changes is the region where resistance does not vary appreciably with the amount of gas adsorbed. Regions where this is true are shown for butane and dimethyl ether in the Figs. 4 and 5 already referred to. It is in this region of amount adsorbed where the extension of the rod becomes very marked, and to account for the constant resistance values at least two compensating effects must be assumed if the extension of the rod is supposed to cause any alteration in its resistance. Evidence suggesting compensating effects is the curve for ethyl chloride (Fig. 5) for which the widest range of adsorption condition was studied. Here the sharp maximum in the extent of the resistance effect would indicate that more than one factor is involved.

The most striking evidence in support of the finding that extension of the conductor is of secondary importance in the resistance changes is illustrated in Fig. 6. A comparison is there represented between the resistance effect, the

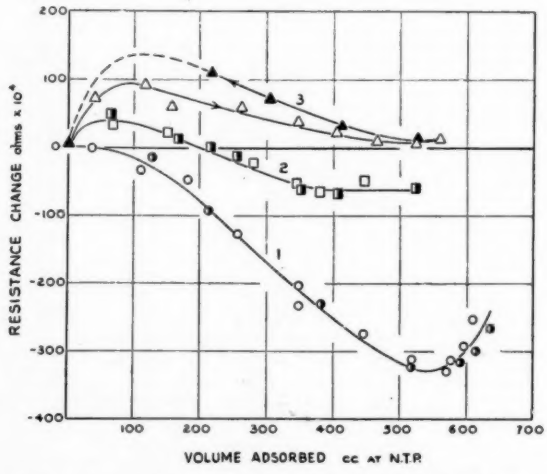

FIG. 5. Comparison of resistance changes of rod No. 13 caused by dimethyl ether and ethyl chloride. Ordinate is resistance change in ohms; abscissa is volume adsorbed in cc reduced to N.T.P. Curve 1—ethyl chloride at 10.0°C; curve 2—dimethyl ether at 20.0°C ⊡ and at 35.0°C ◨. Curve 3—dimethyl ether at 6.5°C.

adsorption isotherm, and the dimensional change of activated carbon when exposed to water vapor. The resistance data were obtained with carbon No. 8 (see Table VI), the extension data with carbon No. 11 (see second paper) and the isotherm was taken from a publication by Morrison and McIntosh[13] for a zinc chloride activated carbon. (It is typical of many adsorption isotherms for water which have been published.) The resemblance between the resistance effect and the adsorption isotherm is clear, and the importance of this similarity is emphasized in view of the contraction of the rod below its original length when water was desorbed. From these particular data it would appear that the resistance effect is determined only by the amount of material adsorbed, and is independent of the relative positions of the crystallites as determined by the film pressures which have been established.

TABLE V. Resistance variations of carbon No. 13 with dimethyl ether and ethyl chloride.

Temperature and adsorbate	P/P_0	Volume adsorbed cc at N.T.P.	Resistance change ohms
Dimethyl ether; 6.5°C	2.5×10^{-4}	41.4	+.0072
P_0 = 2424 mm	1.2×10^{-3}	113	+.0093
	3.22×10^{-3}	157	+.0060
	1.05×10^{-2}	260	+.0060
	2.56×10^{-2}	345	+.0038
	4.80×10^{-2}	402	+.0021
	8.62×10^{-2}	462	+.0008
	1.44×10^{-1}	521	+.0007
	1.83×10^{-1}	559	+.0014
	1.43×10^{-1}	522*	+.0010
	5.00×10^{-2}	410*	+.0030
	1.68×10^{-2}	304*	+.0070
	6.20×10^{-3}	216*	+.0110
Pumped 72 hr. at R. T.		nil	+.0002
Dimethyl ether; 35.0°C	9.5×10^{-4}	66.8	+.0033
P_0 = 5760 mm	4.51×10^{-3}	150	+.0021
	1.00×10^{-2}	211	+.0001
	2.11×10^{-2}	280	−.0022
	3.91×10^{-2}	343	−.0051
	5.68×10^{-2}	378	−.0063
	9.81×10^{-2}	447	−.0049
Dimethyl ether; 20.0°C	6.32×10^{-4}	63.0	+.0046
P_0 = 3762 mm	4.60×10^{-3}	165	+.0012
	1.35×10^{-2}	257	−.0012
	4.52×10^{-2}	355	−.0060
	7.37×10^{-2}	405	−.0068
	1.84×10^{-1}	521	−.0059
Ethyl chloride; 10.0°C		34.1	.0000
P_0 = 691 mm	1.1×10^{-3}	107	−.0031
	4.2×10^{-3}	181	−.0048
	9.7×10^{-3}	254	−.0128
	2.54×10^{-2}	348	−.0204
	7.01×10^{-2}	442	−.0273
	1.36×10^{-1}	515	−.0312
	2.42×10^{-1}	575	−.0316
	3.68×10^{-1}	595	−.0292
	6.74×10^{-1}	609	−.0253
Ethyl chloride; 10.0°C	1.4×10^{-3}	125	−.0014
P_0 = 691 mm	4.7×10^{-3}	211	−.0094
	3.68×10^{-2}	380	−.0230
	1.32×10^{-1}	512	−.0323
	2.77×10^{-1}	587	−.0314
	4.42×10^{-1}	606	−.0300
	7.51×10^{-1}	634	−.0267
	4.14×10^{-1}	613*	−.0300
	2.04×10^{-1}	568*	−.0330
	2.60×10^{-2}	344*	−.0232

* Desorption values.

[13] J. A. Morrison, and R. McIntosh, Can. J. Research **B24**, 137 (1946).

Estimate of the Total Surface Area by the B.E.T. Method

Since an evaluation of the monolayer capacity of the rods was possible from the adsorption data, and since a correlation between the constant portion of the resistance curve and the monolayer capacity V_m would have appeared suggestive, the value of V_m was obtained after the method of Brunauer, Emmett, and Teller.[10] Both the monolayer and multilayer equations were tested. The monolayer equation was not suitable for any of the adsorbates, while the multilayer equation gave excellent straight lines

TABLE VI. Resistance change for water vapor on carbon No. 8. Temperature = 20.2°C. Original rod resistance = 0.6376 ohm.

Percent relative humidity		Resistance change ohms	
96.0		−.0255	Adsorption
100		−.0244	
79.1		−.0242	Desorption
61.9		−.0231	
57.9		−.0230	
53.8		−.0277	
	Pumped 48 hr. at 20.2°C		
nil		−.0003	
44.7		−.0030	Adsorption
52.1		−.0048	
54.9		−.0052	
59.5		−.0070	
67.8		−.0124	
79.6		−.0204	
	Pumped 24 hr. at 20.2°C		
nil		+.0001	Desorption
86.9		−.0244	Adsorption
100		−.0246	
49.0		−.0215	Desorption
44.9		−.0195	
38.5		−.0141	
36.2		−.0090	
	Pumped 24 hr. at 20.2°C		
nil		.0000	
36.0		−.0007	Adsorption
61.0		−.0067	
78.6		−.0210	
95.5		−.0236	
100		−.0234	Desorption
39.6		−.0121	
35.8		−.0044	
	Pumped 24 hr. at 20.2°C		
nil		−.0005	

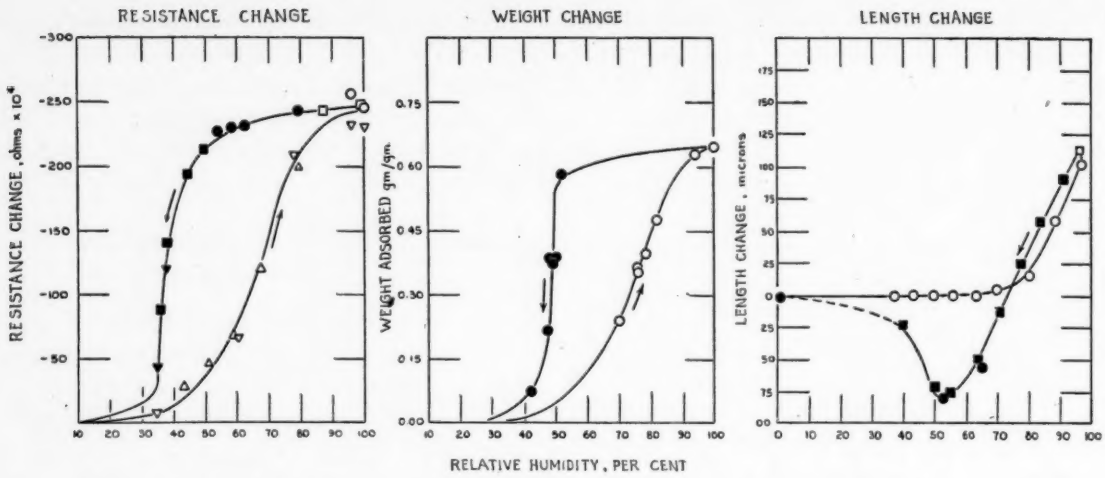

FIG. 6. Comparison of resistance, weight, and length changes of activated carbon caused by water vapor. Ordinates are, respectively: resistance change in ohms $\times 10^4$, weight change in g/gm, and length change in microns. Abscissae are percent relative humidity.

between relative pressures of 1×10^{-2} and about 0.25. The total surface areas are not expressed in terms of area per g of carbon, since the carbon assemblies would have had to be destroyed. This was done, however, for carbon No. 12, and a value of 940 m^2/g was obtained, which is the order of magnitude to be expected for a fairly highly activated carbon. The surface area data, along with calculated spreading pressures at various degrees of saturation of the surface are given in Table III.

As is generally observed, the initial adsorption points of the B.E.T. plots fell below the line, a behavior attributed by Brunauer[14] to the fact that the E_1 value is greater than the average value of E_1 for the surface up to that degree of saturation of the surface. The usual criterion of the applicability of the B.E.T. theory is met, namely that the total surface area values measured with different adsorbates should be the same. The values of Σ for each rod, estimated on the usual assumptions[15] agree within ±5 percent. Ethylene oxide, however, although it did not show any evidence of chemi-sorption, did not conform with either the mono- or multilayer equations, and the surface area was not evaluated with it. These anomalous adsorption data are recorded in Table VII along with resistance changes.

Since the multilayer formula expressed the results satisfactory (although a better procedure would have been to employ the "n" equation in the manner developed by Joyner and others[16]), and since the total amount of gas adsorbed at the highest relative pressure was not much greater than that required to complete a monolayer, it appears that the first layer was not complete even at the highest relative pressures studied. This emphasizes again the somewhat unexpected form of the adsorption layers deduced from the B.E.T. theory, as pointed out by Gregg[17] and more recently by Hill.[18] Since the first layer is not complete it follows that the region where no further resistance change is observed cannot be due to the formation of a complete monolayer. It might signify, however, that further adsorption occurs only in the second and higher layers. However, in the one case where a relative pressure of 0.8 was achieved, that of ethyl chloride, it has been pointed out that a reversal of the direction of resistance change followed the constant portion of the curve. Thus the constant region appears to be the result of compensating factors, and no correlation of this region with V_m would be necessary.

[14] See reference 6, page 158.
[15] P. H. Emmett, and S. Brunauer, J. Am. Chem. Soc. **59**, 1553 (1937).
[16] L. G. Joyner, E. B. Weinberger, and C. N. Montgomery, J. Am. Chem. Soc. **67**, 2182 (1945).
[17] S. J. Gregg, *The Ultra-Fine Structure of Coals and Cokes* (B. C. U. R. A., London, 1944), p. 110.
[18] T. L. Hill, J. Chem. Phys. **14**, 268 (1946).

GENERAL DISCUSSION

It appears from the evidence given above that the contact resistance between the carbon aggregates is not sufficient to explain the resistance changes which were observed. It should also be noted that the resistance decreases for the majority of vapors, which is in agreement with the finding of Schwab and Karkalos,[2] but differs from the observations of Siebel[1] and Sandor.[3] If, in the case of activated carbon, it is assumed that the governing factor in the resistance change is a surface effect, due to the very large surface to volume ratio of the conductor, and to the presence of the adsorbate in the surface region, there are three possibilities to be considered. These are: (1) the conductivity of the adsorbate is responsible for the effect; (2) the adsorbate influences the conductivity of the adsorbent; (3) both factors are involved.

The conductivities of the adsorbates in the bulk state are very much smaller than that of carbon, so that unless properties are attributed to them when adsorbed on a surface which are quite different from the normal, no appreciable resistance change would be observed. Further, no increase in resistance could be brought about unless the adsorbate had influenced the conductor itself, or unless a dimensional change of the conductor is specifically assumed to account for increases in resistance. Increases in resistance would be readily explained, however, by the establishment of "mirror image" forces between the adsorbate and the somewhat metallic surface. A decrease in resistance due to the influence of the adsorbate at the surface would require either an increased mobility or an increased number of conducting electrons in the adsorbent. Without more knowledge of the conducting mechanism of semi-conductors, further discussion of the results is not warranted. It appears, however, that the existence of an effect which cannot be explained by mechanical factors in the conductor has been definitely established.

TABLE VII. Adsorption and resistance data for ethylene oxide on carbons No. 8 and No. 9 at 20.2°C. $P_0 = 1070$ mm

Rod	Pressure, mm of Hg	Volume adsorbed cc at N.T.P.	Resistance change ohms
8	1.0	22.3	+.0007
	2.4	43.3	+.0017
	4.2	63.5	+.0020
	8.5	106	+.0034
	16.4	158	+.0040
	31.5	234	+.0048
	61.5	343	+.0041
	103	434	+.0045
	163	527	+.0049
	204	580	+.0050
	220	605	+.0055
9	0.5	19	+.0024
	1.5	34.8	+.0035
	4.1	57.9	+.0049
	7.0	81.0	+.0067
	10.0	103	+.0068
	21.0	161	+.0086
	59.2	288	+.0087
	107	389	+.0071
	165	533	+.0065
	232	610	+.0062

ACKNOWLEDGMENT

It is a pleasure for one of us (R. M.) to acknowledge the assistance of N. R. S. Hollies, graduate student in Chemistry, McGill University, Montreal, in carrying out certain of the preliminary experiments.

THE JOURNAL OF CHEMICAL PHYSICS VOLUME 15, NUMBER 1 JANUARY, 1947

Length Changes of Activated Carbon Rods Caused by Adsorption of Vapors*

R. S. HAINES AND R. MCINTOSH
Division of Chemistry, National Research Laboratories, Ottawa, Canada

(Received October 1, 1946)

The length variations of two zinc chloride activated carbon rods caused by the adsorption of several vapors are reported. The relationship between percent extension of the rod and calculated spreading pressure of the adsorbed film suggested by Bangham has been tested. The relation agrees well with experiment for organic vapors above about $\frac{1}{3}$ saturation of the monolayer capacity. It does not agree in the low adsorption region nor along the desorption branch of the water isotherm. A marked contraction of the rod below its original length has been noted when water is desorbed, and this contraction may be considered as a proof of the establishment of concave menisci in the capillaries along the desorption branch.

INTRODUCTION

THIS investigation of the length changes of activated carbon rods brought about by adsorption was carried out in an attempt to determine whether a correlation between the electrical resistance variation[1] and the length variation might be made. It was thought that resistance changes might be governed by the dimensional changes altering the contact resistance between the conducting carbon particles. No simple correlation was observed, but several interesting points concerning the dimensional changes themselves were found and are presented here.

Experiments on the expansion of charcoal due to the adsorption of vapors have been performed by Meehan,[2] Bangham and his associates,[3–6] and by McBain.[7] Meehan[2] used an optical extensometer consisting of a light beam focused on a small pivoted mirror which rested on the charcoal rod. He showed that the expansion of carbonized charcoal was isotropic, and that at constant pressure of the gas phase expansion varies with temperature. Bangham[3–6] used a mechanical gain extensometer to determine the behavior of unactivated charcoal rods when such vapors as the lower alcohols, benzene, pyridene, and water were adsorbed. He found the percent linear expansion X of the rods to be a linear function of the film spreading pressure F over a large part of the adsorption range.[4,5] For organic vapors at low adsorption pressures an expansion followed by a slow contraction was observed, the over-all process being an expansion.[5] The large initial expansion was attributed to the formation of an unstable primary film, and the contraction to the conversion of this film to a stable form. McBain[7] used a modified type of optical extensometer and measured the linear expansion of activated charcoal when benzene, heptane, and water vapor were adsorbed. No evidence of an unstable primary film was obtained in his work.

In the experiments reported here an initial contraction in length of the activated charcoal rod was obtained when vapors were adsorbed on it. Since the spreading force F is considered to be positive whenever adsorption occurs when the Gibbs adsorption equation is employed in the form of Eq. (6) below, the relation, X is proportional to F, does not hold in the initial adsorption region. On further adsorption expansion of the rod occurred, and this expansion was found to be approximately proportional to the calculated spreading force evaluated from the equation

$$F=\frac{RT}{\Sigma V_1}\left[V+\frac{BV^2}{2}\right]_0^V, \qquad (1)$$

where Σ is the total surface area of the rod, V_1 is

* Contribution No. 1446 from the National Research Laboratories, Ottawa, Canada.

[1] R. McIntosh, R. S. Haines, and G. C. Benson, J. Chem. Phys. **15**, 17 (1947).

[2] F. T. Meehan, Proc. Roy. Soc. **A115**, 199 (1927).

[3] D. H. Bangham and N. Fakhoury, Proc. Roy. Soc. **A130**, 81 (1930).

[4] D. H. Bangham, N. Fakhoury, and A. F. Mohamed, Proc. Roy. Soc. **A138**, 162 (1932).

[5] D. H. Bangham, N. Fakhoury, and A. F. Mohamed, Proc. Roy. Soc. **A147**, 152 (1934); **A147**, 175 (1934).

[6] D. H. Bangham and R. I. Razouk, Proc. Roy. Soc. **A166**, 572 (1938).

[7] J. W. McBain, J. L. Porter, and R. F. Sessions, J. Am. Chem. Soc. **55**, 2294 (1933).

the molar volume of the adsorbate at N.T.P., V is the amount of material adsorbed expressed in cc of gas at N.T.P., and B is an empirical constant whose significance is made clear below. The expansion was also found to be nearly independent of the nature of the adsorbate. No hysteresis of a significant magnitude was found on desorbing the vapors.

In the case of water vapor, however, the adsorption and desorption values of the dimensional changes were very different. Most noteworthy was the large contraction of the rod below its original value as the relative humidity was lowered, a phenomenon which supports the view presented by Morrison and McIntosh[8] concerning the difference in apparent density of adsorbed water along the adsorption and desorption isotherms

APPARATUS AND MATERIALS

The vacuum system, adsorption apparatus, thermostats, preparation, and evacuation of the rods and the purity of the vapors employed have been discussed previously in the first paper.[1] Since an optical type of extensometer would present certain experimental difficulties attributed to the transmission of the light beam through the thermostats, and since the mechanical gain type of instrument employed by Bangham required at least one spring to hold the pointer, and this might apply a compressional force to the rod, a somewhat different form of extensometer was developed. In this instrument the change in length of the carbon was observed through the change in capacitance of a condenser.

The extensometer proper consisted of an electrical condenser, the movable plate of which was attached to one end of the charcoal rod. A somewhat similar arrangement has been described by Schulze and Zickner.[9] Two such extensometers of slightly different form were used and are denoted as the parallel plate condenser and the double leaf condenser.

Parallel Plate Condenser

The parallel plate condenser is shown in Fig. 1. The movable plate was attached to one end of the charcoal rod through a universal joint and clamp. A guide rod that moved through the precision machined collars at each end of the guide cylinder was attached to the back of the movable plate. This guide mechanism made certain that the movable plate traveled parallel to the fixed plate with a minimum of friction. The other end of the charcoal rod was held in a clamp screwed to a stationary plate. The guide cylinder, fixed condenser plate, and stationary plate were fastened by collars with set screws to four quartz rods that formed the frame. The guide cylinder and fixed plate could be further adjusted during assembly by threaded collars which moved over the collars fastened to the quartz rods. The condenser assembly was suspended in the housing by Pyrex glass cylinders placed over the guide cylinder at one end and the stationary plate at the other end. The instrument was always used in the horizontal position shown in the diagram. All metal parts were machined from duraluminum 17S-T, except the brass pins used in the universal joint.

Calibration of this condenser was carried out in the following manner. The clamp holding the charcoal rod at the stationary plate was loosened, thus permitting the condenser plate to be moved. The distance between the movable and fixed plates was determined at a number of positions

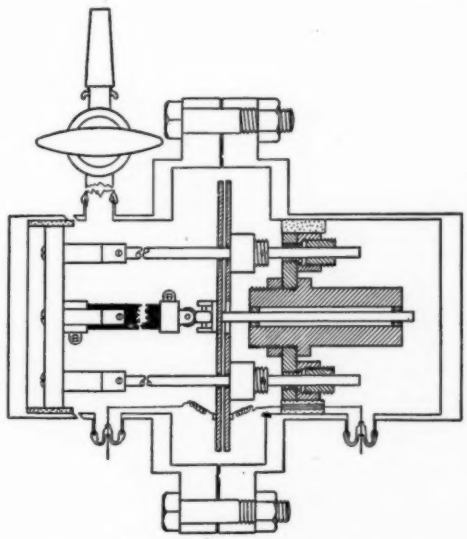

FIG. 1. Parallel plate condenser. Quartz rod out from plane of paper removed, circular condenser plates and guide mechanism sectioned, glass insulators dotted, and metal glass housing shown in outline.

[8] J. A. Morrison and R. McIntosh, Can. J. Research **B24**, 137 (1946).

[9] A. Schulze and G. Zickner, Arch. f. Elecktrotechnik **24**, 111 (1930).

by means of a Gaertner traveling microscope reading in microns. The capacitance values at these positions were also measured. When a plot of capacitance multiplied by distance between the plates against distance between the plates was made, a straight line was obtained over the range employed. Thus capacitance values were converted into values of the distance between the plates, and from these into variations in the length of the carbon rod.

The vacuum jacket was made in two pieces with an inch flange on each section. One flange had a V-shaped groove into which the corresponding ridge of the other flange squeezed an annealed iron gasket when the two sections were bolted together with twelve $\frac{3}{8}''$ bolts. The jacket was made from copper tubing and plate, silver soldered together, except for the flange which was made of machined rolled steel and copper plated. The two fine copper leads from the condenser were brought through the jacket wall by using commercially manufactured copper Nonex seals with tungsten sealed through the glass. A similar copper Nonex seal was used to make the connection between the metal jacket and the glass adsorption system.

Double Leaf Condenser

The double leaf condenser is shown in Fig. 2. In this arrangement the movable set of plates

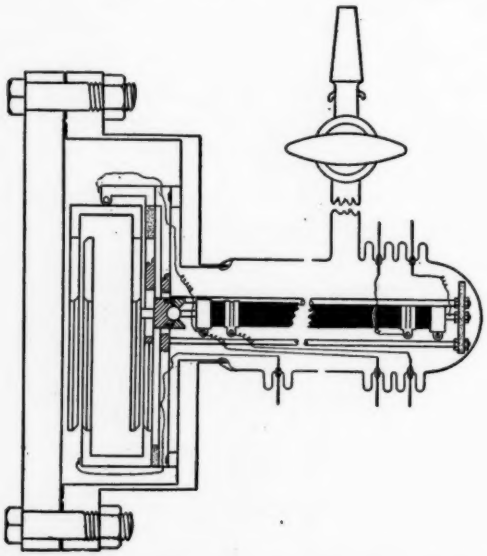

FIG. 2. Double leaf condenser. Ball and socket joint sectioned, mykroy insulator dotted, and glass metal housing shown in outline.

was pivoted from a precision hinge which was insulated from the stationary set by a mykroy insulator. The charcoal rod was connected with one of the movable plates by a precision built ball and socket joint (with no pressure on the ball), and by a clamp. The other end of the charcoal rod was held in a clamp passing through a mykroy disk. The mykroy disk and support of the condenser were held together by three invar rods, insulated with glass sleeves. These invar rods formed the frame.

This condenser was arranged for calibration by attaching a metal strip to the mykroy disk and another to the clamp holding the charcoal rod. By adjusting the nuts on the screw passing through the mykroy disk, when the charcoal rod was in position, the capacitance of the condenser was varied. For each capacitance value the distance between the two attached metal strips was noted with the Gaertner traveling microscope. The logarithm of the capacitance was plotted against the change in length of the set screw, and this plot was used to obtain the change of length of the rod from capacitance values during the adsorption experiments.

As it was also desired to follow the electrical resistance changes with the same assembly, two special type spring clamps, separated from the charcoal by a strip of platinum, were attached to the rod. To make connections for passing the current through the rod one fine copper wire was silver soldered to the end of the set screw passing through the mykroy disk, and another fine copper wire, closely coiled to prevent it applying tension to the rod, was connected from the clamp on the charcoal rod at the ball and socket end to the low potential side of the condenser. The measurement of resistance was carried out exactly as described previously.[1]

The containing jacket consisted of a Nonex glass section and a metal section that housed the condenser. The two sections were connected through a $1\frac{1}{4}''$ copper Nonex seal. The five fine copper electrical leads passed out through tungsten seals in the Nonex glass, and the glass connection to the adsorption system was also attached to the Nonex glass. The condenser assembly was held in position in the metal section by four set screws from the condenser support to the housing wall. The jacket was sealed with

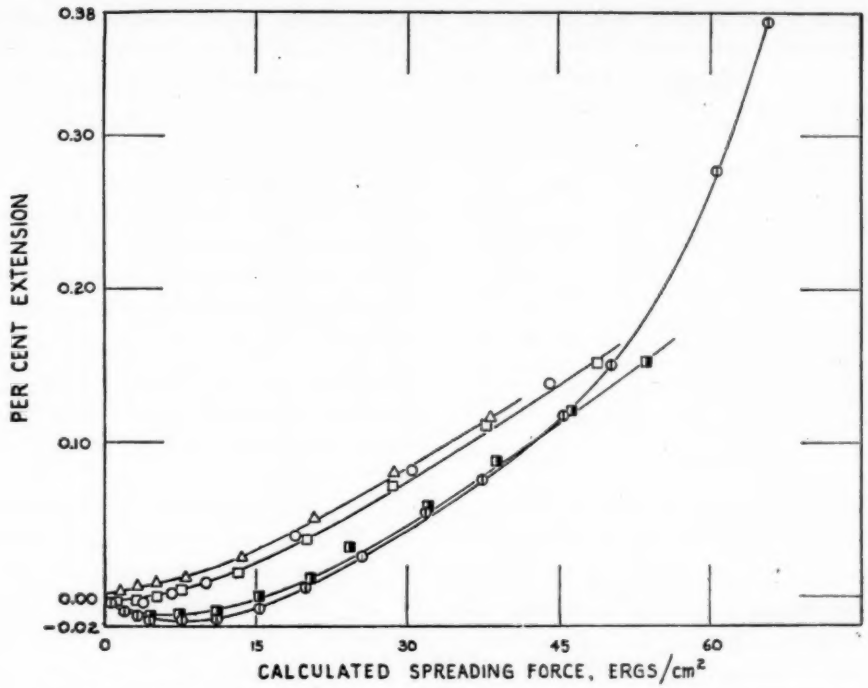

FIG. 3. Length changes of rods No. 11 and No. 13. Ordinate percent extension; abscissa calculated spreading force, ergs/cm².

⊙ Butane on No. 11 at 20.0°C.
△ Dimethyl ether on No. 11 at 25.0°C.
⊡ Ethyl chloride on No. 11 at 25.0°C.
◑ Ethyl chloride on No. 13 at 10.0°C.
◨ Dimethyl ether on No. 13 at 6.5°C.

TABLE I. Comparison of data obtained with two types of extensometer.

Volume of vapor adsorbed cc*	Charcoal rod No. 11 Butane at 20.0°C % length change of rod	Force ergs/cm²	Dimethyl ether at 20.0°C % length change of rod	Force ergs/cm²	Ethyl chloride at 25.0°C % length change of rod	Force ergs/cm²	Charcoal rod No. 13 Ethyl chloride at 10.0°C % length change of rod	Force ergs/cm²	Dimethyl ether at 6.5°C % length change of rod	Force ergs/cm²
25	−0.0036	1.58	+0.0024	1.49	−0.0018	1.39	−0.0053	0.89	−0.0044	0.86
50	−0.0036	3.78	+0.0054	3.29	−0.0024	3.10	−0.0106	1.94	−0.0088	1.89
75	+0.0012	6.61	+0.0072	5.15	.0000	5.13	−0.0133	3.12	−0.0098	3.06
100	+0.0084	10.1	+0.0121	7.80	+0.0048	7.52	−0.0155	4.46	−0.0115	4.37
150	+0.0386	18.8	+0.0253	13.6	+0.0157	13.2	−0.0173	7.56	−0.0124	7.45
200	+0.0807	30.4	+0.0506	20.6	+0.0373	20.2	−0.0159	11.2	−0.0106	11.2
250	+0.139	44.1	+0.0807	28.8	+0.0724	28.5	−0.0088	15.5	−0.0018	15.5
300			+0.116	38.3	+0.112	38.0	+0.0053	20.3	+0.0106	20.4
350					+0.152	48.9	+0.0248	25.5	+0.0319	24.6
400							+0.0531	31.8	+0.0593	32.0
450							+0.0752	37.3	+0.0885	38.6
500							+0.118	45.5	+0.121	46.2
550							+0.151	49.8	+0.154	53.9
600							+0.279	60.5		
624							+0.367	65.8		

*A common set of volume values was chosen and the spreading forces evaluated for these quantities. The length changes were read from the smoothed curves at the corresponding volume values.

a bolted flange and gasket as described for the parallel plate assembly.

For both condenser assemblies experimentally determined corrections were made to the capacitance readings for the capacitance of the jacket, for the leads to the bridge, and for the effect of the vapors between the plates during adsorption. The parallel plate condenser gave an increase in

TABLE II. Data illustrating reversibility of length changes.

Rod	Adsorbate and temperature, °C	Amount adsorbed cc at N.T.P.	Length increment, microns Adsorption	Desorption
11	Ethyl chloride at 25.0°C	234	53	55
11	Ethyl chloride at 25.0°C	348	124	127
11	Butane at 20.0°C	178	50	55
11	Dimethyl ether at 20.0°C	256	68	66
13	Dimethyl ether at 6.5°C	410	76	77
13	Ethyl chloride at 10.0°C	344	33	32
13	Ethyl chloride at 10.0°C	568	205	203

capacitance for an extension of the rod and was thus more sensitive after the rod had extended and the plates were closer together. The sensitivity of this condenser at its initial setting was 0.18 mmf per micron. The double leaf condenser gave a decrease in capacitance as the rod extended, and thus had its greatest sensitivity at the lowest adsorption points. Its initial setting gave a sensitivity of 1 mmf per micron.

Bridge System

The capacitance readings were measured with a Schering bridge constructed for the experimentation. The bridge was fed by an oscillating source of 1000 cycles at 80 volts through a coupling transformer. The detector was a cathode-ray oscillograph connected with the bridge through a coupling transformer, and thus amplifying the signal 4000 times. The bridge was grounded so that one of the leads going to the measuring condenser and the metal housing of the condenser were at ground potential. The bridge was sensitive to a change of 0.05 mmf and gave with some certainty changes of 0.15 mmf. Thus the bridge detected a change of 1 micron at the initial setting of the parallel plate condenser and a change of 0.2 micron at the initial setting of the double leaf condenser.

RESULTS

Whenever vapor was admitted to the evacuated charcoal assembly an immediate expansion of the rod was registered. The expansion was closely followed by a slow contraction but steady values of the length were established well under the 2–3 hours allowed for adsorption equilibrium. The instantaneous expansion, which was observed until about half the calculated monolayer capacity had been adsorbed, was attributed to the increased temperature of the rod brought about by the exothermic adsorption process. Such an increase in temperature has been observed experimentally by Sandor,[10] who placed a thermocouple near the carbonized coal samples which he studied. In this work no evidence suggesting an unstable primary film such as Bangham obtained was found; however the evidence may have been obscured by the large thermal effect.

The first adsorption runs were made with rod No. 11 using the parallel plate condenser. With this carbon and extensometer a net contraction of the rod was observed with butane, methyl propene, and ethyl chloride until about $\frac{1}{3}$ of the monolayer capacity had been adsorbed. On studying the effect of dimethyl ether, however, an expansion of the rod was obtained all along the adsorption curve. In order to study the initial region of adsorption with greater precision, the double leaf condenser was constructed and measurements made with it on a longer carbon (No. 13), using dimethyl ether and ethyl chloride. With this assembly dimethyl ether also showed an initial net contraction of the rod up to about $\frac{1}{3}$ the monolayer capacity. Typical data are given in Table I and Fig. 3 which show the contraction and the subsequent extension of both rods as the amount adsorbed is increased. No desorption points have been included here as the data have been compiled by interpolation of the curves. It is important to emphasize, however, that the length changes for these vapors were reversed as the gas was desorbed. Where it was possible to measure the gas desorbed, the length values corresponded well with the adsorption length values considering that errors in determining the amount of material adsorbed are cumulative. Examples of this correspondence are given in Table II. Although it was not possible to measure the quantities of gas retained on the carbon as the minimum of the extension *vs.* amount adsorbed curve was approached, it was clearly

[10] J. Sandor, *The Ultra-fine Structure of Coals and Cokes* (B.C.U.R.A., London, 1944), p. 347.

TABLE III. Typical data used to test Williams-Henry equation.

	Dimethyl ether rod No. 13 at 6.5°C		Dimethyl ether rod No. 11 at 20.0°C		Butane rod No. 11 at 20.0°C		Ethyl chloride rod No. 11 at 25.0°C		Methyl propene rod No. 11 at 20.0°C	
	V in cc at N.T.P.	V/P cc/cm	V cc at N.T.P.	V/P cc/cm	V cc at N.T.P.	V/P cc/cm	V cc at N.T.P.	V/P cc/cm	V cc at N.T.P.	V/P cc/cm
Adsorption	113	377	44.4	88.9	42.9	858	46.9	390	63.1	451
	157	200	99.8	58.6	123	191	99.6	192	122	204
	260	102	142	37.5	185	53	176	87.3	187	63.1
	345	55.6	177	26.9	216	30.6	236	48.0	223	32.9
	402	34.6	213	19.0	233	20.6	284	30.1	235	22.0
	462	22.1	265	11.9	255	14.1	307	24.5	258	17.9
	521	14.9	300	8.8	271	11.4	348	17.7	271	15.2
	559	12.6	337	6.5			378	14.5	280	12.6
									293	11.3
									307	10.8
Desorption	522	15.0	256	14.6	173	60.8	348	17.9		
	477	20.3	184	28.8			234	46.9		
	410	34.0	137	45.7						
	304	74.9								
	216	143								

TABLE IV. Typical data used to test B.E.T. multiplayer formula.

Dimethyl ether rod No. 13 at 6.5°C		Dimethyl ether rod No. 11 at 20.0°C		Butane rod No. 11 at 20.0°C		Ethyl chloride rod No. 11 at 25.0°C		Methyl propene rod No. 11 at 20.0°C		
P/P_0	$\frac{P}{V(P_0-P)}$ cc^{-1}	P/P_0	$\frac{P}{V(P_0-P)}$ cc^{-1}	P/P_0	$\frac{P}{V(P_0-P)}$ cc^{-1}	P/P_0	$\frac{P}{V(P_0-P)}$ cc^{-1}	P/P_0	$\frac{P}{V(P_0-P)}$ cc^{-1}	
1.24×10^{-3}	1.10×10^{-5}	1.33×10^{-3}	3.0×10^{-5}	3.00×10^{-4}	7.01×10^{-5}	1.00×10^{-3}	2.15×10^{-5}	7.34×10^{-4}	1.14×10^{-5}	Adsorption
3.22×10^{-3}	2.06×10^{-5}	4.52×10^{-3}	4.56×10^{-5}	3.84×10^{-3}	3.14×10^{-5}	4.37×10^{-3}	4.41×10^{-5}	3.16×10^{-3}	2.59×10^{-5}	
1.05×10^{-2}	4.06×10^{-5}	1.00×10^{-2}	7.13×10^{-5}	2.10×10^{-3}	1.16×10^{-4}	1.70×10^{-2}	9.78×10^{-5}	1.57×10^{-3}	8.49×10^{-5}	
2.56×10^{-3}	7.60×10^{-5}	1.74×10^{-2}	1.01×10^{-4}	4.38×10^{-3}	2.12×10^{-4}	4.14×10^{-2}	1.83×10^{-4}	3.57×10^{-2}	1.66×10^{-4}	
4.80×10^{-3}	1.24×10^{-4}	2.98×10^{-2}	1.44×10^{-4}	6.79×10^{-3}	3.12×10^{-4}	7.94×10^{-3}	3.03×10^{-4}	5.64×10^{-2}	2.54×10^{-4}	
8.62×10^{-3}	2.05×10^{-4}	5.93×10^{-2}	2.39×10^{-4}	1.09×10^{-1}	4.79×10^{-4}	1.05×10^{-1}	3.84×10^{-4}	7.62×10^{-2}	3.20×10^{-4}	
1.44×10^{-1}	3.20×10^{-4}	9.11×10^{-2}	3.35×10^{-4}	1.42×10^{-1}	6.10×10^{-4}	1.65×10^{-1}	5.66×10^{-4}	9.42×10^{-2}	3.84×10^{-4}	
1.83×10^{-1}	4.00×10^{-4}	1.34×10^{-1}	4.59×10^{-4}			2.19×10^{-1}	7.42×10^{-4}	1.17×10^{-1}	4.72×10^{-4}	
								1.37×10^{-1}	5.40×10^{-4}	
								1.50×10^{-1}	5.74×10^{-4}	
1.43×10^{-1}	3.19×10^{-4}	4.65×10^{-2}	1.90×10^{-4}	1.72×10^{-2}	1.01×10^{-4}	1.63×10^{-1}	5.59×10^{-4}			Desorption
9.72×10^{-2}	2.25×10^{-4}	1.69×10^{-2}	9.32×10^{-5}			4.20×10^{-2}	1.86×10^{-4}			
5.00×10^{-3}	1.41×10^{-4}									
1.68×10^{-2}	5.61×10^{-4}									

shown that the rod passed through this region along the desorption branch by pumping off the adsorbate slowly, and allowing the system to stand with the pump turned off when the capacitance readings indicated that this region had been entered. Thus the contraction region must be considered as representing an equilibrium state of the system.

It is necessary at this point to consider whether unexpected experimental errors could cause the differences observed with dimethyl ether for carbons No. 11 and No. 13, and whether the contraction of the rod is real or apparent. The two rods, may, of course, have been somewhat different in structure, as pointed out in dealing with the resistance determinations,[1] and this might account for the different behavior with dimethyl ether. A more likely explanation appears to be that the difference was caused by friction in the parallel plate assembly since the contraction of the rod when exposed to the other vapors was less and since the thermal effect noted above took appreciably longer to disappear than in the double leaf assembly.

The contraction of the rod appears to be real. A possible source of error such as an apparent change of capacitance due to the adsorption of vapors on the plates does not appear likely in view of the tests made with a fixed plate condenser when the effect of the dielectric constant of the vapors was determined. In the low relative pressure region any correction for the effect of the vapor was negligible.

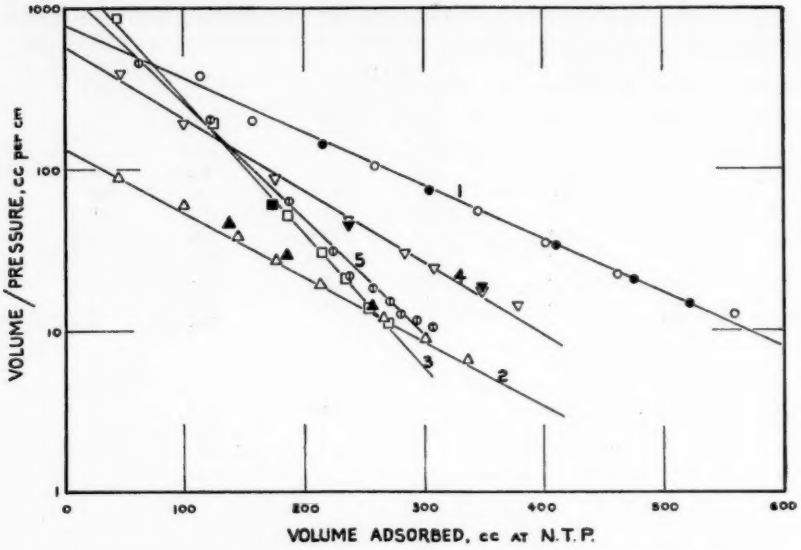

FIG. 4. Williams-Henry plot of adsorption data. Ordinate volume/pressure, cc at N.T.P. per cm of Hg. Abscissa volume absorbed, cc at N.T.P.

1. Dimethyl ether on No. 13 at 6.5°C.
2. Dimethyl ether on No. 11 at 20.0°C.
3. Butane on No. 11 at 20.0°C.
4. Ethyl chloride on No. 11 at 25.0°C.
5. Methyl propene on No. 11 at 20.0°C.

Solid symbols represent desorption values.

Estimation of Film Spreading Pressure from the Adsorption Data

In order to test the relationship $X=\lambda F$ proposed by Bangham and to compare extensions caused by different adsorbates, the relation

$$\sigma_0-\sigma=F=\frac{RT}{\Sigma V_1}\int_0^P\frac{V}{P}dP \qquad (2)$$

was employed. As Harkins and Jura[11] have emphasized an accurate evaluation of the integral requires a large number of experimental points in the low pressure region unless an analytical representation of volume as a function of pressure may be found. Representation of the data according to the multilayer formula of the B.E.T. theory[12] was not satisfactory in the low pressure region, that is below a relative pressure of about 1×10^{-2}.[13] The Williams-Henry[14] equation in the form

$$\ln V/P=A-BV, \qquad (3)$$

where V is the volume of gas adsorbed expressed as cc reduced to N.T.P., P is the equilibrium pressure, and A and B are empirical constants, represented the adsorption data well down to the lowest relative pressures, in many cases down to values of 5×10^{-4}. Deviations from the formula were both positive and negative at the lowest adsorption point, and appeared to be due therefore to experimental error in the determination of the low equilibrium pressure values. Typical data used to test Williams-Henry and the B.E.T. equations are given in Tables III and IV and shown in Figs. 4 and 5. Since the Williams-Henry equation was valid over the adsorption range studied, the film pressures were evaluated from the expression

$$F=\frac{RT}{\Sigma V_1}\left[V+\frac{BV^2}{2}\right]_0^V, \qquad (1)$$

where B is the slope of the line obtained from the plot of $\ln V/P$ *vs.* V. From this expression for the film spreading force the equation of state

[11] W. D. Harkins and G. Jura, in Alexander's *Colloid Chemistry* (Reinhold Publishing Corporation, New York, 1946), Vol. VI, p. 10 *et seq.*

[12] S. Brunauer, P. H. Emmett, and E. Teller, J. Am. Chem. Soc. 62, 1723 (1940).

[13] S. Brunauer, *The Adsorption of Gases and Vapors, Vol. I, Physical Adsorption* (Princeton University Press, Princeton, 1945), p. 158.

[14] S. Brunauer, reference 13, p. 84 *et seq.*

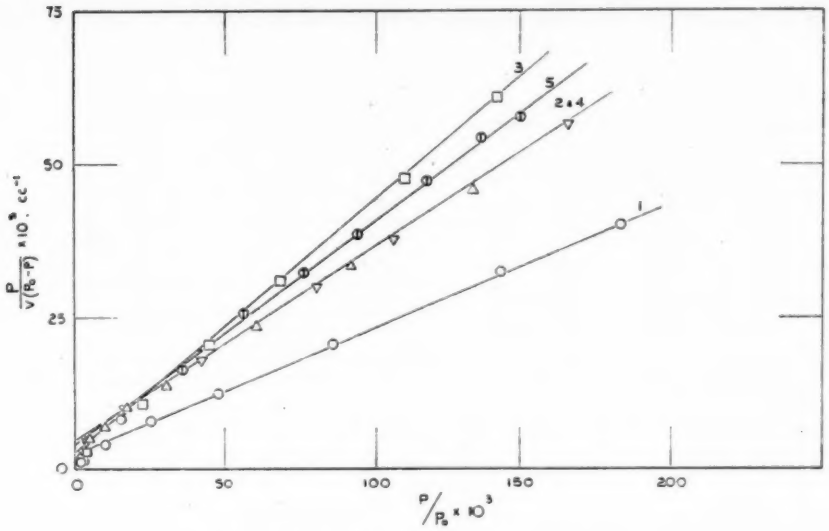

FIG. 5. B.E.T. multilayer plot of adsorption data.

Ordinate $\frac{P}{V(P_0-P)}\times 10^5$ cc^{-1}, abscissa $P/P_0\times 10^3$.

1. Dimethyl ether on No. 13 at 6.5°C.
2. Dimethyl ether on No. 11 at 20.0°C.
3. Butane on No. 11 at 20.0°C.
4. Ethyl chloride on No. 11 at 25.0°C.
5. Methyl propene on No. 11 at 20.0°C.

of the film

$$FA=\frac{RT}{N}\left[1+\frac{BV_1\Sigma}{2N}\cdot\frac{1}{A}\right], \qquad (4)$$

where A is the area per molecule in the film and N is Avogadro's constant, follows directly. When this equation is compared with a generalized equation of state such as that of Onnes,

$$PV=RT\left(1+\frac{B^1}{V}+\cdots\right), \qquad (5)$$

where P is the pressure, V is the volume per mole, and B^1 is an empirical constant, it is seen to be the two dimensional analogue of a gas under moderate compression.

In Table I and in Fig. 3 typical data illustrate the region of contraction of the rod. Since F is positive on the assumptions implicit in the Gibbs adsorption equation in the form

$$-d\sigma=RT\Gamma_1 d\ \ln P=dF, \qquad (6)$$

where $-d\sigma$ is the decrease in Gibbs surface tension of the solid, Γ_1 is the surface excess of adsorbate in moles per unit surface area, P is the equilibrium pressure of the gas phase, and dF is the increase in film spreading pressure. Bangham's relation $x=\lambda F$ does not hold in this region. The mechanism by which the contraction is produced is not known, although several plausible ones may be suggested.

Firstly, contraction along the length of the rod may have occurred while an expansion took place along the diameter. A direct check of this possibility was not feasible with the experimental arrangement. Solution of adsorbate in the adsorbent might also explain the observation, and here again no discriminatory test was possible. Adsorption in narrow crevices where the range of attractive forces is as great as the crevice diameter has been suggested by DeBoer[15] as an explanation for high initial energies of adsorption and might be suggested here to account for the observed contraction. Evidence of high initial adsorption energies has already been noted in the thermal effects and in the deviation of the adsorption data from the B.E.T. formulation in the low range.[13] On the other hand, however, the successful application of the Williams-Henry

[15] J. H. DeBoer, *Electron Emission and Adsorption Phenomena* (Cambridge University Press, Cambridge, 1935) p. 46.

TABLE V. Evaluation of spreading pressures at equivalent fractions of the surface covered.

Adsorbate	Rod	Temperature, °C	B.E.T. constant V_m	B.E.T. constant C	Density of liquid adsorbate g/cm³	Area covered by adsorbate molecule A^2	Total surface area of rod m^2	Spreading force ergs/cm² $V_m/3$	Spreading force ergs/cm² $V_m/2$	Spreading force ergs/cm² V_m
*Ethyl chloride	11	25.0	313	64	0.887	26.6	2.25×10^3	8.0	14.1	40.7
*Dimethyl ether	11	20.0	300	67	0.661	25.9	2.10×10^3	7.7	13.6	38.5
*Methyl propene	11	20.0	264	138	0.596	31.6	2.26×10^3	7.4	13.4	41.0
*Butane	11	20.0	242	126	0.575	33.1	2.16×10^3	7.3	13.4	41.3
*Ethyl chloride	13	10.0	450	111	0.909	26.0	3.18×10^3	7.6	13.3	38.2
Dimethyl ether	13	6.5	479	104	0.681	25.3	3.29×10^3	8.4	14.9	43.4
Dimethyl ether	13	20.0	452	65	0.661	25.8	3.15×10^3	8.6	15.3	45.5
Dimethyl ether	13	35.0	433	82.5	0.637	26.4	3.09×10^3	7.9	14.0	40.0

* These values have already been tabulated in Table III of reference 1, where more extensive data have been summarized.

TABLE VI. Comparison of λ and E (Young's modulus) for carbons No. 11 and No. 13 with coal samples studied by Bangham.

Sample	Adsorbed vapor	λ cm/dyne	Σ_1* cm²/g	$E=100\Sigma_1 d/\lambda$ dynes/cm²††
†Northumberland weakly caking coal (methanol extracted)	Methanol	0.026	186×10^4	10×10^9
†Northumberland weakly caking coal (unextracted)	*n*-Hexane	0.029	168×10^4	8.5×10^9
Charcoal rod No. 13 at 10°C	Ethyl chloride	0.0039*	941×10^4	5.3×10^{11}
Charcoal rod No. 13 at 6.5°C	Dimethyl ether	0.0039*	974×10^4	5.5×10^{11}
Charcoal rod No. 11 at 20°C	Butane	0.0038*	907×10^4	5.3×10^{11}
Charcoal rod No. 11 at 10°C	Ethyl chloride	0.0040*	945×10^4	5.2×10^{11}

* Values calculated from $x=\lambda F$ for a spreading force between 20 and 35 ergs/cm².
The weights of carbons No. 11 and No. 13 were estimated from a comparison of their volumes and the known volume and weight of carbon No. 12. See reference 1.
† Values from *The Ultra-fine Structure of Coal and Coke* (B.C.U.R.A., London, 1944), p. 122, Table I.
†† Assuming an absolute density d of 2.29 g/cc for this charcoal.

formula, which also assumes that the differential energy of adsorption is independent of the amount of adsorbate on the surface, suggests that the deviation from the B.E.T. formulation is not caused by that factor. Least likely is any explanation based on the conception of the formation of concave menisci and adsorption by capillary condensation, since the pore diameters estimated on that basis are too small.

In the range of adsorption where expansion occurs the relation $dx/dF=\lambda$ is approximately true, and as the calculated spreading pressure is nearly independent of the adsorbate for equal fractions of the total surface covered, the extension of the rod is nearly equal at this same condition for all the adsorbates. Data illustrating this finding are given in Tables V and VI. Table V summarizes the relevant adsorption data while in Table VI are given the values of λ for the two rods studied. Comparison is also made with values of λ and E, the Young's modulus of the rods, obtained by Bangham[16] for coal samples.

[16] D. H. Bangham and F. A. P. Maggs, *The Ultra-fine Structure of Coals and Cokes* (B.C.U.R.A., London, 1944), p. 118.

In Table VII data for one rod using dimethyl ether at three temperatures are included. The data are too meager to decide whether the relationship between spreading force and extension applies accurately for a range of tempera-

TABLE VII. Length changes of rod No. 13 caused by adsorption of dimethyl ether at 6.5°C, 20.0°C, and 35.0°C

Temperature, °C	Vol. adsorbed cc at N.T.P.	Calculated spreading force, ergs/cm²	Length change, percent
6.5	50.0	1.89	−0.0088
	150	7.45	−0.0124
	250	15.5	−0.0018
	300	20.4	+0.011
	400	32.0	+0.059
	500	46.2	+0.121
	550	53.9	+0.154
20.0	50.0	2.09	−0.0030
	100	4.91	−0.0070
	200	12.7	−0.0030
	300	23.5	+0.025
	400	37.2	+0.080
	450	45.1	+0.112
35.0	50.0	2.18	−0.0031
	200	12.6	−0.0030
	300	22.7	+0.025
	400	35.4	+0.074
	450	42.8	+0.098

tures. Again the relation appears to be valid within experimental error.

Water Vapor

The data obtained with water vapor are of interest in determining the mechanism of its adsorption. McBain[7] first emphasized that a critical test of the theory of capillary condensation could be made by measuring the dimensional change of the adsorbent. If the unusual isotherm for water were caused by condensation in the adsorbent capillaries with the formation of concave menisci, the adsorbent should be under tension, and a contraction of the adsorbent should result. McBain, therefore, determined the behavior of a charcoal rod when exposed to water vapor and found an extension to occur as with other adsorbates.

An extension of the rod on exposure to water vapor was found also in this investigation (see Fig. 6 and Table VIII). Expansion became appreciable as the relative humidity was raised above 75 percent. Up to that relative humidity no expansion was observed although reference

TABLE VIII. Length change for water vapor on carbon No. 11 at 20.0°C

Percent relative humidity	Extension, cm	*Desorption points
37.1	+.0001	
42.8	+.0001	
49.1	+.0001	
56.1	+.0001	
62.8	+.0002	
70.2	+.0006	
79.8	+.0019	
88.2	+.0061	
96.1	+.0104	
*64.1	−.0054	Run no. 1
*52.5	−.0077	
On pump 24 hr. at 20.0°C		
nil	nil	
96.2	+.0112	
*91.5	+.0093	
*84.0	+.0057	
*78.2	+.0025	
*70.5	−.0013	
*64.0	−.0053	
*54.5	−.0075	Run no. 2
*51.0	−.0068	
*40.0	−.0021	
On pump 24 hr. at 20.0°C		
nil	nil	
66.6	+.0005	
*52.8	−.0008	
On pump 24 hr. at 20.0°C		Run no. 3
nil	nil	

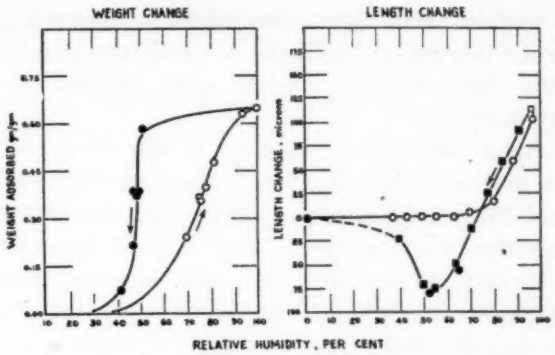

FIG. 6. Comparison of weight adsorbed and length change as a function of relative humidity for water vapor. Adsorption isotherm from data of Morrison and McIntosh on granular zinc chloride activated carbon at 20.0°C, length change for carbon No. 11 at 20.0°C.

to an adsorption isotherm of another zinc chloride activated charcoal made by Morrison and McIntosh[8] shows that about 50 percent of the saturation weight has been taken up at this humidity. The behavior in this adsorption region was therefore found to be similar* to that of organic vapors, and gave no evidence of capillary condensation along the adsorption branch.

The desorption data for water were quite dissimilar from that obtained with the organic adsorbates. Between 96 percent and 53 percent relative humidity an almost linear contraction of the rod was observed until the length was much less than it had been before any adsorption had occurred. This result was reproducible, and except for the extent of the contraction, could be obtained without exposing the rod to the high relative humidity of 96 percent. (See run No. 3 of Table VIII.) Over the range of contraction (96 percent − 53 percent relative humidity) almost no water is desorbed as is shown by reference to the adsorption isotherm.[8] However, when the relative humidity was reduced below 53 percent the rod expanded again toward the original length.

These data are most easily explained by assuming that the desorption branch of the water isotherm is caused by evaporation from concave menisci which are formed as the relative humidity

* In fact using carbon No. 13 and the double leaf condenser a slight contraction of the rod was observed in this range, exactly as with organic vapors. The complete adsorption range could not be investigated with this condenser, because of the contraction on desorption which would have injured the assembly.

is reduced from high values towards 53 percent. When desorption begins fewer capillaries remain filled and the rod extends again towards its original value.

Some independent support of this view may be derived from the observations of Morrison and McIntosh[8] on the apparent density of the adsorbed water phase. In that work it appeared necessary to assume that the adsorbed film coalesced in some manner along the desorption branch in order to explain the difference is apparent density of the adsorbed film along that branch from that found along the adsorption branch. The formation of a coalesced film with concave menisci was suggested, and the film in that form was presumed to block off a small amount of the internal voids, thus causing low values of the apparent density. The two types of observations, therefore, appear to be explicable by the same qualitative interpretation.

At first sight it also appeared possible to deduce a value of the wetting angle of the film in the capillaries from a knowledge of the Young's modulus for the rod and the measured contraction, provided that a model of the types suggested by Bangham[16] was assumed. However, unless a knowledge of the form and distribution of the film between the outer and inner surfaces of the equivalent surface (hollow cylinder, for example) is obtained, such a calculation does not appear feasible.

One other consideration is of interest in connection with these data. It is of importance to know which branch of the isotherm represents the stable state of the film. Bangham[5] has shown that at constant pressure of the gas phase the stable film should have the higher value of the spreading pressure. On the basis that the dimensional change in the rod is a measure of the spreading pressure, the adsorption branch of the isotherm would appear to represent the stable form of the film, and the desorption branch a highly unstable system, since F_{de} appears to be negative because the rod extension is negative.

There are two cases, therefore, where identification of the observed spreading force (by length change) with the calculated spreading force estimated from thermodynamical considerations does not appear to be valid. These are: (a) within the region of contraction observed when organic vapors are adsorbed at low relative pressures and (b) along the desorption branch of the water isotherm. Therefore, for the zinc chloride activated charcoal rods studied here, the assumption made by Bangham that the percent extension of the rod may be employed as a measure of the lowering of the Gibbs surface tension of the adsorbent does not apply in all cases. It is apparently correct for the organic vapors in the adsorption range above about $\frac{1}{3}$ of the monolayer capacity, but not below this region, and does not apply along the desorption branch of the water isotherm.

ACKNOWLEDGMENT

The authors wish to express their appreciation to Dr. G. C. Benson for helpful discussions concerning the theoretical interpretation of certain of the data, and to Mr. J. Ravenscroft and Mr. A. J. Grant of the Physics Division for advice concerning the construction of the oscillator and bridge.

THE JOURNAL OF CHEMICAL PHYSICS VOLUME 15, NUMBER 1 JANUARY, 1947

The Raman Spectrum of Hexafluoroethane

D. H. RANK AND E. L. PACE*
School of Chemistry and Physics, The Pennsylvania State College, State College, Pennsylvania
(Received October 18, 1946)

The Raman spectrum of hexafluoroethane in the liquid phase has been obtained. The polarization of the lines appearing in the spectrum has been measured qualitatively. An assignment of the frequencies has been made from the spectrum.

INTRODUCTION

COMPOUNDS containing only carbon and fluorine are relatively rare. With the exception of CF_4,[1] Raman spectra of specific fluorocarbons are non-existent. Some years ago, small amounts of higher molecular weight fluorocarbons were prepared at The Pennsylvania State College by Dr. J. H. Simons. Raman spectra of various samples of these fluorocarbons of different molecular weights were obtained by Weber.[2] Unfortunately, little was known about the samples studied by Weber except the molecular weight and the knowledge that only fluorine and carbon were present in the molecule. Weber's samples were in the C_3 to C_8 molecular weight range.

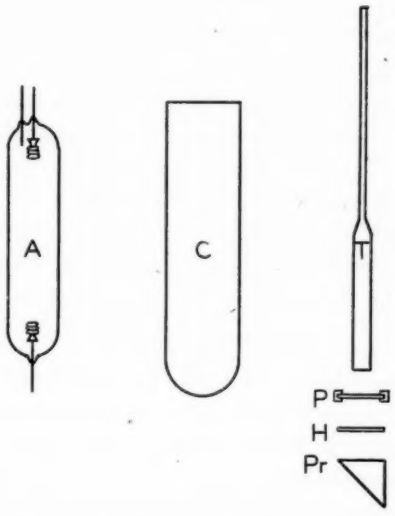

FIG. 1. Schematic diagram of light source and optical appurtenances. *A*, mercury arc; *C*, cylindrical lens; *T*, scattering tube; *P*, Polaroid disk; *H*, half-wave plate; *Pr*, prism.

Recently, we have been fortunate to obtain a sample of hexafluoroethane of high purity. This material was furnished by Dr. J. H. Simons, Director of the Fluorine Laboratory of The Pennsylvania State College and had been prepared and purified under his direction. The amount of impurity as determined from the melting point data was of the order of less than 0.1 percent.

EXPERIMENTAL

Hexafluoroethane has a boiling point of 195°K and a melting point of 173°K. The spectrum was obtained of the liquid phase which was maintained at 195°K by suitable refrigeration.

The main features of the method of excitation of the spectrum were described by one of us[3] previously. However, in this particular case, certain modifications in the experimental procedure were occasioned by the nature of the material under investigation. Figure 1 shows a schematic diagram of the apparatus. The tube *C* contained water since no filter was necessary for isolation of the λ4358 group from its short wave neighbor λ4047. (It was known that no frequencies as high as 1800 cm^{-1} would appear in the Raman spectrum of a fluorocarbon and thus overlapping of lines excited by the above-mentioned two groups of mercury lines was impossible.) Tube *P* contained a saturated solution of praseodymium ammonium nitrate, the effective thickness of which was about 2 cm.

Scattering tube *T*, Fig. 1, was about 14 mm in diameter and had a capacity of about 17 ml. The scattering tube was immersed in a quartz Dewar flask (not shown in Fig. 1) which had plane windows on the bottom to allow the light scattered at 90° to fall on the totally reflecting prism Pr. The upper part of the scattering tube

* Phillips Petroleum Fellow.
[1] Don M. Yost, E. N. Lassettre, and S. T. Gross, J. Chem. Phys. **4**, 325 (1936).
[2] R. L. Weber, Dissertation, The Pennsylvania State College (1938).
[3] D. H. Rank, R. S. Pfister, and H. H. Grimm, J. Opt. Soc. Am. **33**, 31 (1943).

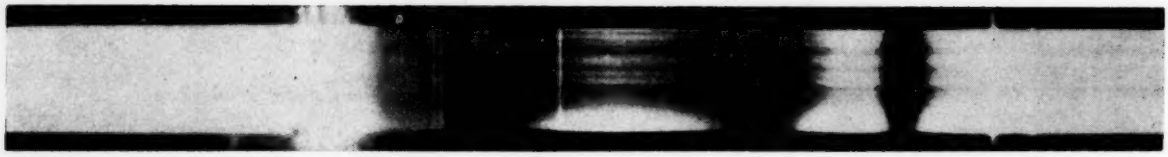

FIG. 2. Enlarged reproduction of spectrogram.

was provided with a close-fitting sheet-copper jacket to assist in thermal conduction of heat from the tube. The cooling was accomplished by directing a stream of cold dry air into the Dewar. The air was cooled by passing through a copper coil immersed in liquid air. A thermocouple inserted into the Dewar allowed a rough estimate of the temperature to be obtained. The temperature could be regulated by varying the flow of cold air into the Dewar. In order to reduce the Fresnel reflection from the windows of the scattering tube, methyl alcohol was poured into the Dewar to a depth of about a cm after the scattering tube had been inserted.

The spectrograph was essentially the same instrument as used by Rank, Scott, and Fenske.[4] However, the f:4.5 Tessar has been replaced by an f:3.4 "Spectro-aplanat" designed by one of us. This lens gives definition much superior to the Tessar over the necessary small field and is considerably faster than the Tessar. Exposure times varied from 2 to 5 hours. Wave-length measurements were made against iron comparison spectra. The wave number shifts should be accurate to ± 2 cm^{-1} in most cases.

Qualitative depolarization measurements were made by photographing the $\parallel$ and $\perp$ components separately by the use of the Polaroid P, Fig. 1. H is a half-wave plate made from a selected piece of Cellophane mounted on a glass slide. Quantitative measurement of the depolarization factors of the Raman lines in this spectrum was not attempted. It has been shown[3] that the method of excitation used by us yields essentially correct depolarization factors. However, as can be seen from Fig. 2, the plates obtained would not be suitable for accurate photographic photometry. The apparent "dust lines" seen in Fig. 2 are not dust lines but are produced by somewhat-out-of-focus images of small bubbles in the two quartz windows of the bottom of the Dewar flask.

TABLE I. The Raman spectrum of hexafluoroethane, point group D_{3d}.

Frequency cm^{-1}	Intensity	Polarization	Assignment		
			Designation	Species	Description
349	10 (s)	mp	ν_3	A_{1g}	CC stretching
380	10 (b)	dp	ν_{12}	E_g	Bending
620	10 (b)	dp	ν_{11}	E_g	CF_3 deformation
655	1		$2\nu_9$	A_{1g}, E_g	?
809	50 (s)	sp	ν_2	A_{1g}	CF_3 deformation
1237	4 (b)	dp	ν_{10}	E_g	CF stretching
1420	5 (b)	?	ν_1	A_{1g}	CF stretching

Results of the experiments described above are summarized in Table I. The assignment of frequencies (Designation, Species, and Description) is according to nomenclature used by Herzberg[5] for ethane. The 655 cm^{-1} frequency shift might be explained as $2\nu_9$. ν_9 is the $\perp$ bending frequency which should appear in the infra-red.

Qualitatively, the magnitudes of the CF stretching frequencies found by us for hexafluoroethane are in general agreement with Weber's[2] results for the spectra of fluorocarbons ranging from C_3 to C_6 inclusive. The highest frequency observed by Weber was 1382 cm^{-1}.

It might be significant to note that the Raman spectrum of hexafluoroethane is only about $\frac{1}{10}$ as intense as the spectra of ordinary hydrocarbons.

ACKNOWLEDGMENT

We are deeply indebted to Dr. J. H. Simons, Director of the Fluorine Laboratory of The Pennsylvania State College for loan of the hexafluoroethane.

These experiments were performed at the suggestion of Dr. J. G. Aston, of the Cryogenic Laboratory, in order to obtain information useful for thermodynamic calculations. The results of the cryogenic work will appear in another publication.

[4] D. H. Rank, R. W. Scott, and M. R. Fenske, Ind. Eng. Chem. Anal. Ed. **14**, 816 (1942).

[5] G. Herzberg, *Infrared and Raman Spectra* (D. Van Nostrand Company, New York, 1945), p. 343.

THE JOURNAL OF CHEMICAL PHYSICS VOLUME 15, NUMBER 1 JANUARY, 1947

Studies on Aging of Precipitates and Coprecipitation

XXXIX. Low Temperature Conductivity of Silver Bromide*

I. SHAPIRO AND I. M. KOLTHOFF
School of Chemistry, University of Minnesota, Minneapolis, Minnesota
(Received October 4, 1946)

The following expression is proposed for the electrical conductivity of silver bromide

$$\chi=(Ae^{-W/2kT}+KS)e^{-U/kT},$$

in which S is the magnitude of the active surface. When $Ae^{-W/2kT}\gg KS$ the high temperature kind of conductivity predominates. In the opposite case the low temperature kind of conductance predominates. Conductivity-temperature curves of fresh (large S) and well-aged (small s) silver bromide have been determined. In agreement with theoretical expectations it is found that

$$\chi=3.0\times10^{5}e^{-18,000/RT}+A_{i}e^{-8300/RT}$$

in which A_i varies in proportion to the active surface of the product. A pellet prepared from freshly precipitated silver bromide was found to have about 500 times as large a conductance as a pellet prepared from the fused product. At a given temperature the following relation exists between χ and the pressure p applied to the pellet: $d\ln\chi/dp=-k$. The value of k increases with decreasing active surface and with increasing temperature. The temperature effect is accounted for by the contribution of the active surface.

INTRODUCTION

THE theory of the ionic conductivity in crystals based upon Frenkel[1] and Schottky[2] disorders has been reviewed by Mott and Gurney[3] and by Barrer.[4] The agreement of the theoretical considerations with experimental findings has been satisfactory in most cases; however in some salts at low temperatures certain discrepancies are found.

In general the experimental ionic conductivity-temperature curves for salts can be divided into two parts, a reversible high temperature curve obeying a law

$$\chi=Ae^{-E/kT} \tag{1}$$

and families of low temperature curves obeying analogous laws

$$\chi_1=A_1e^{-E_1/kT} \quad (E_1<E). \tag{2}$$

The value of the constant A_1 in Eq. (2) depends upon the previous history and treatment of the specimen.

The equation for the electrical conductivity in solids also can be expressed by

$$\chi=n\epsilon v, \tag{3}$$

where n is the number of carriers (e.g., number of positions of disorder), ϵ is the ionic charge, and v is the mobility of the carriers. Considering the case of a Frenkel disorder in a crystal (i.e., some cations occupying interstitial positions instead of normal positions) the number of carriers, n, in thermal equilibrium at temperature T is given by

$$n=Ne^{-W/2kT}, \tag{4}$$

where W is the work necessary to move an ion from a normal position to a distant interstitial position. The mobility of these carriers can be expressed by

$$v=Be^{-U/kT}, \tag{5}$$

where U is a potential barrier and B is a constant. Therefore Eq. (3) can be rewritten as

$$\chi=Ae^{-(\frac{1}{2}W+U)/kT}. \tag{6}$$

By comparing Eq. (6) with Eq. (1),

$$E=\tfrac{1}{2}W+U. \tag{7}$$

[1] J. Frenkel, Zeits. f. Physik **35**, 652 (1926).
[2] W. Schottky and C. Wagner, Zeits. f. physik. Chemie **B11**, 163 (1930).
[3] N. F. Mott and R. W. Gurney, *Electronic Processes in Ionic Crystals* (Oxford Press, 1940), p. 42.
[4] R. M. Barrer, *Diffusion in and through Solids* (Macmillan Company, New York, 1941), p. 239.

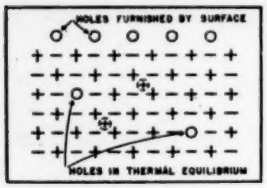

FIG. 1. Frenkel-type lattice disorder.

Several explanations for the break in the conductivity-temperature curves in ionic crystals have been given by workers in this field. Some workers hold the view that at the higher temperatures the exponential in the conductivity equation is governed by $(\frac{1}{2}W+U)$, but at the lower temperatures the positions of disorder are "frozen in" and only part of the exponential is used, namely U. Koch and Wagner[5] carried out some unique experiments on mixed crystals of AgBr-$PbBr_2$ and have shown that small additions of lead bromide greatly increase the conductivity of silver bromide. On the basis of these mixed crystal measurements Koch and Wagner believe that the low temperature conductivity is governed primarily by impurities in the crystals.

In view of the work carried out by Smekal[6] and other workers, it seems that the break in the curves is more regular than a mere dependence upon impurities or the "freezing of the positions of disorder" at some temperature. In any real crystal there exist cracks and imperfections which may be considered as internal surface. Any surface, internal or external, should be capable of furnishing a high concentration of "holes" to the crystal since an ion near the surface can migrate to a vacent lattice position (of which there are many) on the surface just as well as to a vacant lattice position in the interior of the crystal (see Fig. 1). Therefore at any temperature the total concentration of holes (note: a "hole" can be considered as a "carrier") will be dependent upon the active surface present and the normal concentration of holes existing in thermal equilibrium. The temperature function of the holes (or carriers) in the lattice in thermal equilibrium is given by Eq. (4) while the concentration of holes in the surface practically is independent of the temperature (as long as no aging occurs in the material). Hence Eq. (6) should be rewritten as

$$\chi=(Ae^{-W/2kT}+KS)e^{-U/kT}, \tag{8}$$

where S is magnitude of active surface and K is a proportionality factor. When the temperature T is such that

$$Ae^{-W/2kT}\gg KS, \tag{9}$$

then the high temperature form of the conductivity equation becomes predominant and Eq. (8) reduces to Eqs. (1) or (6). On the other hand when the temperature T is such that

$$Ae^{-W/2kT}\ll KS, \tag{10}$$

then the low temperature curve becomes the more important and Eq. (8) reduces to Eq. (2). This reasoning explains why compressed pellets of powdered silver bromide have a higher conductivity than those of the fused salt at low temperatures but that the conductivity of the former becomes equal to that of the latter at higher temperatures.[6] Also the increase in conductivity with addition of lead bromide to silver bromide[5] can be explained in the light of the above discussion because each molecule of lead bromide added creates a cation hole in the crystal lattice. These created holes behave identically with the surface holes of the crystals.

The validity of Eq. (8) can be checked indirectly by measuring the pressure effect on conductivity. Jost and Nehlep[7] have shown that in the high temperature range

$$d\ \ln\chi/dp=-\beta\ \ln C/\alpha T=\text{a constant} \tag{11}$$

where β is the coefficient of compressibility, α is the coefficient of expansion, T is the absolute temperature, and C is a constant which is determined by

$$\exp(-(\alpha V_0/k)\cdot(dE/dV)).$$

It is obvious from Eq. (11) that the slope of the conductivity-pressure curve numerically will decrease with increasing temperature. However, in the low temperature range, Eq. (11) need not apply. The pressure effect at low temperatures will be considered in more detail after the experimental data are given.

[5] E. Koch and C. Wagner, Zeits. f. physik. Chemie **B38**, 295 (1937).

[6] A. Smekal, *Handbuch der Physik* (1933), Vol. 24, Part 2, page 881.

[7] W. Jost and G. Nehlep, Zeits. f. physik. Chemie **B34**, 348 (1936).

The experiments on the effects of temperature and pressure upon ionic conductivity of silver bromide powders have been carried out in conjunction with a study on the "aging" phenomena of powders.[8] The effect of the change in surface of the powder upon ionic conductivity could be followed by conductance measurements.

EXPERIMENTAL PROCEDURE

Preparation of Samples

The preparation of the silver bromide samples and the subsequent measurements of the electrical conductivity at various temperatures and pressures are given in detail in the thesis of the Junior author. All of the silver bromide used in these experiments were prepared by a precipitation method using analytical grade reagents and conductivity water. Solutions of 0.4*N* silver nitrate were added to equivalent amounts of potassium bromide solutions with vigorous stirring. The precipitates were washed five times with large volumes of water, then five times with acetone, and finally five times with thiophene-free benzene. Dry air was passed through the precipitate on a Büchner funnel until the odor of benzene no longer was detectable. All precipitations and treatment of the silver bromide were carried out in photographically inactive red light.

Portions of the silver bromide powder were thermally aged by heating the powder to various temperatures (measured with a nichrome-constantan thermocouple) for definite periods of time in a Pyrex tube placed in a well of a copper block furnace. To prevent loss of bromine from the silver bromide at the elevated temperatures (above 100°C) a stream of bromine vapor was maintained over the powder in the furnace. The temperature and heating time of the "aged" powders are given with the experimental data.

In most cases the electrical conductivity measurements were made on pellets prepared from compressed powders but in several instances the pellets were formed by fusing the silver bromide and machining the congealed melt to the correct size on a lathe. The pellets formed from the powders were compressed under 3000 atmospheres pressure. Previous work on the pressure effect of silver bromide powders indicate that under these conditions the apparent density of the powders is within one percent of the true density of silver bromide. Therefore the data on compressed powder and fused-cut pellets should be comparable.

Electrical Conductivity Measurements

A sketch of the conductivity cell is shown in Fig. 2. In this cell the electrical conductivity of the silver bromide could be measured under various conditions of temperature and pressure. The pistons which served as electrodes were silver plated and a lamina of Bakelite served as an insulator between the pistons and die. The pressures on the silver bromide pellets were measured with a calibrated gage on the hydraulic press, and the temperatures were measured with a copper-constantan thermocouple connected to a type-*K* potentiometer. An electric heater and stirrer in an oil bath were used to obtain the various high temperatures while freezing mixtures, e.g., dry ice and acetone, were used for the low temperatures.

A direct current was used for measuring the conductivity of the pellets. The current flowing through a pellet under a given voltage was read on a three-range combination micro-milliammeter. For the source of voltage nine 1½v dry cells and three 45v "*B*" batteries were wired in such a manner that various voltages in the range of 1½v to 135v could be applied by turning the

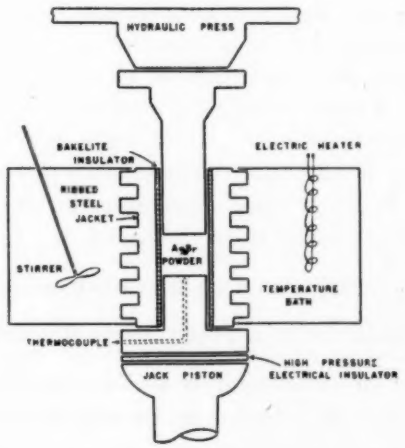

FIG. 2. High pressure conductivity cell.

[8] I. M. Kolthoff, Tekniska Samfundets Handlingar **3**, 119 (1939).

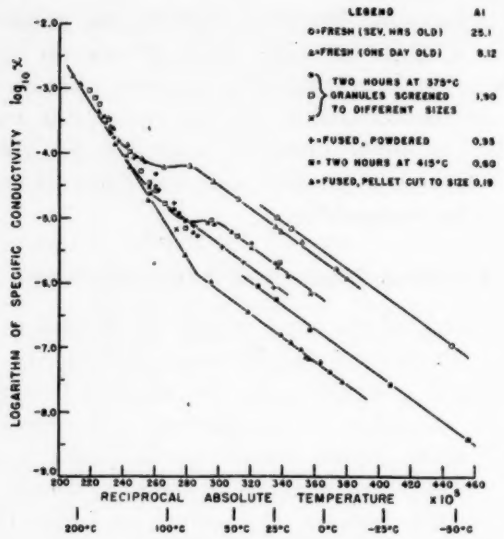

FIG. 3. Electrical conductivity of silver bromide as a function of temperature.

knob of a double gang switch. The actual voltage used depended upon the resistance of the pellet so that the current always was within a definite range. A voltmeter was used to measure accurately the various voltages. The dimensions of the pellets were measured with a micrometer at the conclusion of the experiments. All electrical and mechanical measurements were reproducible to within 1 percent.

A continuous direct current must not be allowed to flow through a pellet otherwise dendritic silver bridges will form across the electrodes and will cause a short-circuit through the pellet. For that reason the actual current was kept to a minimum and was allowed to flow through the pellet just long enough (few seconds for each reading) to obtain the necessary data. Since the total quantity of electricity passing through a pellet during the course of the experiment was negligibly small compared to the quantity of electricity necessary to produce the silver "bridges," the error introduced by the transport of ions can be disregarded.

RESULTS AND DISCUSSION

Conductivity of Fresh Silver Bromide

Fused silver bromide is an ionic conductor in which only the silver ions are migrating.[9] Since fresh silver bromide at room temperature has a conductivity that may be more than 10^4 times as great as the conductivity of the fused product under similar conditions, the possibility of a change in mode of conductivity with age was investigated. Transference experiments of fresh silver bromide (to be published) show that there is no change in mode and that the fresh silver bromide is an ionic conductor in which only the silver ions are migrating through the silver bromide crystals.

Conductivity as a Function of Voltage

Since it has been found convenient to vary the voltage dependent upon the resistance of the silver bromide samples (resistance varies greatly with "age" and temperature) so that the current always will be within a definite range, the validity of the application of Ohm's law to the data was checked. It was found that Ohm's law is applicable for the entire range of voltages used in these experiments and is not affected by variation of temperature and/or pressure.

Conductivity as a Function of Temperature

The dependence of conductivity upon temperature for the various aged silver bromide samples is shown in Fig. 3. All temperature experiments were carried out under a constant pressure of 925 atmos. after the pellets had been subjected to pressures of 3000 atmos. From pressure-conductivity experiments it was found that one could obtain reproducible results at the high pressures whereas the measurements at low pressures might be influenced by poor contact between electrodes and pellet.

An inspection of the curves in Fig. 3 reveals three outstanding features: (1) The slopes of the curves for all samples are approximately the same at low temperatures; (2) At high temperatures all curves merge into one straight line whose slope is greater than that at the low temperature; and (3) At any one low temperature the conductivity is strongly dependent upon the "age" (including thermal treatment) of the samples of silver bromide. Empirically all the curves in Fig. 3 can be expressed by the following equation:

$$\chi = 3.0\times 10^5 e^{-18{,}000/RT} + A_i e^{-8300/RT},$$

[9] C. Tubandt, *Handbuch der experimental Physik* (Leipzig, 1932), Vol. 12, p. 389, 397.

where the values of A_i depend upon the previous history of the particular samples. The values of A_i are listed in the legend of Fig. 3. The Q-values of 18,000 cal. (high temperature) and 8300 cal. (low temperature) are in excellent agreement with the values obtained by Koch and Wagner[5] on mixed crystals of AgBr-$PbBr_2$.

The slight dip in the curves for the comparatively fresh powders shown in Fig. 3 is due to thermal aging as the specimens are heated. The actual shape of the dip in the curves depends upon experimental conditions (e.g., rate of heating, etc.). As long as the temperature is sufficiently low, the low temperature curves are reversible, but as soon as appreciable aging occurs, the curves follow a line of correspondingly lower conductivity. Of course, the high temperature curve is reversible regardless of the age of the specimen.

Conductivity as Function of Age of Powder

The total surface of the unpressed powders of the various aged samples of silver bromide were measured by the dye adsorption method[10] by using wool violet and a Cenco photelometer. Direct measurements of the surface after the powder once is compressed are unobtainable. However, experiments on the change of conductivity with pressure as the powders are compressed afford an approximate method for evaluating the change in surface with pressure. (The data on the electrical conductivity during the compaction of silver bromide powders will be published in a subsequent article.) Calculations of the surface in the compressed powder at room temperature give values which are approximately proportional to the (low temperature) conductivity of the pellets. This proportionality between surface and conductivity at a fixed (low) temperature bears the view that the low temperature conductivity is predominantly a "surface" conductivity (Eq. (10)). Further evidence substantiating this theory is given in the next section.

TABLE I. Effect of pressure on conductivity of silver bromide pellets at room temperature.

Sample no. (corresponds to curve no. in Fig. 4)	"Age," heat treatment of silver bromide	Conductivity at zero pressure (extrapolated) $\chi_{p=0}$, Ω^{-1} cm^{-1}	k/atmos. $\times 10^4$
1	Fresh (less than 1 day old)	2.20×10^{-5}	0.644
2	Fresh (one day old)	1.03×10^{-5}	1.25
3	Unheated (20 days old)	7.9×10^{-6}	1.27
4	Heated 4 hours at 110°C	4.0×10^{-6}	1.63
5	Heated 2 hours at 375°C	2.4×10^{-6}	1.59
6	Heated 2 hours at 375°C	2.1×10^{-6}	1.53
7	Fused, quenched, powdered	1.4×10^{-6}	1.45
8	Fused, powdered, screened: 14–20 mesh	1.1×10^{-6}	1.65
9	Fused, powdered, screened: mixed size	1.1×10^{-6}	1.73
10	Fused, powdered, screened: 10–14 mesh	9.8×10^{-7}	1.68
11	Fused, powdered, screened: 8–10 mesh	9.0×10^{-7}	1.64
12	Fused, cooled slowly, powdered	3.0×10^{-7}	2.11
13	Fused pellet, cut to size	1.9×10^{-7}	2.22
14	Fused pellet, cooled slowly, arreated, cut to size	6.9×10^{-8}	2.50

[10] I. M. Kolthoff and A. S. O'Brien, J. Am. Chem. Soc. 61, 3409 (1939).

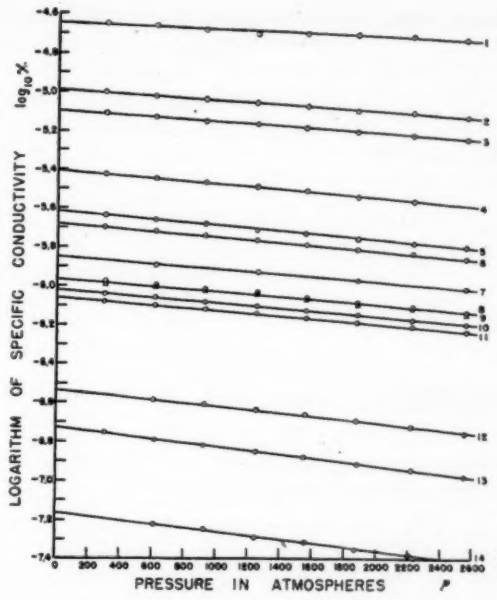

FIG. 4. Conductivity of pellets of silver bromide as function of recompression pressure 25°C (reversible).

Conductivity as a Function of Recompression Pressure

The effect of recompression upon the conductivity of silver bromide pellets at room temperature is shown in Fig. 4. It is observed that each curve can be expressed by

$$d\ln\chi/dp = -k, \qquad (12)$$

where k is a constant. The "age" or heat treatment of the various samples before compaction, the extrapolated conductivity at zero pressure ($\chi_{p=0}$), and the k-values for the samples are listed in Table I. The proportionality between surface and conductivity can be seen by comparing the "age" of the powder with its conductivity at room temperature. Of course, the

TABLE II. Effect of temperature upon the conductivity-pressure function

Age of sample	Temp. of press. exp. $t°C$	k/atmos. $\times 10^4$
Fresh (1 day old)	−10.5	0.284
	4.0	0.621
	25.8	1.30
	205.0*	1.86
Heated 2 hr. at 375°C	25.5	1.49
	38.6	1.58
	51.5	1.62
	64.1	1.73
	93.2	2.90
Fused-powdered	25°	1.68
	112°	1.77
	151*	2.28

* In high temperature region.

"fresh" powders had "aged" somewhat as a result of the pressure effect, nevertheless the trend still can be recognized clearly from the data of Table I.

From an inspection of Fig. 3 it is obvious that room temperature (25°C) is in the low temperature conductivity range hence only part of Eq. (8) need be considered here, so

$$\chi = KSe^{-U/RT}. \qquad (13)$$

Thus at a fixed temperature the exponential of Eq. (13) is constant and the conductivity is proportional to the active surface in accordance with experimental facts.

The slight increase in the value of k (Table I) with age of the sample can be explained on the basis of a surface conductivity. The low temperature conductivity is proportional to the number of "continuous paths of surface" between the electrodes. Since isolated surfaces, especially if oriented perpendicular to the line of direction between electrodes, do not contribute materially to an increase in conductivity, these so-called "paths of surface" refer to "active" surface and not necessarily "total" surface. As pressure is applied to a pellet, the number of "paths of surface" decreases. Since there are more "paths" in a pellet formed from a fresh powder than from a well-aged or fused powder, the relative decrease in number of paths will be less for the fresh powder pellet and therefore its conductivity will be less sensitive to pressure.

The effect of temperature upon the conductivity-pressure function is given in Table II. Regardless of the age of the sample the value of k increases with the temperature of the experiment. However from Eq. (11) one finds that the value of k should decrease with increasing temperature were only the mobility of the ions affected by pressure. By considering the influence of surface this anomaly can be reconciled. By taking the logarithm of Eq. (13) and differentiating with respect to pressure, we get

$$d\ln\chi/dp = d\ln S/dp - (1/RT)(dU/dp). \qquad (14)$$

Experiments on the compressibility of silver bromide powders (in press) show that the change in the logarithm of porosity (related to surface) of a powder with pressure is a constant, and that the numerical value of the constant increases with temperature and/or age of the powder. By assuming that a similar function exists between surface and pressure for compressed pellets, then the value of k from Eq. (12) will depend more upon the surface term in Eq. (14) than upon the energy term. Indeed calculations based upon known data show that the energy term of Eq. (14) is much smaller than the experimentally determined values so that the assumption seems justified.

THE JOURNAL OF CHEMICAL PHYSICS VOLUME 15, NUMBER 1 JANUARY, 1947

Dielectric Behavior of Solutions of Electrolytes in Solvents of Low Dielectric Constant
I. A Calorimetric Method for Measuring Losses[1]

A. H. SHARBAUGH, JR.,[2] C. SCHMELZER,[3] H. C. ECKSTROM, AND C. A. KRAUS
Metcalf Research Laboratory, Brown University, Providence, Rhode Island

(Received October 16, 1946)

The experimental equipment and method used to determine calorimetrically the energy absorption in a radiofrequency field by several electrolytes in solvents of low dielectric constant is described. The dipole conductivity and the loss factor for these systems are then calculated from the experimental data.

FOR some time, the attention of this laboratory has been directed toward a thorough investigation of the behavior of electrolytes in solvents of low dielectric constant. Such investigations are of interest because of the large interionic attractive forces which cause association into ion-pairs and other increasingly complex aggregates. One of the more important aspects of the theory accounting for the behavior of these solutions was the postulation of the existence of the ion-pair, or dipole.[4] Such postulation became fact when dielectric constant measurements yielded values for the dipole moments of a number of quaternary and ternary ammonium salts in benzene which required separation of unit electronic charges by distances of the order of molecular dimensions.[5]

To gain complete insight into these low dielectric constant systems, it has been necessary to investigate their properties by means of several methods, *viz.*, conductance, dielectric constant, and cryoscopic measurements. The method to be described here was developed to give still another approach which would yield information as a direct consequence of the existence of the ion-pair. Certainly, it is to be expected that these large and highly polar molecules dispersed in nonpolar solvents should exemplify systems with large dielectric losses at readily accessible radiofrequencies. Therefore, the quantity of heat generated as a result of energy absorption in a radiofrequency field by several quaternary and ternary ammonium salts in solvents of low dielectric constant have been investigated calorimetrically. This has been accomplished by placing the solution in a two-electrode cell to which is affixed a capillary thermometer tube; thereby, any temperature change in the fluid may be observed directly by a change in the level of the capillary liquid. This method has the advantage of being simple in principle and of giving an absolute measure of dielectric losses of the cell and its contents. It is not a new procedure, having been originated by Harms in 1901,[6] and used more recently by Schmelzer,[7] Oncley,[8] and Conner.[9]

PRINCIPLES OF THE METHOD

Let an alternating voltage, $V = V_{max}\sin\omega t$, be imposed on a thermometer cell which contains the fluid to be investigated. If the fluid-filled cell presents a resistance R, the amount of heat generated in t seconds is given by

$$Q = \int_0^t V^2/R dt. \qquad (1)$$

If one neglects the change in resistance caused by the small temperature change during the flow of current, Eq. (1) becomes

$$Q = V_{R.M.S.}{}^2 t/R = V_{R.M.S.}{}^2 t\kappa/z, \qquad (2)$$

where κ is the specific conductance of the solution

[1] This paper is based on a portion of a thesis submitted by A. H. Sharbaugh, Jr., in partial fulfillment of the requirements for the degree of Doctor of Philosophy at Brown University, June, 1943.
[2] Metcalf Fellow in Chemistry at Brown University, 1941–42. Present address: General Electric Research Laboratory, Schenectady, New York.
[3] Anthony Fellow in Chemistry at Brown University, 1937–38 and 1938–39. Address: 14a Heindenheim/Brenz, Württemberg, 2 Theodor Schaeferstrasse, American Zone, Germany.
[4] R. M. Fuoss, Chem. Rev. **17**, 27 (1935).
[5] Geddes and Kraus, Trans. Faraday Soc. **32**, 585 (1936). Kraus, J. Frank. Inst. **225**, 687 (1938).
[6] F. Harms, Ann. d. Physik **5**, 564 (1901).
[7] C. Schmelzer, Ann. d. Physik **28**, 35 (1937).
[8] Oncley, Ferry, and Shack, Ann. N. Y. Acad. Sci. **40**, 371 (1940).
[9] W. P. Conner, J. Chem. Phys. **9**, 591 (1941).

and z is the cell constant. Therefore, if the rate of heat generation, Q/t, is observed for a given applied alternating voltage, the conductance of the solution may be readily calculated for the frequency of the voltage in question. Equation (2) may also be rewritten as follows:

$$Q = V_{\text{R.M.S.}}{}^2 t\kappa/z = mc\theta = \pi r^2 \Delta h dc/\alpha, \quad (3)$$

where m is the mass, c is the specific heat, θ is the temperature rise, d is the density, Δh is the height of rise in the cell capillary in t seconds, r is the radius of the thermometer tube, and α is the coefficient of expansion of the fluid filling the cell. A subscript 0 will denote quantities of Eq. (3) which are measured at a sufficiently low frequency so that no heat is generated as a result of energy absorption by the ion-pairs or dipoles in the solution. The subscript ω will denote these quantities observed in the same conductance cell at another higher angular frequency $\omega = 2\pi\nu$. When this is done, we may write

$$V_0{}^2 t_0 \kappa_0 / V_\omega{}^2 t_\omega \kappa_\omega = [d_0 c_0 \Delta h_0/\alpha_0]/[d_\omega c_\omega \Delta h_\omega/\alpha_\omega],$$

from which

$$\kappa_\omega = [V_0{}^2 t_0 \kappa_0 / V_\omega{}^2 t_\omega][\alpha_0 d_\omega c_\omega \Delta h_\omega / \alpha_\omega d_0 c_0 \Delta h_0]. \quad (4)$$

Since only the ratio of voltages is now involved, the r.m.s. subscript will be dropped. Equation (4) is further simplified and thermal irregularities are avoided if the low and high frequency observations are made each time for the same solution and for equal temperature rises. Hence, Eq. (4), under these conditions, becomes

$$\kappa_\omega = V_0{}^2 t_0 \kappa_0 / V_\omega{}^2 t_\omega. \quad (5)$$

Furthermore, it will be assumed that the high frequency conductance may be resolved as

$$\kappa_\omega = \kappa_0 + \Delta\kappa = V_0{}^2 t_0 \kappa_0 / V_\omega{}^2 t_\omega,$$

where $\Delta\kappa$ will be referred to as the dipole conductivity. Therefore,

$$\Delta\kappa = [(V_0{}^2 t_0 / V_\omega{}^2 t_\omega) - 1]\kappa_0. \quad (6)$$

The tacit assumptions to be kept in mind when using Eq. (6) are that both the low and high frequency voltages should be measured in the same manner (as peak values of sinusoidal voltages in this investigation); that Ohm's law is obeyed within the range of voltages used; and that t_0 and t_ω are the times required for the same amount of expansion in the thermometer cell.

The complex dielectric constant[10] ϵ may be conveniently expressed as

$$\epsilon = \epsilon' - j\epsilon'',$$

where the prime and double prime represent the real and imaginary parts according to the usual alternating current vector notation. With reference to a medium, ϵ may be defined as the ratio of the admittance of a condenser filled with the medium to the admittance of the condenser when empty.[11] Hence,

$$\epsilon = \epsilon' - j\epsilon'' = Y/Y_0 = [G_\omega + j\omega C_1]/j\omega C_0,$$

where G_ω is the equivalent parallel conductance at the frequency ω, and C_1 and C_0 represent the equivalent parallel capacity of the filled and empty condenser, respectively. Equating real and imaginary parts,

$$\epsilon' = C_1/C_0$$

and

$$\epsilon'' = G_\omega/\omega C_0 = \kappa_\omega \times 1.80 \times 10^{12}/\nu,$$

where ν is the frequency of the applied alternating voltage in cycles per second and κ_ω is the specific conductance in reciprocal ohm-cm at a frequency $\omega = 2\pi\nu$. Furthermore, it is convenient to separate the a.c. and d.c. in-phase components by defining a loss factor $\Delta\epsilon''$ as

$$\Delta\epsilon'' = 1.80 \times 10^{12}(\kappa_\omega - \kappa_0)/\nu = 1.80 \times 10^{12} \Delta\kappa/\nu.$$

Thus, $\Delta\epsilon''$ is a measure of the pure a.c. response of the system, and ϵ' is the usual dielectric constant defined by the ratio of the capacitance with a given material dielectric, to the capacitance of the same system with a vacuum as a dielectric. $\Delta\kappa$ will be called, for convenience, simply the dipole conductivity but, in general, it will be understood that losses dealt with in this investigation may be caused by the existence of higher order complexes, such as quadrupoles, octapoles, etc., as well as to dipoles.

EXPERIMENTAL EQUIPMENT

High frequency energy was furnished by a conventional three-stage short wave generator,

[10] P. Debye, *Polar Molecules* (Chemical Catalog Company, New York, 1929).
[11] Hubert H. Race, Phys. Rev. **37**, 430 (1931).

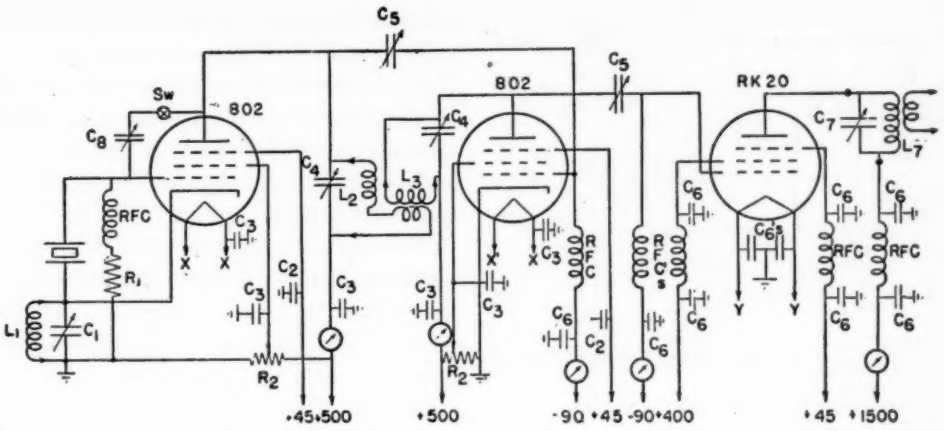

C_1—.00015 max. μf
C_2—.0005 μf
C_3—.01 μf
C_4—.0001 max. μf
C_5—.00005 max. μf
C_6—.005 μf
C_8—3–30 μμf
L_7–C_7—interchangeable tank units

S_w—switch
L_1, L_2, L_3—plug-in inductances
RFC—2.5 mh. r-f choke
R_1—20,000 ohms
R_2—60,000 ohms
XX—6.3 volts
YY—7.5 volts

FIG. 1. High frequency generator.

shown in Fig. 1, capable of delivering up to about 50 watts useful output. Frequencies were controlled by three crystals and, by virtue of frequency multiplication in the Tri-tet oscillator stage, as well as in the buffer-multiplier stage, useful output could be obtained on crystal harmonic frequencies through 28 Mc. The frequencies actually used were 1.83, 3.50, 7.04, 10.51, 14.09, 21.13, and 28.18 Mc. The d.c. voltage supplies consisted of two units: one of 500 volts, to operate the oscillator and multiplier stages and, secondly, a 2000-volt supply for the final amplifier and another low frequency transmitter to be described later. A type 83 and a pair of 866 tubes served as rectifiers for the low and high voltage supplies, respectively. The voltage furnished by the high voltage supply was made continuously variable by means of a Variac inserted in the primary circuit of the high voltage plate transformer. The 115-volt a.c. source was a 500-volt-ampere Sola Constant Voltage transformer. This insured a steady output from the generators since the Sola transformer delivered 115 volts ±1 percent for a total primary variation of about 20 percent.

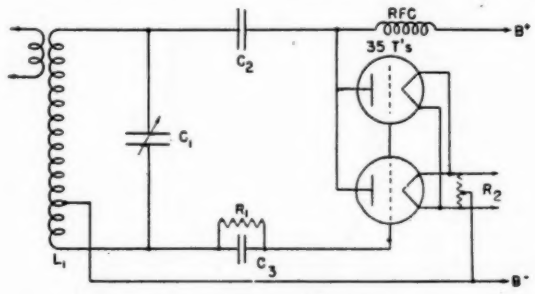

C_1–L_1—resonant tank circuit
C_2—.002 μf
C_3—.00025 μf
R_1—20,000 ohms
R_2—50 ohm C.T.
RFC—r-f choke

FIG. 2. Low frequency generator.

A second generator was constructed for the special purpose of supplying low radiofrequency energy. The Hartley oscillator circuit of Fig. 2 was selected because of its simplicity and the convenience with which the lower frequencies may be obtained, since both plate and grid inductances are shunted by the tuning condenser. Plug-in coils and variable air condensers served to vary the frequency, if desired, although during this investigation, a frequency of 0.1 Mc was principally used. Critical circuit elements were varied until a cathode-ray oscilloscope indicated a substantially pure sine wave output. Frequencies could be set to within ±3 percent with a General Radio Type 574 wave meter.

The third source of cell voltages was that of the 60-cycle power mains. An arrangement for supplying this consisted of a Variac whose output could be connected directly to the cell or first stepped up by a transformer. All 60-cycle voltages were measured with a Weston 341 voltmeter.

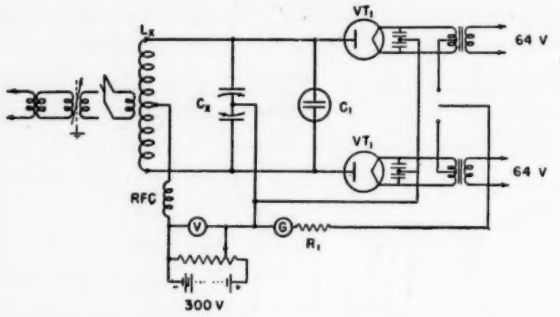

L_2—plug-in coils
VT_1—G.E. custom built water-cooled diodes, 1.60 heater volts
C_2—140 $\mu\mu$f per section
C_1—thermometer cell
R_1—1, 2, or 3 megohms
RFC—r-f choke
By-pass condensers .005 μf

FIG. 3. Cell circuit.

Radiofrequency voltages were determined by voltmeter tubes as used in the circuit of Fig. 3. The circuit is similar to that used by Schmelzer[7] and consists of two diodes in a symmetrical rectifying circuit with provision to exactly compensate the peak radiofrequency voltage with a bank of "*B*" batteries.

Since the calculation of the dipole conductivity requires the ratio of two voltages measured at very different frequencies, careful consideration was given to frequency dependent errors. A serious source of error may arise because of the voltage drop resulting from the self-inductance of the leads working in conjunction with the electrode capacity of the voltage measuring apparatus. This is easily shown by a consideration of the equivalent circuit shown in Fig. 4. Let L_1 and L_2=self-inductance of leads, V=desired high frequency voltage, V_a=apparent voltage operating in the measuring device, and C=capacity of the measuring device. By a general application of Ohm's law:

$$V_a/V=Z_c/Z,$$

where

$$Z=j(\omega[L_1+L_2]-1/\omega C) \quad \text{and} \quad Z_c=-j/\omega C.$$

Therefore,

$$V/V_a=\omega C(1/\omega C-\omega L),$$

where

$$L=L_1+L_2.$$

Finally,

$$V=V_a(1-\omega^2 LC).$$

Estimating L to be 0.1μh and C to be 0.6 $\mu\mu$f, the error in the apparatus described here would be only about +0.2 percent at 28 Mc.

Calculation also reveals that the transit time of the electrons need not be considered with the tubes (about 1.5 mm electrode spacing) and voltages used in this investigation up to frequencies of about 50 Mc.

Because of electron pressure, a very small "resting" current ($<10^{-6}$ amp.) flowed in the d.c. circuit when no potential was applied to the diodes. The reading of the galvanometer under this condition served as the null point for future balances of the r-f voltage by the biasing d.c. voltage. The two tubes had slightly different "rest" currents; hence, for convenience, when rapidly obtaining cut-off voltages, a single null position was established for both tube balances, and then, later, a small correction could be applied if necessary.

The cut-off voltages were measured on a calibrated Weston Model 45 voltmeter. Currents were indicated by a "loop" galvanometer similar to that described by Deubner.[12] The movement is a piece of aluminum foil (about 1 micron thick), shaped as a "U" and held in the field fissure of a permanent magnet. The loop of foil is protected from air currents by a glass housing and the entire assembly is completely shielded. Observation of the loop displacement as a result of current flow is done subjectively by a telescope (80×magnification) containing an ocular scale, illumination being furnished by a lamp within

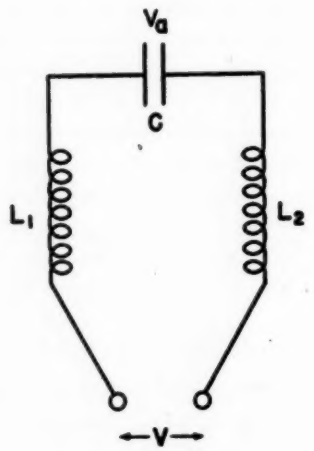

FIG. 4.

[12] A. Deubner, Zeits. f. tech. Physik **11**, 163 (1930).

the housing. Three degrees of freedom are furnished by sliding carriages so that the loop can be located at will with respect to the ocular scale. It was found that observation of the movement was facilitated by having a small glass fiber cemented to the foil. This galvanometer is especially suited to its application here because of the extremely small inertia of the loop movement. The specifications are: total time of oscillation, 0.2 sec.; loop resistance 5–10 ohms; sensitivity, 7×10^{-7} amp. per scale division.

The cell circuit was link (inductively) coupled to the radiofrequency generators through a Faraday shield as shown in Fig. 3. Various inductances could be plugged into this circuit to obtain resonance at the different frequencies. (Also additional shunt capacity was necessary in the case of 0.1 Mc.) A measurement of some of the amplitudes of the harmonics present in the cell circuit showed them to be less than 2 percent of the fundamental if they were measurable at all; hence, a tuned intermediate resonant circuit between generator and cell circuit seemed unnecessary.

The thermometer cell bulb and associated components were immersed in a constant temperature air-bath. The temperature of the vessel was controlled by a flow of constant temperature water supplied from a large reservoir, the temperature of which could be held to 25°C within $\pm0.001°$ for a day at a time. This water was circulated continuously by two pumps; one line supplied the top cover of the air bath and water jackets of the voltmeter tubes (which were located in the air-bath with the cell in order to obtain the shortest possible leads), and the other line supplied a copper water jacket at the sides and bottom of the air thermostat. Pipe lines, as well as air bath, were thermally insulated to minimize the effect of the ambient temperature. Over a period of several hours, the air bath temperature varied on the average by less than 0.01°C, depending on room temperature fluctuations and the quantity of heat lost from the cell.

TABLE I. Cell characteristics.

	Physical volume (cc)	Effective vol.* (cc)	Cell constant	Separation electrodes (mm)	$\Delta\lambda/\Delta t$ cm/deg. (approx.)	Capillary diam. (mm)	Approx. usable range (ohm^{-1} cm^{-1})
Cell No. 1	39.3	4.29	0.002326	1	7.0	0.95	10^{-3}–10^{-8}
Cell No. 2	8.5	0.741	0.01347	1	6.0	0.50	10^{-4}–10^{-6}
Cell No. 3	3.0	0.354	0.1119	2	2.1	0.50	10^{-7}–10^{-5}

* Calculated volume between the electrodes of the cell.

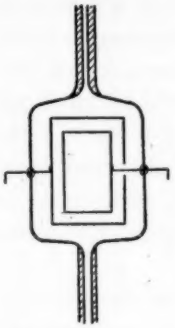

FIG. 5. Thermometer cell.

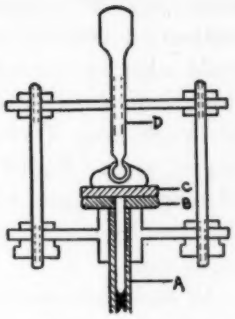

FIG. 5a. Method of closure of thermometer cell on bulb end. *A*, capillary leading to bulb; *B*, plane glass surface; *C*, optically plane glass plate; *D*, screw arrangement for holding *C* against *B*.

Three thermometer cells of the type shown in Fig. 5 were used in the investigation. The characteristic constants of these cells are listed in Table I, where benzene is the filling liquid. In order to avoid losses by evaporation, each thermometer cell was equipped on the bulb end with an optically plane glass surface which could be fitted against a similar surface of a glass disk for closing (see Fig. 5a) or to a suction apparatus for filling. With such an arrangement, having an air gap next to the polished glass surfaces, a solution could be kept for weeks without any noticeable evaporation. The capillary of the cell projected from the air-bath where the fluid meniscus could be viewed with a telescope. While in use, the open end of the capillary was connected to a glass bulb containing vapor of the investigated fluid. The dimensions of all these cells were negligibly small in comparison to one-quarter of the shortest wave-length used (10 meters). This, of course, refers to the wave-length in the fluid-filled cell which is smaller than the wave-length in free space by the factor $(1/\epsilon')^{\frac{1}{2}}$.

Rising times of the capillary fluid were measured with a synchronous-motor Cenco timer. These times ranged from about 4 sec. to 100 sec., depending on the field strength and conductance of the solution in the cell. To make a continuous time record of a rising meniscus in the capillary, a "Visasig" was used. This instrument delivered a

paper tape at a constant speed on which were marked intervals corresponding to seconds. There could also be recorded simultaneously on the paper indications of a pen actuated by closing a telegraph key. Therefore, a time record of the height of the liquid column as observed by a telescope equipped with an ocular scale could be obtained by measuring the time intervals on this paper tape.

All audiofrequency conductances (assumed to be the conductance at 0.1 Mc) were measured by the substitution method on a special bridge built around the Campbell-Shackelton shielded ratio box by Leeds and Northrup. The conductance cells used with this bridge were cleaned with fuming nitric acid, steamed, and baked in an oven at 140° overnight. While cooling, a current of dry air was blown through them. When making measurements, the cells were placed in an air bath and observations made when temperature equilibrium had been established.

PRACTICAL ASPECTS OF MAKING MEASUREMENTS

The determination of dipole conductivity, using Eq. (6), is reduced to measuring two rates of rise of the meniscus—once, at a sufficiently low frequency where $\Delta\kappa$ is zero; and, again, at the desired higher frequency, each time reading the accompanying voltages. Once a reliable r-f voltage measuring arrangement has been constructed, the experimental determination of the rates of rise presents the greatest problem. The question of constancy of the rising rate arises immediately, since the low and high frequency time measurements must be made under identical conditions to be used in Eq. (6). A number of plots of meniscus height *vs.* time were made with the "Visasig" chronograph for each of the three thermometer cells. These were studied carefully to ascertain within just what limits a linear relationship existed. In general, all determinations were made using actual rising heights from 1 to 10 mm (corresponding to 0.01°–0.2°C), depending on the conductance of the solution and size of cell. For best reproducibility, it was necessary to wait for complete thermal equilibrium between each measurement. However, with the largest cell used, satisfactory results could be obtained by operating the cell slightly above its equilibrium temperature and measuring the rate of cooling. The exponential cooling curve was approximated by a linear relationship and so used to correct the rising rate. It was found unnecessary to correct for any effect of temperature shifts of the air-bath.

TABLE II.

	Temp.	V_0	t_0	$V_0^2 t_0 \times 10^{-5}$
ν=0.1 Mc	3.835	129.4	30.3	5.07
	3.840	149.0	22.5	4.99
	3.842	173.0	17.2	5.15
	3.847	219.6	11.2	5.40
	3.849	219.4	10.8	5.19
	3.850	309.4	5.46	5.23
	3.852	377.4	12.0*	5.12
	3.853	456.2	8.32*	5.20
	3.852	523.0	6.36*	5.22
				Av. 5.17±1.6%
	Temp.	V_ω	t_ω	$V_\omega^2 t_\omega \times 10^{-5}$
ν=21.1 Mc	3.860	44.3	16.9	0.330
	3.860	44.3	16.6	0.325
	3.859	46.0	15.8	0.334
	3.862	103.1	10.2*	0.327
	3.855	103.1	10.2*	0.327
	3.860	105.1	9.74*	0.325
	3.850	138.7	5.59*	0.322
	3.846	156.4	4.55*	0.334
	3.851	159.1	4.39*	0.334
				Av. 0.329±1.2%

* For Δh=10 mm where the V^2t values have been reduced to a Δh=3 mm rise.

Within the range of voltages (0.1–6.0 kv/cm) used and within the experimental error, no variation of the observed high frequency conductance with field strength was found. An apparent decrease in conductance with increasing voltages was initially observed, but the effect was eventually traced back to a zero correction on the voltage measurement. According to Onsager's theory,[13] for uni-univalent salts which are very slightly dissociated, the increase in conductance caused by high field strengths (second Wien effect) is given by

$$\kappa_E/\kappa_0 = 1+3.33\times10^{-3}e^3V/4\epsilon' k^2T^2 = 1+4.818\,V/\epsilon' T^2,$$

where V is the field strength (average volts cm^{-1}), e is the electronic charge (statcoulombs), κ_E is the increased conductance due to the field, and the other symbols have their usual significance.

[13] Lars Onsager, J. Chem. Phys. 2, 599 (1934).

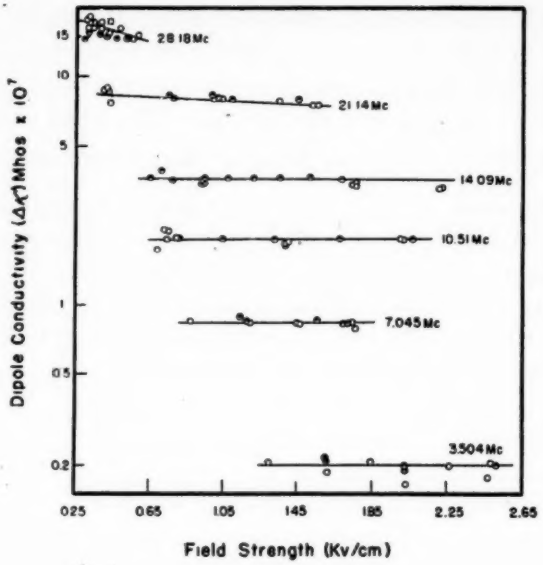

0.0934 molar i = Am_3NHPi in C_6H_6
$\kappa_0 = 5.30 \times 10^{-8}$
Shaded circles—Cell 3
Open circles—Cell 2

FIG. 6. Dipole conductivity as a function of frequency and field strength.

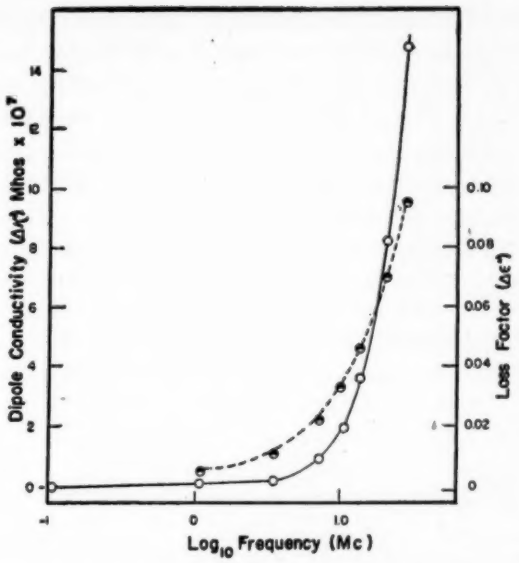

0.0934 molar i = Am_3NHPi in C_6H_6.
Open circles—observed dipole conductance, ordinates left.
Shaded circles—observed loss factors, ordinates right.
Solid and dashed curves—theoretical curves for dipole conductance and loss factor, respectively, based on $\epsilon_0 - \epsilon_\infty = 1.44$; $\nu_c = 430$ Mc.

FIG. 7. The dependence of dipole conductivity and loss factor on frequency.

Thus, for benzene,

$$\kappa_E/\kappa_0 = 1 + 23.8 \times 10^{-6} V,$$

and in the example cited where $V = 2(2.5 \times 10^3)/\pi = 1.6 \times 10^3$, we could expect a maximum of about a 4 percent increase in conductance. However, the Langevin relaxation time, which is the time required to establish equilibrium between charge distribution and the external electric field, is only about 2 microseconds.[14] Our working frequencies correspond to periods of from 0.04–0.6 microsecond so that in this range there was not time for the Wien effect to appear in the cells.[15] However, no systematic increases in conductance with increasing field strengths were observed at 60 cycles or at 0.1 Mc where the periods are long enough to allow the effect to exist. Further work at these frequencies is in progress.

Wherever necessary, a correction was made for the heating of the glass of the cells. These corrections were calculated from data obtained with only pure solvent in the cells with the aid of Eq. (4). Observable heating was found at only the highest frequencies and the correction amounted to only a few percent except for the very dilute solutions. The apparent glass conductance varied with the first to second power of the frequency depending upon the cell geometry.

For each concentration studied, the density, refractive index, viscosity, and audiofrequency dielectric constant, all pertinent to the Debye theory, were measured. All observations were made at 25.0°C.

Individual rates of rise per volt squared for a constant voltage could be reproduced with a mean deviation of about ±1 percent. The rate of rise per volt squared for a two- or threefold voltage increase could be measured with a mean deviation of ±5 percent.

The conductances measured at 60 cycles and 0.1 Mc agreed within the allowable experimental error.

EXAMPLE OF A MEASUREMENT

In Table II, is presented a typical set of data for a 0.0934 molar solution of tri-*iso*amylammonium picrate in benzene in Cell No. 2. The solution was allowed to return to temperature equilibrium between each application of the voltage. A temperature value of 3.854, in the

[14] L. Onsager, reference 13. For benzene solutions, the Langevin relaxation time $\tau_L = \epsilon'/72\pi \times 10^{11}\kappa = 10.1 \times 10^{-14}/\kappa$.
[15] Mead and Fuoss, J. Am. Chem. Soc. **62**, 1720 (1940).

second column, corresponds to 25.000°C; V = peak voltage of the field; t = time in sec. for $\Delta h = 3$ mm or 10 mm rise, as indicated; κ_0 = audiofrequency conductance = 5.30×10^{-8} ohm^{-1} cm^{-1}; density = 0.8825 g cm^{-3}; viscosity = 0.00657 poise; dielectric constant (1000 cycles) = 3.60; and index of refraction = 1.5000.

According to Eq. (5), the values of the dipole conductivity and loss factor at 21.1 Mc would be

$$\kappa_\omega = V_0^2 t_0 \kappa_0 / V_\omega^2 t_\omega = (5.17)(5.30\times10^{-8})/0.329 = 83.4\times10^{-8}\ \text{ohm}^{-1}\ \text{cm}^{-1},$$

$$\Delta\kappa' = \kappa_\omega - \kappa_0 - \kappa_{\text{glass}} = (83.4 - 5.30 - 0.3)\times10^{-8} = 78.0\times10^{-8}\ \text{ohm}^{-1}\ \text{cm}^{-1},$$

$$\Delta\epsilon'' = \Delta\kappa'(1.80\times10^{12})/\nu = (78.0\times10^{-8})(1.80\times10^{12})/21.1\times10^{6} = 6.65\times10^{-2}\ \text{ohm}^{-1}\ \text{cm}^{-1}/\text{cycle}.$$

Plots of the dipole conductivity *vs.* voltage and frequency for this solution are shown in Figs. 6 and 7. In Fig. 7, the experimental values are represented by the plotted points while the course of the solid curves is determined by calculation based on the Debye theory.

THE JOURNAL OF CHEMICAL PHYSICS VOLUME 15, NUMBER 1 JANUARY, 1947

Dielectric Behavior of Solutions of Electrolytes in Solvents of Low Dielectric Constant. II. Dielectric Absorption[1]

A. H. SHARBAUGH, JR.,[2] H. C. ECKSTROM, AND C. A. KRAUS
Metcalf Research Laboratory, Brown University, Providence, Rhode Island

(Received October 16, 1946)

The dielectric losses in solutions of salts in several low dielectric constant solvents are studied as a function of frequency and concentration, using the calorimetric method. The results are interpreted according to the Debye theory, and critical frequencies, molecular radii, and dipole moments are evaluated wherever feasible. Solutions of tri-*iso*amylammonium picrate in benzene and diphenylmethane behave as a monodisperse system having a single well-defined polar structure relatively independent of concentration. Corresponding solutions of tetra-*n*-butylammonium thiocyanate, in contrast, show a marked departure from theoretical behavior for a monodisperse system, having a broad distribution of relaxation times and a high degree of association strongly dependent on concentration. Di-*n*-butyldioctadecylammonium thiocyanate shows monodisperse behavior at low concentrations, with more physically and electrically different polar bodies appearing as the concentration is increased. These results are in good agreement with polarization, conductance, and cryoscopic measurements for these systems.

THE experimental approach for measuring the dipole or "absorption conductivity" of solutions of electrolytes described in Part I of this series has been used for the study of solutions of tri-*iso*amylammonium picrate, tetra-*n*-butylammonium thiocyanate, di-*n*-butyldioctadecylammonium thiocyanate, di-*n*-butyldioctadecylammonium octadecylsulfate, tetra-*n*-butylammonium bromide, and *n*-butyl alcohol. Benzene and diphenylmethane were selected as solvents because their dielectric constants are sufficiently low to cause marked ion association and the difference in their viscosities also provides a check against theory. These results are interpreted on the basis of the Debye theory of polar molecules.[3]

EXPERIMENTAL

Commercial, thiophene-free benzene was purified by stirring with successive portions of concentrated sulfuric acid until the acid was no longer colored. The acid was removed by stirring with dilute sodium hydroxide solution, followed

[1] This paper is based on a portion of a thesis submitted by A. H. Sharbaugh, Jr., in partial fulfillment of the requirements for the degree of Doctor of Philosophy at Brown University, June, 1943.

[2] Metcalf Fellow in Chemistry at Brown University, 1941–42. Present address: General Electric Research Laboratory, Schenectady, New York.

[3] P. Debye, *Polar Molecules* (Chemical Catalog Company, New York, 1929).

by water. After drying over calcium chloride for several days, the benzene was placed in a still and refluxed over sodium-lead alloy for several more days. All solutions were made up from freshly distilled solvent. The specific conductance varied between 10^{-13}–10^{-14} ohm^{-1} cm^{-1}.

Eastman diphenylmethane was distilled, fractionally crystallized two to three times and dried over calcium chloride. M.P., 25°–26°C. Specific conductance, 4×10^{-13} ohm^{-1} cm^{-1}.

Commercial *n*-butyl alcohol was washed with sodium acid sulfite, boiled with strong sodium hydroxide solution, washed with water, and dried over ignited calcium oxide. It was distilled from fresh calcium oxide, the middle fraction being collected. Immediately before using, this product was refluxed several hours over activated alumina and distilled from it. B.P., 116.8°C. Specific conductance, 5.56×10^{-8} ohm^{-1} cm^{-1}.

Tri-*iso*amylammonium picrate was prepared by mixing equimolar quantities of tri-*iso*amylamine and picric acid in hot ethyl alcohol solution. It was purified by recrystallization from ethylene dichloride and petroleum ether. M.P., 126.5°–127.2°C (corrected).

Tetra-*n*-butylammonium thiocyanate was prepared by the method described by Kraus and Fuoss.[4] This salt was hygroscopic and all solutions were, accordingly, made from freshly vacuum-dried material. M.P., 125.5°–126.5°C (corrected).

Di-*n*-butyldioctadecylammonium thiocyanate was prepared by Dr. L. E. Strong, of this laboratory.[5] M.P., 84°–85°C (corrected).

Di-*n*-butyldioctadecylammonium octadecylsulfate was prepared by Dr. W. E. Thompson, of this Laboratory.[6] M.P., 92°–93°C (corrected).

The absorption conductivities were determined with the calorimetric dielectric absorption apparatus as described in Part I of this series.[7]

Audiofrequency measurements of conductance and dielectric constant were made by the substitution method on a special bridge built around the Campbell-Shackleton shielded ratio box for this laboratory by Leeds and Northrup.[5] With this bridge and the available conductance cells, specific conductances of the order of 10^{-13} ohm could be measured to one or two significant figures. The conductance cells were cleaned with fuming nitric acid, steamed, and baked in an oven at 140°C overnight. They were allowed to cool while a current of dry air was blown through them. In all cases, the conductance cell was placed in an air-bath and allowed to come to equilibrium before measuring. The dielectric constant and conductance measurements were made simultaneously since this bridge contained a three-terminal, quartz-insulated condenser which covered the range from 35–170 $\mu\mu$f. The condenser was calibrated and was linear to better than 0.1 $\mu\mu$f. The dielectric constant of benzene was taken to be 2.276 at 25°C[8] and the cells were calibrated against dry air and constants checked by filling with pure ether. In Table I, are listed the constants for the conductance cells where C_0 is the inherent capacity owing to leads and other strays and C is the capacity of the cell after this correction, C_0, is applied.

Viscosity measurements were made with an Ostwald viscometer which was equipped with stopcocks to prevent evaporation. The viscometer was placed in a battery jar of constant temperature water which was lagged with thermal insulating material. A synchronous motor timer was used to measure time and all the measurements were made relative to benzene.

Refractive index measurements were made with a thermostatically controlled Pulfrich refractometer.

Density measurements were accomplished by means of a Westphal balance.

THEORY

Several mathematical theories have been advanced to account for the variation of dielectric properties with the frequency of an applied

TABLE I. Characteristics of conductance cells used in bridge measurements.

	Cell constant	C($\mu\mu$f)	C_0($\mu\mu$f)
Cell *S* No. 1	0.002888	30.75	2.38
Cell *S* No. 2	0.003048	29.47	0.82
Cell *B* No. 4	0.01724	5.15	0.79

[4] Kraus and Fuoss, J. Am. Chem. Soc. **55**, 21 (1933).
[5] L. E. Strong, Thesis, Brown University (1940).
[6] W. E. Thompson, Thesis, Brown University (1941).
[7] Sharbaugh, Schmelzer, Eckstrom, and Kraus, J. Chem. Phys. **15**, 47 (1947).
[8] Smyth, *Dielectric Constant and Molecular Structure* (Chemical Catalog Company, New York, 1931).

alternating voltage. Although such theories may present different physical pictures for the mechanism of the absorption, they all postulate some form of an exponential relaxation function relating the decrease of absorption current with time. Therefore, certain relaxation frequencies where the dielectric loss per cycle reaches a maximum are predicted.

Following Debye,[3] the generalized dielectric constant ϵ may be expressed as the sum of a real and an imaginary part

$$\epsilon=\epsilon'-j\epsilon'', \tag{1}$$

where

$$\epsilon'=\epsilon_\infty+\frac{\epsilon_0-\epsilon_\infty}{1+x^2} \tag{2}$$

and

$$\epsilon''=\frac{(\epsilon_0-\epsilon_\infty)x}{1+x^2}, \tag{3}$$

$x=\omega\tau(\epsilon_0+2)/(\epsilon_\infty+2)$, ϵ_0 is the audiofrequency value of the dielectric constant, ϵ_∞ is the corresponding value at optical frequencies, $\omega=2\pi\nu$, where ν is the frequency in cycles per second. Assuming Stokes' hydrodynamics, the relaxation time for the molecules is called τ and for a spherical molecule

$$\tau=4\pi\eta a^3/kT, \tag{4}$$

where η is the viscosity of the solvent, a is the molecular radius, k is the Boltzmann constant, and T is the absolute temperature.

In order to obtain a relationship between ϵ' and ϵ'' and physically measurable quantities, we may define the complex dielectric constant ϵ of a medium in a condenser as the ratio of the admittance of the filled condenser Y to the admittance of the empty condenser Y_0.[9] It is further assumed that the filled cell may be represented by the equivalent circuit of Fig. 1; where C_0 and C_1 represent the vacuum and solution-filled capacities, respectively, G_0 is the d.c. ionic conductivity, and ΔG is the absorption conductivity. Therefore,

$$\epsilon=\epsilon'-j\epsilon''=Y/Y_0=(G_0+\Delta G+j\omega C_1)/j\omega C_0$$

and, hence,

$$\epsilon'=C_1/C_0 \tag{5}$$

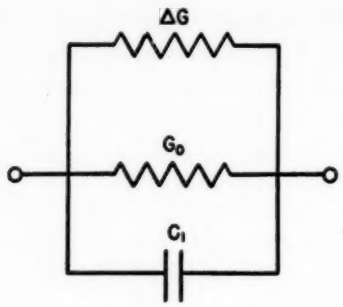

FIG. 1.

and

$$\epsilon''=(\kappa_0+\Delta\kappa)1.80\times10^{12}/\nu=\kappa_\omega 1.80\times10^{12}/\nu,$$

where κ_ω, by definition, the specific conductance of a solution at a frequency ω, equals $(G_0+\Delta G)/9\times10^{11}\times4\pi C_0$. Then, also by definition,

$$\Delta\epsilon''=\epsilon''-1.80\times10^{12}\kappa_0/\nu=1.80\times10^{12}\Delta\kappa/\nu. \tag{6}$$

$\Delta\kappa$ is in ohm^{-1} cm^{-1} and ν in cycles sec.$^{-1}$. Therefore, assuming that there is no ionic a.c. loss,[10] $\Delta\kappa$ represents the conductance owing to pure a.c. response and will be called the absorption conductivity. The quantity $\Delta\epsilon''$ is called the loss factor and gives a measure of the energy absorption per cycle. From Eq. (5), it is seen that the real part of the generalized dielectric constant, ϵ', is the quantity commonly known as dielectric constant.

By equating the derivative of Eq. (3) to zero, it may be seen that ϵ'' (which is identical to $\Delta\epsilon''$ of Eq. (6) since Eq. (3) was derived on the basis that $G_0=0$) reaches a maximum value when

$$\omega\tau=(\epsilon_\infty+2)/(\epsilon_0+2). \tag{7}$$

Under this condition, then

$$\nu_c=(\epsilon_\infty+2)/2\pi\tau(\epsilon_0+2), \tag{8}$$

where ν_c is called the critical frequency. In terms of ν_c, then Eqs. (2), (3), and (6) become

$$\epsilon'=\epsilon_\infty+\frac{\epsilon_0-\epsilon_\infty}{1+\nu^2/\nu_c^2}, \tag{9}$$

$$\Delta\epsilon''=\frac{(\epsilon_0-\epsilon_\infty)\nu/\nu_c}{1+\nu^2/\nu_c^2}, \tag{10}$$

[9] Hubert H. Race, Phys. Rev. **37**, 430 (1931).

[10] Mead and Fuoss, J. Am. Chem. Soc. **67**, 1566 (1945).

and

$$\Delta\kappa=\frac{(\epsilon_0-\epsilon_\infty)\nu^2/\nu_c}{(1+\nu^2/\nu_c^2)1.80\times10^{12}}. \qquad (11)$$

From the classical Debye theory, ν_c, as defined above, becomes

$$\nu_c=[kT/8\pi^2\eta a^3][(\epsilon_\infty+2)/(\epsilon_0+2)],$$

and when $\nu^2\ll\nu_c^2$, Eq. (11) reduces to

$$\Delta\kappa=(\epsilon_0-\epsilon_\infty)\nu^2/1.80\times10^{12}\nu_c. \qquad (12)$$

If a correction for heating of the glass of the cell is applied to $\Delta\kappa$, the corrected quantity will be denoted by $\Delta\kappa'$. These equations will be found useful in interpreting the experimental data.

In a previous paper,[7] it has been shown that the conductance at an angular frequency ω is obtained by measuring the rate of rise $\Delta h/t$ cm sec.$^{-1}$ of the level of the solution in the thermometer cell when a r.m.s. voltage $V_{\text{R.M.S.}}$ is applied to the electrodes of the cell. The relationship thus obtained is as follows:

$$\kappa_\omega=\left\{\left(\frac{\pi r^2}{0.239}\right)\left(\frac{dc}{\alpha}\right)(z)\right\}\frac{\Delta h}{V_{\text{R.M.S.}}{}^2t}, \qquad (13)$$

where r = capillary radius (cm), z = cell constant (cm^{-1}), d = density of solution (g cm^{-3}), c = heat capacity of the solution (cal. g^{-1} degree^{-1}), and α = coefficient of expansion of the solution (degree^{-1}). It was further shown that

$$\kappa_\omega=V_0{}^2t_0\kappa_0/V_\omega{}^2t_\omega \qquad (13a)$$

if the low and high frequency observations are made each time for the same solution in the same cell and for equal temperature rises. When the proportionality constant in Eq. (13) between κ_ω and $\Delta h/V_{\text{R.M.S.}}{}^2t$ is evaluated by low frequency data, a value for benzene solutions of $\alpha/dc=0.00300$ is obtained. This value of α/dc is used in the calculation of κ_ω for those solutions where the correction owing to the conductance of the glass is large in comparison with that for the solution, unless, in using Eq. (13a), the conductance of the glass cell does not dominate the conductance of the solution itself.

In most cases, however, the proportionality constant between κ_ω and $\Delta h/V_{\text{R.M.S.}}{}^2t$ was determined for each individual solution by a determination of $\Delta h/V_{\text{R.M.S.}}{}^2t$ at 60 cycles or 0.1 Mc where the conductance was assumed to be that measured at audiofrequencies. Generally, $\Delta h/V_{\text{R.M.S.}}{}^2t$ was obtained from the slope of the straight line plot of $(\Delta h/t)^{\frac{1}{2}}$ *vs.* V. In some cases, it was found that, because of small errors in the voltage measurement, the intercept did not always pass exactly through the origin. Within the limits of experimental error, a straight line plot, indicating no variation of conductance with field strength, was always obtained. All values of absorption conductivity have been corrected for heating of the glass in the cell. These corrections were negligibly small except in the case of the very dilute solutions.

We have calculated the values of the dipole moment by using the following equation, derived by Debye,[11] for dilute solutions (where the loss is proportional to the mole fraction of the solute), where $\omega^2\tau^2\ll1$ and $\epsilon''\ll\epsilon'$:

$$\mu=\{w[3/(\epsilon_0+2)]^2[2M_1/\omega^2d_1]\times[3kT/N\tau][1/N_2E^2]\}^{\frac{1}{2}}. \qquad (14)$$

Here, μ = dipole moment (e.s.u.), w = heat generated (ergs cc^{-1} sec.$^{-1}$), ϵ_0 = static dielectric constant of solvent at low frequencies (e.s.u.), M_1 = molecular weight of solvent, ω = angular frequency (ra. sec.$^{-1}$), d_1 = density of solvent (g cm^{-3}), $k=1.37\times10^{-16}$ (ergs degree^{-1}), T = absolute temperature, N_2 = mole fraction of solute, $N=6.06\times10^{23}$, τ = relaxation time (sec.) and E = field strength (peak statvolts cm^{-1}). From considerations of the thermometer cell, it is seen that

$$w=4.18\times10^7d_1c\pi r^2\Delta h/\alpha tAx, \qquad (15)$$

where A, the effective area of the cell electrodes, is calculable from the cell constant, and where x is the separation of the electrodes. When w is expressed in terms of the loss factor $\Delta\epsilon''$ with the help of Eqs. (6) and (13) and substituted in Eq. (14), we have

$$\left.\begin{aligned}\mu&=1.12\times10^{-21}(\Delta\epsilon''/\nu\tau c)^{\frac{1}{2}}\text{ e.s.u.}\\&\qquad\text{for benzene solutions, and}\\\mu&=1.05\times10^{-21}(\Delta\epsilon''/\nu\tau c)^{\frac{1}{2}}\text{ e.s.u.}\\&\qquad\text{for diphenylmethane solutions,}\end{aligned}\right\} \qquad (16)$$

where ν is the frequency in megacycles, τ is in seconds and c is molarity. It is understood that the multiplier, $(1+[2\times10^6\pi\nu\tau]^2)^{\frac{1}{2}}$, must be used

[11] P. Debye, Physik. Zeits. **35**, 101 (1934).

in Eq. (14) when $[2\times10^{6}\pi\nu\tau]^2$ is not very much less than unity.

RESULTS

In Table II are presented the dielectric constants measured for all investigated solutions as a function of concentration and frequency. The number of significant figures listed for each value was determined by the favorability of experimental conditions of frequency, conductance and cell geometry. The last digit of each constant must be considered doubtful. All figures are relative to that of benzene, whose dielectric constant was taken to be 2.276 at 25°C.[8] Some solutions exhibit a large variation with frequency around 1000 cycles and these values must be regarded with caution as they undoubtedly do not represent the true dielectric constant. In these cases, the asymptote values have been taken as ϵ_0. Further investigations must be carried out to explain completely these pseudodispersons.

TABLE II. Audiofrequency dielectric constant data.

Molarity	Frequency (cycles/second) 200	500	1000	2000	4000	6000	7500
A. Tetra-n-butylammonium thiocyanate in benzene							
1.51×10^{-4}	2.276	2.275	2.276	2.276	2.275	2.276	2.275
3.66×10^{-3}	2.289	2.287	2.288	2.278	2.288	2.287	2.293
9.36×10^{-3}	2.34	2.322	2.319	2.315	2.315	2.312	2.310
1.72×10^{-2}	2.45	2.425	2.409	2.400	2.389	2.384	2.374
2.66×10^{-2}	4.28	2.78	2.62	2.53	2.56	2.55	2.57
4.28×10^{-2}	14.4	8.8	5.24	3.52	2.95	2.91	2.86
in diphenylmethane containing 17% benzene							
9.73×10^{-3}	2.606	2.605	2.602	2.598	2.597	2.597	2.597
B. Tri-isoamylammonium picrate in benzene							
8.49×10^{-3}	2.41	2.40	2.411	2.409	2.414	2.393	2.412
9.34×10^{-3}	3.86	3.70	3.69	3.67	3.69	3.69	3.71
in diphenylmethane							
1.03×10^{-2}	2.786	2.784	2.783	2.780	2.780	2.781	2.780
6.89×10^{-2}	4.62	3.98	3.77	3.71	3.68	3.64	3.65
C. Dibutyldioctadecylammonium thiocyanate in benzene							
8.99×10^{-4}	2.26	2.279	2.277	2.277	2.276	2.276	2.279
8.41×10^{-3}	2.42	2.37	2.360	2.345	2.335	2.331	2.314
1.12×10^{-2}	2.49	2.437	2.411	2.395	2.386	2.370	2.370
1.37×10^{-2}	2.79	2.617	2.541	2.509	2.495	2.488	2.487
in diphenylmethane containing 30% benzene							
8.34×10^{-3}	2.732	2.700	2.684	2.680	2.674	2.653	2.650
D. Tetra-n-butylammonium bromide in benzene							
3.67×10^{-3}	—	2.282	2.280	2.280	2.280	2.280	2.280
E. Butyl alcohol in benzene							
2.11×10^{-3}	2.271	2.272	2.271	2.273	2.272	2.272	2.272
F. Dibutyldioctadecylammonium octadecylsulfate in benzene							
4.00×10^{-4}	2.27	2.285	2.284	2.284	2.284	2.284	2.284
G. Pure butyl alcohol							
—	18.2	17.8	17.7	17.7	17.7	17.6	17.7

In Table III are summarized all quantities pertinent to the Debye theory. The dielectric constants are taken from Table II for 1000 cycles or the asymptotic limit in cases of dispersion, and benzene was the solvent in all cases except as indicated. Polarizations were calculated on the basis of the Clausius-Mosotti relationship. The symbols used are m, molality; c, molarity; κ_0, specific conductance at 1000 cycles; ϵ_0, dielectric constant (either at 1000 cycles or asymptote value); n, index of refraction; d, density; η, viscosity (poises); P_2, molar polarization of solute (cc) and P_1, molar polarization of the solvent (cc).

DISCUSSION

A. Solvents.—In general, determinations were made with the non-polar solvent benzene. A few observations were made with diphenylmethane as the solvent in order to shift the relaxation frequency to lower frequencies since its viscosity is nearly five times that of benzene. With thermometer cell No. 3 filled with pure benzene, a loss factor $\epsilon''=0.0025$ was measured which was independent of frequency. With the other two thermometer cells, the apparent loss factor was about one-tenth as great and varied somewhat with frequency, approaching a constant value with increasing frequency. Since the trends and amounts of these losses could be reproduced with pure diphenylmethane in the cell, it was concluded that these losses must be caused by the heating of the glass and, possibly, by the leads going to the electrodes. In all cases, a correction has been made for this heating which was negligibly small in all but the most dilute solutions.

B. Pure Butyl Alcohol.—On making the assumption attendant to Eq. (12), *viz.*, that the critical frequency is sufficiently high to make the measuring frequency small by comparison, a straight line plot is to be expected for the absorption conductivity as a function of the square of the frequency. Figure 2 indicates this to be the case here. Applying Eq. (12), a value of 1600 Mc (19 cm) is found for the critical frequency. The values of ν_c found for butyl alcohol by different observers,[12] are not in complete agreement and the underlying reasons need to

[12] C. Schmelzer, Ann. d. Physik 28, 35 (1937).

TABLE III. Constants measured for all investigated solutions and pure solvents at 25°C.**

Salt	m	c	d	η	ϵ_0	κ_0	$\epsilon_\infty = n^2$	P_2 or P_1
Bu_4NCNS	1.73×10^{-4}	1.51×10^{-4}	0.8735	0.00607	2.276	2.45×10^{-11}	2.244	5000
Bu_4NCNS	4.17×10^{-3}	3.66×10^{-3}	0.8747	0.00606	2.288	1.92×10^{-9}	2.244	740
Bu_4NCNS[1]	9.84×10^{-3}	9.73×10^{-3}	0.9890	0.0223	2.597	7.83×10^{-9}	2.451	—
Bu_4NCNS	1.07×10^{-2}	9.36×10^{-3}	0.8740	0.00614	2.310	6.91×10^{-9}	2.244	910
Bu_4NCNS	1.98×10^{-2}	1.72×10^{-2}	0.8743	0.00623	2.374	4.06×10^{-8}	2.244	1040
Bu_4NCNS	3.07×10^{-2}	2.66×10^{-2}	0.8750	0.00635	2.57	1.59×10^{-7}	2.244	1600
Bu_4NCNS	4.95×10^{-2}	4.28×10^{-2}	0.8762	0.00668	2.86	6.54×10^{-7}	2.244	2100
i-Am_3NHPi	9.72×10^{-3}	8.49×10^{-3}	0.8770	0.00612	2.411	1.15×10^{-11}	2.246	2600
i-Am_3NHPi	1.11×10^{-1}	9.34×10^{-2}	0.8825	0.00657	3.69	5.30×10^{-8}	2.250	1610
i-Am_3NHPi[2]	1.07×10^{-2}	1.03×10^{-2}	1.0030	0.0290	2.780	3.13×10^{-10}	2.415	2600
i-Am_3NHPi[2]	6.94×10^{-2}	6.89×10^{-2}	1.0060	0.0318	3.65	1.19×10^{-7}	2.480	1920
Bu_2Oct_2NCNS	1.03×10^{-3}	8.99×10^{-4}	0.8735	0.00607	2.277	2.79×10^{-10}	2.242	1200
Bu_2Oct_2NCNS	9.69×10^{-3}	8.41×10^{-3}	0.8735	0.00624	2.314	2.21×10^{-8}	2.242	1040
Bu_2Oct_2NCNS[3]	8.67×10^{-3}	8.34×10^{-3}	0.9620	0.0165	2.650	4.46×10^{-8}	2.402	—
Bu_2Oct_2NCNS	1.30×10^{-2}	1.12×10^{-2}	0.8743	0.00638	2.370	4.55×10^{-8}	2.242	1600
Bu_2Oct_2NCNS	1.58×10^{-2}	1.37×10^{-2}	0.8750	0.00644	2.487	7.89×10^{-8}	2.242	2120
$Bu_2Oct_2NOctSO_4$	4.58×10^{-4}	4.00×10^{-4}	0.8735	0.00607	2.284	3.00×10^{-11}	2.243	5300
$BuOH$	2.41×10^{-3}	2.11×10^{-3}	0.8735	0.00608	2.272	1.22×10^{-12}	2.244	—
Bu_4NBr	4.21×10^{-3}	3.67×10^{-3}	0.8735	0.00609	2.280	9.21×10^{-10}	2.242	—
C_6H_6	Pure solvent		0.8735	0.00605	2.276	10^{-13}–10^{-14}	2.243	$(P_1)26.6$
$BuOH$	Pure solvent		0.8082	0.0246	17.7	5.56×10^{-8}	1.954	$(P_1)77.6$
Ph_2CH_2	Pure solvent		1.0028	0.0289	2.591	4×10^{-13}	2.484	$(P_1)58.1$

** The solvent was benzene except as indicated. Bu, butyl; Ph or Φ, phenyl; Oct., octadecyl; Pi, picrate.
[1] Solvent: 83 percent diphenylmethane—17 percent benzene.
[2] Solvent: Diphenylmethane.
[3] Solvent: 69 percent diphenylmethane—31 percent benzene.

be further investigated. In all likelihood, the discrepancies are caused by losses contributed by unknown amounts of unknown electrolyte impurities in the alcohol, depending on the degree of purification.

C. Dibutyldioctadecylammonium Octadecylsulfate.—This salt was investigated to determine the magnitude of the absorption by a salt having a long chain group on both the cation and the anion. Unfortunately, the salt is not very soluble in benzene at 25° and, hence, only a single concentration was within the range of the apparatus. These values are subject to considerable error because of large corrections for heating of the cell. Figure 3 shows the same linearity of absorption conductivity with the square of the frequency as with butyl alcohol. Therefore, this salt at this concentration behaves as a monodisperse system where Debye's equations are valid. The nearly perfect agreement with theory is shown in Fig. 4 where the drawn-in curves, calculated from Eqs. (10) and (11) for $\epsilon_0=2.284$, $\epsilon_\infty=2.243$, and $\nu_c=1500$ Mc, coincide well with the experimental points. The effective radius $a=3.8\times10^{-8}$ cm is surprisingly small in comparison with that of other molecules calculated on the same basis.

D. Tri-isoamylammonium Picrate.—This salt was selected as being representative of a weak electrolyte in a benzene solution. Both its ions are unsymmetrical with respect to shape and charge; the major portion of the positive charge being located on the nitrogen atom of the Am_3NH^+ ion, and most of the negative charge of the picrate ion being centered on the oxygen atom. Determinations were made at two concentrations of this salt in both benzene and diphenylmethane in order to study the effects of concentration and solvent viscosity. The results are plotted in Fig. 5 on a log-log scale in order to cover the wide range of values. First, it is to be noted that, according to the Debye theory, this type of plot should yield a straight line with a value of $d(\log\Delta\epsilon'')/d\log\nu=1$, if the measurement frequencies are small in comparison with the critical frequency. Within the limits of experimental error, this is seen to be the case here, there being some small deviation from linearity at the lowest frequencies for the two diphenylmethane solutions. It should be remembered that the probable error for the values of $\Delta\epsilon''$ at low frequencies is greater than at higher frequencies where the amount of absorption is much larger. In Fig. 5, the theoretical straight line was drawn in for comparison with the experimental results, and calculations have been made

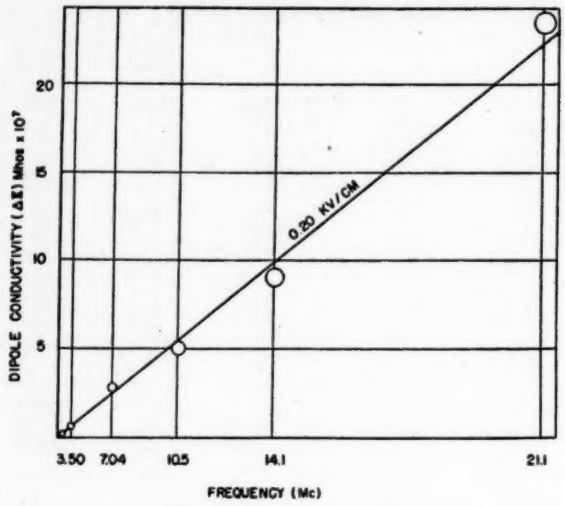

Pure butyl alcohol
$\kappa_0 = 5.56 \times 10^{-8}$
Field strength = 0.20 kv/cm.

FIG. 2. Dipole conductivity as a function of frequency squared.

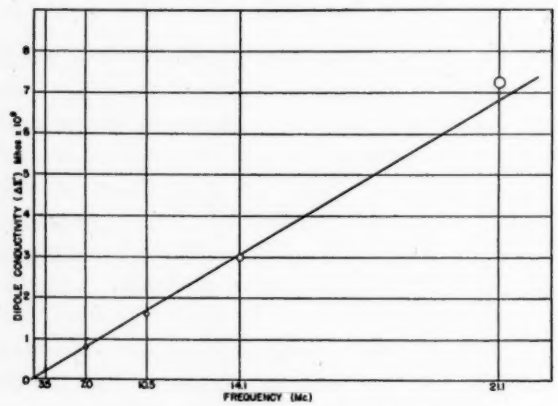

4.00×10^{-4} molar $Bu_2Oct_2NOctSO_4$ in C_6H_6
$\kappa_0 = 3.00 \times 10^{-11}$
Field strength = 1.5 kv/cm.

FIG. 3. Dipole conductivity as a function of frequency squared.

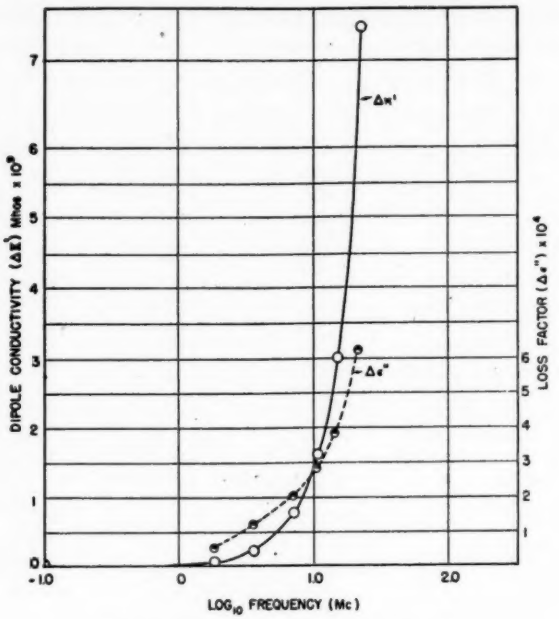

4.00×10^{-4} molar $Bu_2Oct_2NOctSO_4$ in C_6H_6
$\kappa_0 = 3.00 \times 10^{-11}$
Field strength = 1.5 kv/cm.

FIG. 4. The dependence of dipole conductivity and loss factor on frequency.

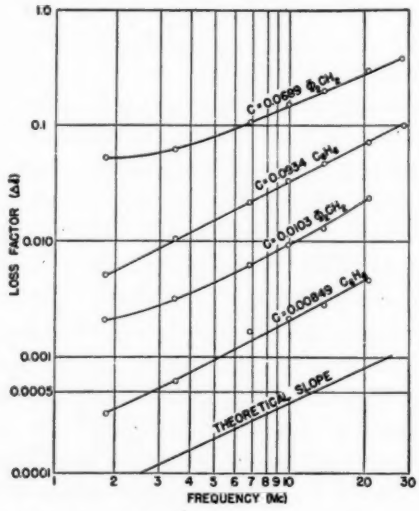

FIG. 5. The dependence of loss factor on frequency for *i*-Am_3NHPi in C_6H_6 and Φ_2CH_2.

on the basis of the straight line portions of the curves. From Eqs. (12), (8), and (4), values for the critical frequency, relaxation time and molecular radius have been calculated and are listed in Table IV. Unfortunately, the cell corrections for heating of the glass were large in comparison with the absorption heating for the two most dilute solutions, and, therefore, calculated figures for these two solutions can only be regarded as approximate.

The good agreement of the loss factor-frequency curves with theory affords evidence that this salt at these concentrations forms a monodisperse system and thus indicates the existence of rotating dipolar body of well-defined dimensions. The calculated radii show good agreement and show that the effective spherical radius remains the same in spite of tenfold concentration and fivefold viscosity changes. The excellent

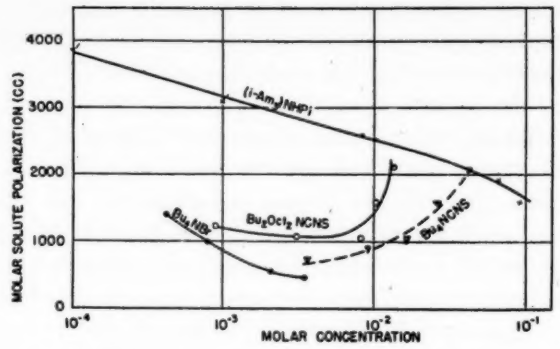

FIG. 6. Dependence of molar solute polarization on concentration (points with tails measured by Strong and by Geddes).

agreement with theory is to be noted in the case of the 0.0934 molar benzene and 0.0694 molar diphenylmethane solutions.

Although there are large cell corrections for the two dilute solutions, it is seen that the loss is roughly proportional to the concentration times viscosity at a given frequency. For a precise determination of the dipole moment, it would be necessary to investigate a larger number of concentrations making an extrapolation to infinite dilution, but it is interesting to note the value of $\mu = 12\times10^{-18}$ e.s.u. obtained by the use of Eq. (14). This value is in good agreement with the value of 13.3×10^{-18} e.s.u. obtained by dielectric constant (ϵ') measurements.[13]

The molecular radius obtained from the loss measurements on the more concentrated solutions is 5.2×10^{-8} cm. This figure compares favorably with the value of 5.05×10^{-8} cm which was independently obtained from polarization

TABLE IV. Constants calculated on the basis of the Debye theory.

Salt	Molar concentrations, c	Critical frequency ν_c(Mc)	Relaxation time τ(sec.)	Molecular radius a(A)	Dipole moment μ(D)	Solvent
$Bu_2Oct_2NOctSO_4$	4.00×10^{-4}	1500	1.1×10^{-10}	3.8	27.6	C_6H_6
$i\text{-}Am_2NHP_i$	8.49×10^{-3}	700	2.2×10^{-10}	4.9	11.8	C_6H_6
$i\text{-}Am_2NHP_i$	9.34×10^{-2}	430	2.8×10^{-10}	5.2	12.7	C_6H_6
$i\text{-}Am_2NHP_i$	1.03×10^{-2}	380	3.9×10^{-10}	3.5	15.9	Ph_2CH_2
$i\text{-}Am_2NHP_i$	6.89×10^{-2}	87	1.5×10^{-9}	5.3	12.5	Ph_2CH_2
Bu_2Oct_2NCNS	8.34×10^{-2}	4.5	3.5×10^{-8}	21	8.7	69% Ph_2CH_2, 31% C_6H_6
Bu_2Oct_2NCNS	8.41×10^{-3}	21	7.5×10^{-9}	16	5.7	C_6H_6
Bu_2Oct_2NCNS	1.12×10^{-2}	3.5	4.4×10^{-8}	28	6.6	C_6H_6
Bu_2Oct_2NCNS	1.37×10^{-2}	1.8	8.7×10^{-8}	35	7.7	C_6H_6
Bu_4NCNS	9.73×10^{-3}	150	1.0×10^{-9}	5.2	11.0	83% Ph_2CH_2, 17% C_6H_6
Bu_4NCNS	9.36×10^{-3}	384	4.1×10^{-10}	6.0	8.0	C_6H_6

[13] C. A. Kraus, J. Frank. Inst. 225, 687 (1938).

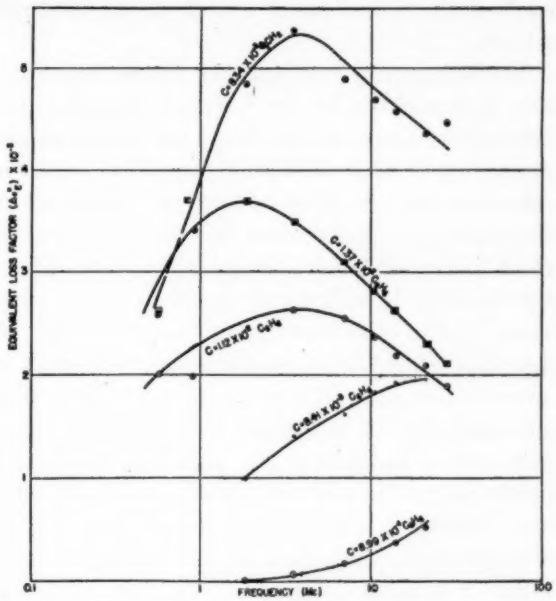

FIG. 7. Equivalent loss factor as a function of concentration and frequency for Bu_2Oct_2NCNS in C_6H_6 and Φ_2CH_2.

measurements. This latter value represents the minor diameter of an ellipsoidal model, where the ratio of major to minor axes is taken as 2:1 and is calculated by an equation developed by Fuoss.[14] These dimensions are also in accord with the value of 5.54×10^{-8} cm calculated from cryoscopic measurements for the ellipsoidal model, using the value of 12.9×10^{-18} e.s.u. for the dipole moment.

Examination of the values of molar solute polarization P_2 (Fig. 6) for this salt shows a relatively slow decrease with increasing concentration. This is interpreted as meaning that the loss factor per mole should be nearly constant (for constant frequency and relaxation time) and association of the dipole ion-pairs into non-polar quadrupoles or other higher order non-polar aggregates is occurring only on a small scale. This interpretation has been further confirmed by cryoscopic measurements for this salt in benzene where it has been found that the polymerization number is only about 1 at 0.01 molar and 1.5 at 0.1 molar.[15] Since our loss measurements show $\Delta\epsilon''$ to be proportional to the (concentration)$\times$(viscosity) and the molecular radius is constant, we are in complete agree-

[14] R. M. Fuoss, J. Am. Chem. Soc. 56, 1031 (1934).
[15] Copenhafer, Thesis, Brown University (1942).

ment with these other independent determinations.

Audiofrequency conductance values as a function of concentration for tri-*iso*amylammonium picrate[5] are also in accord with the simple dipole picture for this salt with unsymmetrical ions. No inflections are observed beyond the minimum of the equivalent conductance-concentration curve, which increases uniformly up to a value where the viscosity is sufficiently large to cause a decrease in the observed conductance. It is to be observed that the conductance-concentration curve is very steep at concentrations above that corresponding to the minimum in the conductance curve, indicating the presence of ions of higher degree of clustering than triple-ions. However, the very low conductance of this salt in benzene shows that the total ionic concentration is but a minute fraction of the stoichiometric concentration for ternary ammonium salts; hence, most of the salt is present as non-conducting ion-pairs, at any rate, neutral aggregates. The absence of inflections at concentrations above the minimum is in accord with the assumption that association is predominantly dipolar so that a spread of relaxation times would not be expected.

E. Dibutyldioctadecylammonium Thiocyanate. —Structurally speaking, this salt offers a transition between the highly unsymmetrical ions of tri-*iso*amylammonium picrate, previously discussed, and the highly symmetrical ions of tetra-*n*-butylammonium thiocyanate; that is, the dipole of this ion-pair (Bu_2Oct_2NSCN) is composed of an unsymmetrical positive ion and a symmetrical negative ion.

Figure 7 shows the dependence of the equivalent loss factor on frequency, the equivalent loss factor being simply the conventional quantity divided by the number of moles per liter. This type of presentation has been used in order to emphasize the relation between the loss and concentration. Measurements were made at four different concentrations in benzene and one in diphenylmethane. The values measured at the lowest concentration were nearly out of the range of the apparatus and, hence, must be regarded as giving order of magnitude only. The scattering of points is marked at the low frequencies because of the low losses involved but, if the expected logarithmic symmetry prevails, these points line up with the expected curve within experimental error.

TABLE V. Theoretical and experimental absorption maxima for dibutyldioctadecylammonium thiocyanate.

Moles/Liter	Solvent	$(\epsilon_0-\epsilon_\infty)/2$	$\Delta\epsilon_{max}''$(expt.)	α
8.99×10^{-4}	C_6H_6	0.0175	—	0
8.41×10^{-3}	C_6H_6	0.0360	0.017	0.43
1.12×10^{-2}	C_6H_6	0.0640	0.029	0.46
1.37×10^{-2}	C_6H_6	0.122	0.050	0.50
8.34×10^{-3}	Φ_2CH_2	0.124	0.045	0.56

Examination of these curves shows an increasing amount of loss per mole with increasing concentration. This means that the polarity of the complex formed is increasing as indicated by the rising molar polarizations (Fig. 6), calculated from the dielectric constant measurements. From the dispersion theory, we expect the maximum loss to be $(\epsilon_0-\epsilon_\infty)/2$ for a given dispersion region. In Table V are listed these computed maxima for the dibutyldioctadecylammonium thiocyanate solutions measured, along with the experimental maxima. It is noted that in common with dispersion data in general, the measured loss factor is considerably lower than that predicted by theory. In accordance with the empirical equation suggested by the Coles,[16] the parameter α may be computed from the maximum values of $\Delta\epsilon''$. These are listed in Table V where it is seen that α is of the order of magnitude of one-half. Mathematically, a value of this parameter $\alpha\neq0$ is consistent with a general spread of the loss factor values about a center relaxation frequency and a simultaneous decrease of the maximum from the value $(\epsilon_0-\epsilon_\infty)/2$. It is found that all the curves agree qualitatively over the frequency range covered with the values predicted by the Cole equation where $\alpha=0.5$. The regular increase of α with concentration is to be noted. The value of $\alpha=0$ for the 8.99×10^{-4} solution was determined by the linear dependence of $\Delta\epsilon''$ upon frequency for this concentration at frequencies much lower than the critical frequency. This means that, at low concentrations, the salt is behaving as a monodisperse system with a single, well-defined polar structure, and that more physically and electrically different polar bodies are appearing with increasing concentration giving rise to the spread of relaxation times.

[16] K. S. and R. H. Cole, J. Chem. Phys. 9, 341 (1941).

The shift of critical frequencies to lower values with increasing concentrations would seem to indicate that larger polar aggregates are being formed. The molecular radii computed from the mean relaxation frequencies are listed in Table IV and show that an extremely large aggregate ($a=35\times10^{-8}$ cm) has been formed by the time the concentration has reached 1.37×10^{-2} molar. Since $a=28\times10^{-8}$ at 1.12×10^{-2} molar, the polar cluster is undergoing a very rapid change in size in this concentration range.

Again, to check the validity of the assumed theory, measurements were made at approximately the same concentration in both the solvents—benzene and diphenylmethane. For 8×10^{-3} molar solutions with a 1:2.7 ratio of viscosities, a shift in critical frequencies of 1:4.7 was found. The quantitative agreement is not very good but is probably satisfactory in view of the departure from typical Debye behavior which all the more concentrated solutions of the salt show.

With increasing concentration, the benzene solutions of dibutyldioctadecylammonium thiocyanate show a steady increase in dipole moment as listed in Table IV. These moments were calculated from Eq. (16) using values of the loss factor measured at each of the critical frequencies. The values of solute polarization for 8.41×10^{-3}, 1.12×10^{-2}, and 1.37×10^{-2} molar benzene solutions were calculated to be, respectively, 1040, 1600, and 2120 from the measured values of ϵ_0. The ratio of these polarizations is 0.49:0.75:1 as compared with the ratio of the squares of the dipole moments which is 0.55:0.74:1. The agreement with theory is, therefore, satisfactory. Here, as with other salts of more symmetrical ions, a minimum in the polarization-concentration curve is found (see Fig. 6) around 0.005 molar. Fuoss[14] has shown that in the limit for dilute solutions, the polarization values should decrease linearly with increasing concentration when there is anti-parallel association of polar dipoles into non-polar quadrupoles. The existence of the minimum would indicate that a competing interaction is taking place which results in forming increasing numbers of polar aggregates of higher complexity.

In view of the large radii calculated for this salt at these concentrations, the charges must be located with a high degree of symmetry and the charge centroids separated by a distance of the order of molecular dimensions. An idea of the comparatively small separation of unit point charges to give $\mu=7.7\times10^{-18}$ e.s.u. may be found by dividing by the unit charge 4.77×10^{-10}, giving a separation of 1.6×10^{-8} cm.

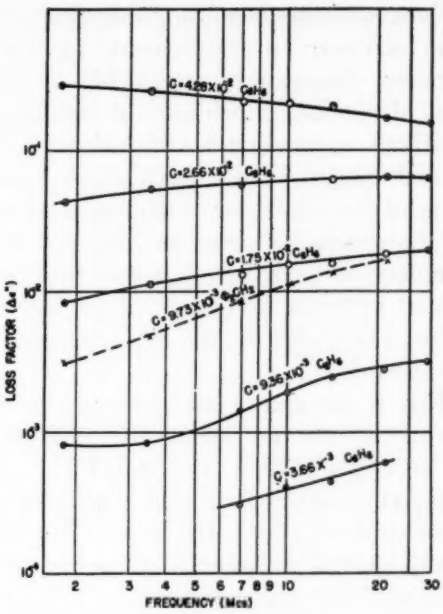

FIG. 8. Loss factor as a function of concentration and frequency for Bu_4NCNS in C_6H_6 and Φ_2CH_2.

Conductance data of Strong[5] for solutions of dibutyldioctadecylammonium thiocyanate in benzene show the characteristics of triple-ion formation up to about 0.1 molar where an aggregate of high stability is formed at the expense of other conducting particles. The rapid increase in polarization and molecular radius observed in the loss measurements above 0.01 molar concentration may be interpreted as evidence in support of the formation of a large and stable polar cluster indicated in the conductance measurements.

That an extremely high degree of association for these long chain salts takes place is demonstrated by cryoscopic measurements[15] on *n*-octadecyltri-*n*-butylammonium formate which has already reached a polymerization number of 10 at 0.001 molal and 21.5 at 0.00326 molal. These data are qualitatively in accord with the results derived from the loss data for dibutyldioctadecylammonium thiocyanate.

F. Tetra-n-butylammonium Thiocyanate.—This salt, in contrast to the ternary picrate and quaternary thiocyanate previously discussed, consists of two ions which may be considered to be relatively symmetrical with respect to both shape and charge. For such symmetrical salts in solvents of low dielectric constant, all the evidence from dielectric constant, cryoscopic and conductance measurements points to a highly associated molecule accompanied by a complex behavior. The dielectric loss measurements here are no exception.

In Fig. 8 are shown the loss factor *versus* frequency results for 3.66×10^{-3}, 9.36×10^{-3}, 1.75×10^{-2}, 2.66×10^{-2}, and 4.28×10^{-2} molar solutions in benzene. It is seen that within this range of concentrations, the absorption peak is gradually shifted to lower frequencies with increasing concentration until, with the most concentrated solution, the portion of the curve has been reached when the loss factor is decreasing with increasing frequency. Table III shows that the viscosity change with concentration could not be very effective in changing the relaxation times for the benzene solutions of tetra-*n*-butylammonium thiocyanate; hence, the increase of relaxation times must be ascribed chiefly to an increase in the size of the polar aggregate. The flatness of the curves suggests that with this salt we have a large spread of relaxation times about some mean value.

With the 2.66×10^{-2} molar solution, we are close to the absorption maximum at 30 Mc, reaching a value of $\Delta\epsilon''=0.065$. For this concentration, $\epsilon_0=2.62$ and $\epsilon_\infty=2.244$; hence, the predicted maximum is $(\epsilon_0-\epsilon_\infty)/2=0.188$, which is three times as large as the experimentally measured loss. From the relation between ϵ_0, ϵ_∞, and $\Delta\epsilon_{max}''$, we may compute $\alpha=0.58$ and, using this value of α, the solid curve drawn in Fig. 8 was computed for this concentration ($2.66\times10^{-2}M$) from the modified Debye equation.[16] The lineup, with the experimental points as indicated by the circles, is excellent.

If we may assume that the points for the 3.66×10^{-3} molar solution lie on a straight line and, therefore, that the measurement frequencies are very much lower than the critical frequency, we see that $\Delta\epsilon''$ is increasing with the 0.75 power of the frequency. Accordingly, $\alpha=0.25$ for this concentration, indicating less spread of relaxation times than for the more concentrated solutions.

From Table III, it is seen that the ratio of viscosities for 9.7×10^{-3} and 9.4×10^{-3} molar solutions in diphenylmethane-benzene mixture and in benzene, respectively, is 3.7:1, while the ratio of the relaxation times computed from Eqs. (12) and (8), using the average slopes of the $\Delta\epsilon''$-frequency curves, is 2.4:1. It is to be noted that here the relaxation times are more nearly proportional to η/V_m (where V_m is the molecular volume) than they are to η.

The gradual increase of the loss factor per mole with increasing concentration is consistent with the molar polarization-concentration curve for this salt (see Fig. 6). Of course, a part of this increase is due to the shifting of the relaxation frequency to lower values with increasing concentration. With a nominal frequency coverage of only one decade, it is impossible to separate these two effects.

The existence of a large number of aggregates of different sizes with overlapping dispersion regions is concordant with cryoscopic measurements on this salt. The freezing point measurements show that the polymerization number increases from 2.7 to 12.3 in the range from 0.004 to 0.049 molal.[15]

Conductance measurements[5] for this salt as a function of concentration yield a very complex curve having a minimum followed by some five inflections which indicate equilibria between a variety of neutral and charged ionic species of higher order.

ACKNOWLEDGMENT

The authors are grateful to Professor Raymond M. Fuoss for his advice and for much helpful discussion in the preparation of the first two papers in this series.

THE JOURNAL OF CHEMICAL PHYSICS VOLUME 15, NUMBER 1 JANUARY, 1947

Pressure Broadening in the Infra-Red and Optical Collision Diameters*

NORMAN D. COGGESHALL AND ELEANOR L. SAIER
Gulf Research and Development Company, Pittsburgh, Pennsylvania

(Received October 29, 1946)

The pressure broadening effects of a number of foreign gases on the infra-red absorption of methane at 7.65μ have been determined. Also the pressure broadening effects of a number of foreign gases on the absorption of carbon dioxide at 4.3μ and 14.8μ have been investigated. The data have been analyzed to obtain optical collision diameters for the various gases and the absorbers. By optical collision is meant any collision which is effective in interrupting the processes of radiation absorption. The data are discussed in terms of the Lorentz theory of pressure broadening and are shown to confirm it. From the results obtained, it is clear that the pressure broadening effects of certain gases on one absorber cannot be reliably extrapolated to predict the effects on another absorber. Also the effects at one wave-length are not in general the same at another wave-length for the same absorber. The optical collision diameter effective for a foreign gas and an absorbing gas at a particular wave-length is a specific function of the two gases and the wave-length. Empirical results on the shape of the curves obtained are presented. The deviation from Beer's law of absorption evidenced by isobutylene at 11.23μ is shown to be not due to pressure broadening.

A NUMBER of gases are known to deviate from Beer's law of absorption when examined in the infra-red region. For example, the optical density of a given gas at a particular wave-length will depend upon the partial pressure but not be directly proportional to it. Also for these gases the optical density will, in general, depend upon the total gas pressure in the sample. For those gases whose molecules possess small moments of inertia and appreciable spacing between the rotational fine structure, these deviations from Beer's law are explained in terms of the Lorentz pressure broadening theory. This subject has been theoretically studied by a number of investigators,[1–3] and their results show that the shape of a rotational line is dependent upon the frequency of molecular collisions. Dennison[2] showed that this change of shape together with a consideration of the energy transmittance of a spectrometer would explain some of the characteristics of the infra-red spectrum of HCl.

A complete application of the theories of Dennison and others to the treatment of experimental data for any particular gas is very difficult unless the data have been obtained with a spectrometer of quite high resolution. However, with instruments of medium resolution, data may be obtained which can be interpreted to give information about the optical collision diameters of the gases studied. The optical collision diameters are the diameters which govern the frequency of effective collisions between molecules of absorbing gas or of absorbing and foreign gas. By effective collisions are meant collisions which are effective in interrupting the processes of radiation absorption.

The present work is an experimental study of the effects of various foreign gases on the infra-red absorption of methane, carbon dioxide, and isobutylene. Optical collision diameters between various pairs of molecules are obtained and discussed. The data show that results for one absorbing gas can only be applied in a general way in predicting the behavior of another.

EXPERIMENTAL DETAILS

The spectrometer used in this work was an NaCl prism type.[4] The method of obtaining optical densities for the gas mixtures was the same as described by us elsewhere.[5] In it, the

* Some of this material was presented at the Symposium on Molecular Spectroscopy and Molecular Structure, Ohio State University, June, 1946.

[1] H. A. Lorentz, *The Theory of Electrons* (Stechert & Company, New York, 1909), note 57.

[2] D. M. Dennison, Phys. Rev. **31**, 503 (1928).

[3] J. H. Van Vleck and V. F. Weisskopf, Rev. Mod. Phys. **17**, 227 (1945).

[4] Model 12-A manufactured by the Perkin-Elmer Corporation, Glenbrook, Connecticut.

[5] N. D. Coggeshall and E. L. Saier, J. App. Phys. **17**, 450 (1946).

radiation intensities are measured by a null method, which allows greater accuracy and convenience than the method of measuring galvanometer deflections. The optical densities were obtained by using a pair of cells. One of these cells was the gas cell and the other an evacuated comparison cell. The gas cell was evacuated, and the ratio of its transmission to that of the comparison cell was obtained for each wavelength being investigated. These ratios were then combined with the corresponding ones obtained for the sample in the gas cell to get the true optical densities.

Two absorption cells were used, one of 9.50 cm length and one of 3.15 cm length. Both had NaCl windows and were mounted in the manner described in reference 5. The spectrometer and gas blending equipment were located in an air conditioned room in which the temperature was kept within 1°C of a mean value. This was significant as the temperature is an important parameter in pressure broadening, and our method of analyzing the data required that it be constant. The blending and mixing of the gases was achieved in either of two ways, depending upon the relative concentrations of the components. One of these involved a special blending system in which mixing was achieved in a reservoir by moving an iron vane by means of exterior magnets. The other method was to introduce both gases into the absorption cell and mix them there by mechanical motion. This was possible as the cell contained a metal vane which lay out of the optical path when the cell was in an operating position, but which could otherwise be moved throughout the interior to mix the gases. A thorough mixing of the components is very important in obtaining data of this sort. The gases used were the purest obtainable commercially,[6] and in each case the impurities present were of such small concentration as not to affect the results.

DATA AND DISCUSSION

According to the Lorentz theory, the absorption for the individual line as a function of frequency has the form,

$$K(\gamma)=\frac{a_i nl(1/\tau)}{4\pi^2(\gamma-\gamma_i)^2+(1/\tau)^2}, \qquad (1)$$

where a_i is a constant characteristic of the individual line; n is the number of absorbing gas molecules per unit volume; l is the length of the absorption cell; τ is the mean time between collisions; and γ_i is the frequency of maximum absorption for the line. In correlating the information included in (1) with actual experimental data the limitations on resolution of the spectrometer used must be considered. For this we use the energy transmittance function $f(\gamma, \gamma_0)$ which gives the energy as a function of frequency in the spectral band width transmitted by the instrument when set to pass radiation of frequency γ_0.[7] The transmission for a sample of gas is given by

$$T=A\int_{-\infty}^{\infty}\exp-\left\{nl\,\Sigma_i\left(\frac{a_i(1/\tau)}{4\pi^2(\gamma-\gamma_i)^2+(1/\tau)^2}\right)\right\}\times f(\gamma,\gamma_0)d\gamma, \qquad (2)$$

where A is a constant which takes into account the integral of the transmittance function over the same spectral region. Although the limits of the integral in Eq. (2) are $-\infty$ and $+\infty$, this does not imply significant contributions from frequencies very far removed from γ_0. Actually the transmittance function $f(\gamma, \gamma_0)$ will be such that it goes to zero very rapidly for values of γ further removed from γ_0 than one-half the spectral slit width. Dennison[2] has found that for the transmittance function both a Gaussian and triangular form are about equally effective in calculating transmissions. The summation in the exponential under the integral in Eq. (2) must be taken over all frequencies which are included in the spectral slit widths. For this reason the analytical evaluation of (2) is very difficult unless a spectral slit width characteristic of an instrument of high resolution is used.

Despite the difficulties of directly using Eq. (2) to correlate theory and experiment or to obtain values of the characteristic constants, use may be made of it to obtain information

[6] The companies from whom the gases were obtained were: The Linde Air Products Co., Buffalo, N. Y.; The Matheson Co., East Rutherford, N. J.; Phillips Petroleum Co., Special Products Division, Bartlesville, Oklahoma; The Ohio Chemical & Mfg. Co., Cleveland, Ohio.

[7] See for example: J. R. Nielson, V. Thornton, and E. B. Dale, Rev. Mod. Phys. 16, 307 (1944).

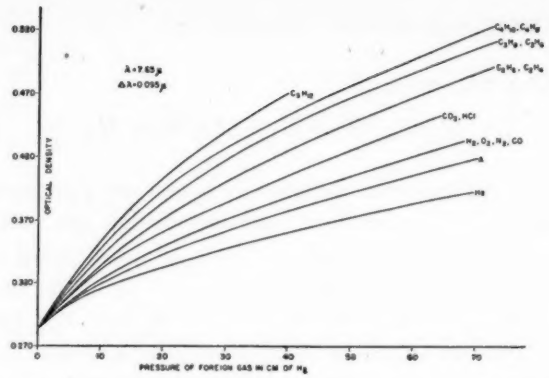

FIG. 1. Effects of various foreign gases on the infra-red absorption of methane at 7.65μ.

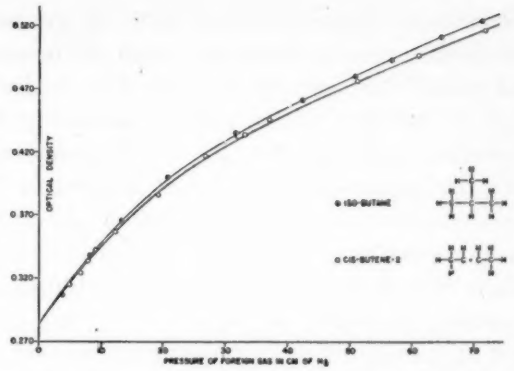

FIG. 3. Detail effects of isobutane and cis-butene-2 on methane absorption at 7.65μ.

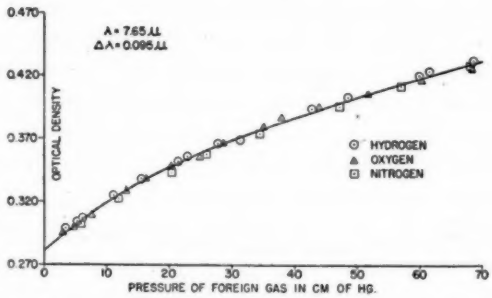

FIG. 2. Detail of similar effects of H_2, O_2, and N_2 on methane absorption at 7.65μ.

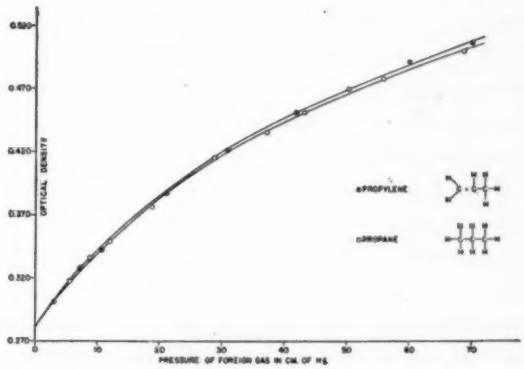

FIG. 4. Detail of effects of propylene and propane on methane absorption at 7.65μ.

concerning the optical collision diameters of various molecules. A consideration of the terms in (2) shows that if the concentration of the absorbing gas, the wave-length, and the slit settings are kept constant, while various foreign, non-absorbing gases are used, the only varying parameter between separate evaluations of (2) will be τ, the mean time between collisions. Figure 1 shows some experimental data taken under the conditions set forth above. Here is plotted the optical density D, $D=\log(1/T)$ for 13.5 cm of Hg pressure of CH_4 in the presence of the different foreign gases indicated. This data was taken with the 9.50 cm cell.

Figure 1 indicates that the effect of foreign gases varies widely and depends upon the individual gases showing a general trend of increasing effect with molecules of increasing multiplicity of atoms. It is to be noticed that for a number of cases more than one foreign gas is represented by one curve. For these cases the effects were so similar that only a single curve was drawn. In Fig. 2 may be seen a more detailed curve for one of these cases. Here it is seen that the foreign gases H_2, O_2, and N_2 have the same effects to within the scattering of the data. It might be inferred that the similar effects were caused by some common characteristic of these gases, but, as will be discussed later, we believe it to be merely fortuitous. In a similar study of the effects of foreign gases on the infra-red absorption of N_2O, Cross and Daniels[8] found the order of gases with increasing effects on the optical density to be as follows: A, O_2, N_2, C_2H_6, CO_2, and H_2. From our data when compared with this it is obvious that the order of increasing effect cannot be extrapolated from one absorbing gas to another, and this will be further confirmed by additional data below.

Figure 3 shows a detail graph of the effects of isobutane and cis-butene-2. This was of interest in view of the much greater chemical reactivity of the olefin and the possible relation of this

[8] P. C. Cross and F. Daniels, J. Chem. Phys. 2, 6 (1934).

difference of chemical reactivity to the pressure broadening effects. A similar graph for propane and propylene may be seen in Fig. 4. From Figs. 3 and 4 it is seen that apparently the chemical reactivity has no direct connection with the pressure broadening, as in one case the more reactive compound of two of about the same molecular weight has a slightly greater effect and in the other case the situation is reversed. It should be mentioned at this point that at the wave-length investigated some of the hydrocarbons used had absorption coefficients which were quite small but not zero. To correct the results for their absorption, Beer's law was assumed to be obeyed by them at this wave-length, and the observed optical density was accordingly corrected. From the general consistency of results discussed below, it is believed that this procedure is correct.

The manner of obtaining data used here wherein only the partial pressure of the foreign gas is varied is equivalent to varying the parameter τ in Eq. (2). Cross and Daniels[8] showed that this procedure may be used to obtain information about the optical collision diameters of the absorbing and foreign gas molecules. Their postulate that the mean free path of the absorbing molecules is the same in all gas mixtures which exhibit the same relative absorption coefficient is equivalent in this case to assuming that Eq. (2) is correct. They showed that if the partial pressures of different foreign gases which produced the same increase of optical density under the conditions above could be experimentally determined, the ratios of their optical collision diameters could be deduced. This is done by straightforward application of the kinetic theory of gases and the result is:

$$D_{AX}/D_{AY}=(p_Y/p_X)^{\frac{1}{2}} \times[M_X(M_A+M_Y)/M_Y(M_A+M_X)]^{\frac{1}{2}}, \quad (3)$$

where D_{AX} is the distance between the centers of absorbing molecule A and the foreign gas molecule X, at which the process of absorption of radiation by A is interrupted. It is then the sum of the optical collision radii of each of the two molecules. D_{AY} is the corresponding quantity for the case of foreign gas Y in the presence of A. P_Y and P_X are partial pressures of gases Y and X which produce the same optical density. M_A, M_X, and M_Y are the molecular weights. For the derivation of (3) from the principle that equal values of τ used in (2) will produce equal optical densities, it is necessary that the temperature of the gas be the same for the different observations. This was achieved in our experiments by allowing equilibrium to be reached between the gas and the room temperature which was controlled.

In the determination of molecular diameters from viscosity or other gas kinetic data, values are obtained which are representative of the distance between molecular centers such that momentum may be transferred. Or, in other words, only those collisions wherein there is a transfer of momentum affect the experimental results. Certainly each such collision would be expected to interrupt the process of radiation absorption by an absorbing molecule. In addition the perturbation of vibrational and rotational states by Van der Waals interactions would be expected to alter the absorption processes in many encounters not close enough to affect momentum transfer. For this reason, a determination of molecular diameters by an application of Lorentz pressure broadening theory gives values called optical collision diameters which are larger than the molecular diameters obtained from kinetic data. The present work gives only ratios between diameters for reasons which will be discussed below. Recently Bleaney and Penrose,[9] in a study of the ammonia bands in the 1-cm region using the microwave technique, have found that the optical diameter effective in

TABLE I. Values of p_Y/p_X for different values of D.

D	p_{He}/p_{CO_2}	p_A/p_{CO_2}	p_{H_2}/p_{CO_2}
0.330	1.86	——	1.33
0.340	1.95	1.43	1.33
0.350	1.99	1.44	1.31
0.360	2.00	1.46	1.29
0.370	1.99	1.44	1.28
0.380	2.00	1.45	1.28
0.390	2.02	1.46	1.28
0.400	——	1.47	1.29
0.410	——	1.47	1.29
0.420	——	1.49	1.31

[9] B. Bleaney and R. P. Penrose, Nature **157**, 339 (1946).

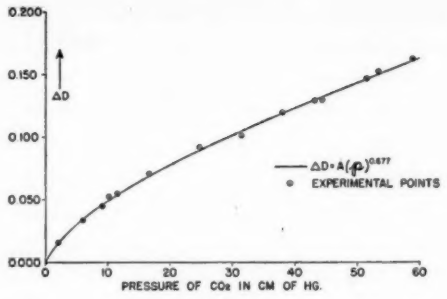

FIG. 5. Increase in optical density of constant pressure of methane as a function of foreign gas pressure.

broadening these bands to be about four times the normal diameter.

Since the optical collision diameters should be independent of gas pressure, Eq. (3) may be used to confirm the physical basis and reasoning used in deriving it. For if these are correct, Eq. (3) may be applied to any pair of partial pressures giving the same optical densities. Therefore the ratio p_Y/p_X should be constant for all values of optical density for which it is determined. Table I gives the values of this ratio for several different pairs of foreign gases at different values of optical density D using the data of Fig. 1.

In this table we may see that the ratios of the pairs of pressure determinations do not vary more than a few percent over the range of optical density used. The greatest variation occurred for the smaller values of optical density, and this could have been caused by experimental difficulties in obtaining the lower end of the curves in Fig. 1. Certainly the values of p_Y/p_X are constant enough to give confirmation to the correctness of Eq. (3).

Returning for the moment to Eq. (2), we note that n, the number of absorbing centers per unit volume, and l, the cell length, enter the integral as a product. Thus, if the product nl is kept constant and the mean time between collisions is kept constant it is possible to achieve the same value of the integral under various experimental conditions. For example, if one has the absorbing gas at a high pressure p_1, in a short cell of length l_1, with no foreign gas present, a certain optical density is obtained. If a second pressure p_2 is used in a cell of greater length l_2, yet adjusted so that $p_1l_1=p_2l_2$, foreign gas must be added to the longer cell to get the same optical density as obtained with the shorter one. This is because the τ due to the absorbing gas alone will change with change of pressure. Using these two different arrangements allows a determination of D_{AA}/D_{AX}. This is given by Eq. (4) which is derived by the same arguments as Eq. (3).

$$D_{AA}/D_{AX}=[p_X/(p_1-p_2)]^{\frac{1}{2}} \times[(M_A+M_X)/2M_X]^{\frac{1}{2}}. \quad (4)$$

Here p_X is the pressure of foreign gas X that must be added to get an optical density using the longer cell equal to that obtained with the shorter one. In our work, the short cell was 3.15 cm in length, and the pressure of methane used in it was 39.70 cm of Hg. The values of p_X used to evaluate Eq. (4) were obtained by reading off from the curves in Fig. 1. The results of using Eq. (4) on the data obtained with the short cell and the data of Fig. 1 are given in Table II.

We note here that, in general, the ratio D_{AA}/D_{AX} decreases with increasing complexity of the X molecules, or in other words the optical diameters of the X molecules increase with increasing size. HCl is somewhat out of place in this respect, but its large optical diameter is believed to be owing to its large dipole moment.

An interesting empirical result is illustrated in Fig. 5. Here ΔD which is the difference between the observed optical density when a foreign gas is used and the optical density obtained for the methane in the cell alone is plotted *versus* the partial pressure of foreign gas, in this case CO_2. Here it is seen that ΔD is given by the equation:

$$\Delta D=Ap^s, \quad (5)$$

where A and s are empirically determined constants. As may be seen the agreement between the points and the curve fitted to two of them is

TABLE II. Values of D_{AA}/D_{AX} for various foreign gases. (A = methane; X = foreign gas used; $\lambda=7.65\mu$.)

X	D_{AA}/D_{AX}	X	D_{AA}/D_{AX}
He	1.72	C_2H_4	0.82
A	1.07	C_2H_6	0.82
H_2	1.59	C_3H_6	0.72
N_2	1.03	C_3H_8	0.73
O_2	1.01	C_4H_8	0.68
CO	1.03	C_4H_{10}	0.66
CO_2	0.87	C_5H_{12}	0.63
HCl	0.88	——	——

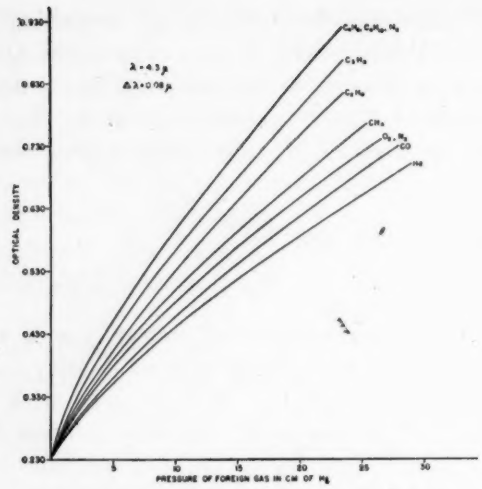

FIG. 6. Effects of various foreign gases on the infra-red absorption of carbon dioxide at 4.3μ.

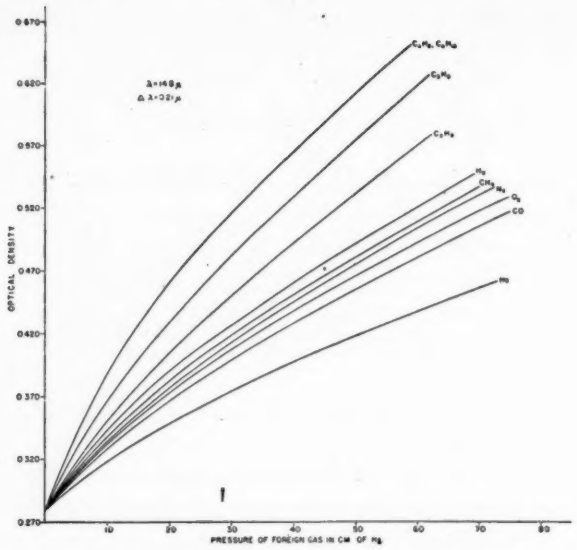

FIG. 7. Effects of various foreign gases on the infra-red absorption of carbon dioxide at 14.8μ.

quite good. From the agreement of the data with Eq. (5) for the case of CO_2 and from constancy of the ratios in Table I we may conclude that agreement may be had for the other foreign gases and that the value of the exponent will be 0.677 for each. A curve of optical density *vs.* pressure for various pressures of methane alone in the 9.50 cm cell gave good agreement with the empirical equation $D=Ap^s$ which is very similar to Eq. (5). The value of the exponent in this case was 0.743.

In addition to the work done on methane the effect of various foreign gases on the absorption of CO_2 was investigated at two different wavelengths 4.3μ and 14.8μ at which absorption takes place due to stretching and bending vibrations respectively. The results for the 4.3μ investigation are seen in Fig. 6, and the results for the 14.8μ work are seen in Fig. 7. Here again the 9.50-cm cell was used, and the partial pressure of CO_2 used at 4.3μ was 3.50 cm of Hg, and at 14.8μ a partial pressure of 9.86 cm of Hg was used. Since with the instrument used the optical path at one place passed through an open space this created some experimental difficulty. This was owing to the fact that if the carbon dioxide content in the room was not constant then the transmittance function $f(\gamma, \gamma_0)$ used in Eq. (2) would not be the same in each case. For this reason data for CO_2 studies were only taken after a CO_2 equilibrium was reached in the room. Reproducibility tests indicated the equilibrium concentration to be nearly the same each day.

An inspection of Figs. 6 and 7 shows that in general the order of increasing effect of the foreign gases is the same for the two different spectral regions. Two exceptions to this are that O_2 and N_2 have the same effect at 4.3μ but distinctly different effects for 14.8μ. Another and more striking exception is that of H_2 which has an effect similar to that of methane for 14.8μ absorption but has a relatively much greater effect at 4.8μ, being of the same magnitude as for isobutane and butadiene. In connection with the latter point, it is interesting to note that the two compounds, isobutane and butadiene, which differ radically in chemical reactivity, have the same pressure broadening effect for CO_2 for both the 4.3μ and 14.8μ bands. From this and the observations on methane it seems safe to conclude that chemical reactivity is not to be directly correlated with optical collision diameters.

The ratios of D_{AA}/D_{AX} were obtained in the same manner as for methane, using the 3.50 cm cell, and the results are given in Tables III and IV.

An examination of the values of D_{AA}/D_{AX} in Tables III and IV shows that for each different gas X considered the values for the two wavelengths are equal to within about 8 percent

except for the gases H_2, C_3H_8, C_4H_{10}, and C_4H_6. These differences, however, plus the variations in order of increasing effect shown for the different absorbing gases confirm our belief that the optical collision diameter ratio is a specific function of the pair of gases under consideration and of definite absorption frequencies. That is, the pressure broadening effect of a gas on one absorber cannot reliably be extrapolated to predict the effect on another. Nor can the results for one particular wave-length be reliably extrapolated to another for the same pair of gases. Thus, optical collision radii have definite quantitative meaning only for specific cases. These conclusions are in line with the recently published work of Foley[10] which indicates the complicated nature of the dependence of the pressure broadening on the molecular interactions. As would be expected, the optical collision diameters depend upon the nature of the Van der Waals interactions and upon the excited states of the gas molecules.

Although data of the type discussed above can give only relative results, i.e., ratios between various optical collision diameters, recent work in microwave technique has demonstrated its possibilities for obtaining absolute values for those wave-length regions.[9, 11, 12]

Another gas given some investigation was isobutylene. If the optical density is plotted *vs.* pressure of isobutylene at the wave-length of 11.23μ (the center of the Q branch) there results a curved line similar in appearance to Fig. 5. This deviation from Beer's law would not seem likely to be caused by pressure broadening due to the large moments of inertia and consequent small spacing between rotational levels for the isobutylene molecule. However, the pressure broadening possibility was checked by comparing the optical density of a particular pressure of isobutylene with the optical density obtained when various pressures of foreign gases were added. In this work a constant pressure of 2.35 cm of isobutylene was used in the 9.50-cm cell. To this were added various pressures of H_2, N_2, and CO_2 ranging from 20 to 75 cm. For each observation regardless of type or pressure of foreign gas the optical density was equal, within experimental error, of the optical density obtained for the isobutylene by itself. This we believe is conclusive evidence that this particular deviation from Beer's law is not due to pressure broadening. It seems likely that it may be owing only to the combined effect of line shape and finite slit widths.

The above data are of interest for applications of infra-red absorption spectroscopy for analytical uses. Gases subject to pressure broadening may be quantitatively measured in mixtures, but allowance must be made for the pressure broadening effects.[5]

The authors are grateful to Dr. M. Muskat for discussions of this work and to Dr. P. D. Foote, Executive Vice President of this Company, for permission to publish this material.

TABLE III. Values of D_{AX}/D_{AA} for various foreign gases. (A = carbon dioxide; X = foreign gas used; $\tau = 4.3\mu$.)

X	D_{AA}/D_{AX}	X	D_{AA}/D_{AX}
H_e	2.18	CH_4	1.26
O_2	1.20	C_2H_6	1.00
N_2	1.19	C_3H_8	0.85
H_2	1.90	C_4H_{10}	0.72
CO	1.29	C_4H_6	0.72

TABLE IV. Values of D_{AA}/D_{AX} for various foreign gases. (A = carbon dioxide; X = foreign gas used; $\lambda = 14.8\mu$.)

X	D_{AA}/D_{AX}	X	D_{AA}/D_{AX}
H_e	1.98	CH_4	1.25
O_2	1.17	C_2H_6	1.07
N_2	1.19	C_3H_8	0.97
H_2	1.64	C_4H_{10}	0.86
CO	1.27	C_4H_6	0.87

[10] H. M. Foley, Phys. Rev. **69**, 616 (1946).

[11] R. Beringer, Phys. Rev. **70**, 53 (1946).

[12] W. E. Good, Phys. Rev. **70**, 213 (1946).

THE JOURNAL OF CHEMICAL PHYSICS VOLUME 15, NUMBER 1 JANUARY, 1947

The Statistical Mechanical Theory of Transport Processes

II. Transport in Gases

JOHN G. KIRKWOOD
Baker Laboratory, Cornell University, Ithaca, New York

(Received October 28, 1946)

By means of the methods developed in the first paper of this series, SMTI, the Maxwell-Boltzmann integro-differential equation, underlying the well-developed Chapman-Enskog theory of transport phenomena in gases of low density, is derived from the principles of statistical mechanics. The derivation supplements and clarifies the usual physical argument employed to establish this important equation.

THE molecular theory of transport in gases of low density is based upon the Maxwell-Boltzmann integro-differential equation, the consequences of which have been developed by Chapman, Enskog, and other investigators.[1] Rigorous mathematical methods, due principally to Enskog, applied to the solution of the Maxwell-Boltzmann equation, have yielded adequate and detailed theories of diffusion, viscous flow, heat conduction, and related phenomena in gases of sufficiently low density to be amenable to binary collision analysis. Little remains to be done along these lines.

The Maxwell-Boltzmann equation is customarily derived by means of a physical argument which, though plausible, leaves certain points rather obscure. The passage from "fine-grained" to "coarse-grained" distribution functions is glossed over and the role of multiply periodic states of motion is not clarified. In order to complete the molecular theory of transport in gases, an analytical derivation of the Maxwell-Boltzmann integro-differential equation from the principles of statistical mechanics is much to be desired. We shall here undertake such a derivation on the basis of the statistical mechanical theory of transport processes outlined in the first paper of this series,[2] SMTI.

We begin with Liouville's equation,

$$\frac{\partial f^{(N)}}{\partial t}+\sum_{l=1}^{N}\left\{\frac{\mathbf{p}_l}{m_l}\cdot\nabla_{R_l}f^{(N)}+(\mathbf{X}_l+\mathbf{F}_l)\cdot\nabla_{p_l}f^{(N)}\right\}=0, \tag{1}$$

$$\mathbf{F}_l=\sum_{i=1}^{N}\mathbf{F}_{il},$$

for the distribution function $f^{(N)}$ in the phase space $(\mathbf{p}_1, \mathbf{p}_N, \mathbf{R}_1, \mathbf{R}_N)$ of systems of N molecules. Here $\mathbf{X}_l$ is the external force acting on molecule l and $\mathbf{F}_l$, the total intermolecular force, assumed the sum of contributions $\mathbf{F}_{il}$, each depending only on the relative configuration of molecules i and l. The distribution function $f_i^{(1)}$ in the 6-phase space of an individual molecule is given by

$$f_i^{(1)}(\mathbf{p}_i, \mathbf{R}_i; t)=\int\int f^{(N)}(\mathbf{p}_i, \mathbf{R}_i, \mathbf{P}, \mathbf{Q}; t)d\mathbf{P}d\mathbf{Q}, \tag{2}$$

where the integration extends over $(\mathbf{P}, \mathbf{Q})$ the residual phase space of the other $N-1$ molecules of the system. The distribution function $\bar{f}_i^{(1)}$ averaged over an interval of time τ subsequent to the instant t is defined by the relation,

$$\bar{f}_i^{(1)}(\mathbf{p}_i, \mathbf{R}_i; t)=\frac{1}{\tau}\int_0^{\tau} f_i^{(1)}(\mathbf{p}_i, \mathbf{R}_i; t+s)ds. \tag{3}$$

[1] See Chapman and Cowling, *Mathematical Theory of Non-Uniform Gases* (Cambridge University Press, 1939).
[2] J. G. Kirkwood, J. Chem. Phys. **14**, 180 (1946).

It is this distribution function $\bar{f}_i^{(1)}$, "coarse-grained" in time, which we shall find to satisfy the Maxwell-Boltzmann equation when the influence of collisions involving more than two molecules is neglected and τ is selected as large relative to the duration of a representative collision. We surmise that an alternative description based upon a distribution function "coarse-grained" in phase space[3] might be constructed, but such a description is not necessary.

Integration of both sides of Eq. (1) over the residual phase space $(\mathbf{P}, \mathbf{Q})$ of all molecules except i and construction of the time average lead to the following equations, Eqs. (49) and (51) of SMTI, for the distribution function $\bar{f}_i^{(1)}$,

$$\frac{\partial \bar{f}_i^{(1)}}{\partial t}+\frac{\mathbf{p}_i}{m_i}\cdot\nabla_{R_i}\bar{f}_i^{(1)}+\mathbf{X}_i\cdot\nabla_{p_i}\bar{f}_i^{(1)}=\sum_{l=1}^{\nu} N_l\nabla_{p_i}\cdot\boldsymbol{\Omega}_{li}^{(1)},$$

$$\nabla_{p_i}\cdot\boldsymbol{\Omega}_{li}^{(1)}=\int\cdots\int(\nabla_{p_i}\cdot\mathbf{K}_{li})f_i^{(1)}(\mathbf{p}_{i0},\mathbf{R}_{i0};t)f_l^{(1)}(\mathbf{p}_{l0},\mathbf{R}_{l0};t)d\mathbf{p}_{i0}d\mathbf{R}_{i0}d\mathbf{p}_{l0}d\mathbf{R}_{l0},$$

$$\mathbf{K}_{li}=-\frac{1}{\tau}\int_0^{\tau}\int\int\mathbf{F}_{li}(t+s)\delta(\mathbf{p}_{i0}+\Delta\mathbf{p}_i-\mathbf{p}_i)\delta(\mathbf{R}_{i0}+\Delta\mathbf{R}_i-\mathbf{R}_i)(1+\vartheta_{li})\times f^{(2/N)}(\mathbf{p}_{i0}\cdots\mathbf{R}_{l0}/\mathbf{P}_0,\mathbf{Q}_0;t)d\mathbf{P}_0d\mathbf{Q}_0ds, \tag{4}$$

$$(1+\vartheta_{li})=\frac{f_{il}^{(2)}(\mathbf{p}_{i0}\cdots\mathbf{R}_{l0};t)}{f_i^{(1)}(\mathbf{p}_{i0},\mathbf{R}_{i0};t)f_l^{(1)}(\mathbf{p}_{l0},\mathbf{R}_{l0};t)},$$

where the symbols have the same significance as in SMTI. $f^{(2/N)}(\mathbf{p}_{i0}\ldots\mathbf{R}_{l0}/\mathbf{P}_0,\mathbf{Q}_0;t)$ is the relative probability density in the residual phase space $(\mathbf{P}_0,\mathbf{Q}_0)$ of the remaining $N-2$ molecules, if the specified pair, i and l, are situated at the point, $\mathbf{p}_{i0}$, $\mathbf{R}_{i0}$, $\mathbf{p}_{l0}$, $\mathbf{R}_{l0}$, in the phase space of that pair. The correlation function in pair space, $(1+\vartheta_{li})$, was denoted by φ_{li} in STMI. If ϑ_{li} is a short range function of the intermolecular distance in a sense presently to be made more precise, that part of $\mathbf{K}_{li}$ arising from ϑ_{li} makes negligible contribution to $\boldsymbol{\Omega}_{li}^{(1)}$ for sufficiently large τ.

We shall assume that the force $\mathbf{F}_{li}$ exerted by molecule l on molecule i has a finite range R_0, vanishing for intermolecular distances R_{il} greater than R_0. For short range intermolecular forces of the van der Walls type, this is not an essential limitation, since an R_0 of molecular order of magnitude may be chosen beyond which such intermolecular forces are of negligible magnitude. If for relative initial configurations of the pair il, for which $\mathbf{F}_{li}$ differs from zero in the subsequent interval τ, the probability of configurations of the remaining $N-2$ molecules, for which their contribution to the force on i also differs from zero, is negligible, it is sufficient to use the *binary collision* approximation,

$$\partial(\Delta\mathbf{p}_i)/\partial s=\mathbf{F}_{li} \tag{5}$$

in the evaluation of the integrals $\mathbf{K}_{li}$ and $\nabla_{p_i}\cdot\boldsymbol{\Omega}_{li}^{(1)}$. The condition for the validity of the approximation is that the ratio of the probability that three or more molecules are situated in region of 3-configuration space, of linear dimension of the order of magnitude of the range of intermolecular force R_0, to the probability that two molecules are situated in the region, be zero. For distributions departing but slightly from statistical equilibrium, this condition is normally fulfilled in the limit of zero density (the assumption of *molecular chaos*). If we make the additional assumption that $f_i^{(1)}$ and $f_l^{(1)}$ have only macroscopic dependence on $\mathbf{R}_i$ and $\mathbf{R}_l$,

$$|\nabla_{R_i}\log f_i^{(1)}|=0(1/L_i),\quad |\nabla_{R_l}\log f_l^{(1)}|=0(1/L_l), \tag{6}$$

where L_i and L_l are macroscopic lengths large relative to the range of intermolecule force, then to terms of order $0(R_0/L_i)$, we may replace $\delta(\mathbf{R}_{i0}+\Delta\mathbf{R}-\mathbf{R}_i)$ by $\delta(\mathbf{R}_{i0}-\mathbf{R}_i)$ in the integral defining $\mathbf{K}_{li}$ and $\mathbf{R}_{l0}$ by $\mathbf{R}_{i0}$ as the configurational argument of $f_l^{(1)}$ in the integral defining $\nabla_{p_i}\cdot\boldsymbol{\Omega}_{li}^{(1)}$, Eq. (4).

[3] See Tolman, *Statistical Mechanics* (Oxford University Press, 1938), Chapter VI, Oxford VI.

We now proceed to evaluate $\mathbf{K}_{li}$ and $\nabla_{p_i}\cdot\boldsymbol{\Omega}_{li}^{(1)}$ of Eq. (4) with the use of Eq. (5) and the other assumptions stated in the preceding paragraph. Changing configuration variables from $\mathbf{R}_{i0}$ and $\mathbf{R}_{l0}$ to $\mathbf{R}_{i0}$ and $\mathbf{R}_{il}^0$, the relative configuration of i and l, and using the properties of the delta functions $\delta(\mathbf{p}_{i0}+\Delta\mathbf{p}_i-\mathbf{p}_i)$ and $\delta(\mathbf{R}_{i0}-\mathbf{R}_i)$, we obtain from Eqs. (4) and (5),

$$\nabla_{p_i}\cdot\boldsymbol{\Omega}_{li}^{(1)}=\int\int\int\psi_{li}f_i^{(1)}(\mathbf{p}_{i0},\mathbf{R}_i;t)f_l^{(1)}(\mathbf{p}_{l0},\mathbf{R}_i;t)d\mathbf{p}_{i0}d\mathbf{p}_{l0}d\mathbf{R}_{il}^0/\tau,$$

$$\psi_{li}=(1+\vartheta_{li})\int_0^\tau\frac{\partial(\Delta\mathbf{p}_i)}{\partial s}\cdot\nabla_{\Delta p_i}\delta(\mathbf{p}_{i0}+\Delta\mathbf{p}_i-p_i)ds \tag{7}$$

$$=(1+\vartheta_{li})\{\delta(\mathbf{p}_{i0}+\Delta\mathbf{p}_i(\tau)-\mathbf{p}_i)-\delta(\mathbf{p}_{i0}-\mathbf{p}_i)\},$$

where the integration of $f^{(2/N)}$ over the residual configuration space $(\mathbf{P}_0,\ \mathbf{Q}_0)$ has been carried out to give unity, since, by Eq. (5), the other factors of the integrand of the expression defining $\mathbf{K}_{il}$ are independent of $\mathbf{P}_0$ and $\mathbf{Q}_0$, depending only on the Lagrange coordinates of the pair il, and $f^{(2/N)}$ is normalized to unity.

If the integral, $\int\vartheta_{li}d\mathbf{R}_{il}^0$, is bounded, it is possible to choose τ of sufficient magnitude to make contributions to $\nabla_{p_i}\cdot\boldsymbol{\Omega}_{li}^{(1)}$, arising from the deviation ϑ_{li}, of the pair correlation function from unity, as small as desired, and we may write,

$$\nabla_{p_i}\cdot\boldsymbol{\Omega}_{li}^{(1)}=\int\int\int\{\delta(\mathbf{p}_i'-\mathbf{p}_i)-\delta(\mathbf{p}_{i0}-\mathbf{p}_i)\}f_i^{(1)}(\mathbf{p}_{i0},\mathbf{R}_i;t)f_l^{(1)}(\mathbf{p}_{l0},\mathbf{R}_i;t)d\mathbf{p}_{i0}d\mathbf{p}_{l0}dR_{il}^0/\tau+0(\tau_k/\tau), \tag{8}$$

$$\mathbf{p}_i'=\mathbf{p}_{i0}+\Delta\mathbf{p}_i(\tau)$$

where τ_k is a time interval of finite magnitude determined by the correlation integral, $\int\vartheta_{li}d\mathbf{R}_{il}^0$. Since the initial distribution is arbitrary there is no *a priori* reason for ϑ_{il} to be short range in the sense that the correlation integral is finite, but it may generally be expected to be so for distributions departing but slightly from statistical equilibrium. The requirement that it be so may be regarded as an auxilliary part of the assumption of *molecular chaos* which must be satisfied for the present analysis to be valid. We shall presently show that the volume in relative configuration space for which $\Delta\mathbf{p}_i(\tau)$ is non-vanishing becomes proportional to τ and that $\nabla_{p_i}\cdot\boldsymbol{\Omega}_{li}^{(1)}$ becomes independent of τ for sufficiently large τ.

We now need to consider in detail the solutions of Eq. (5), the equation of motion for a binary collision. Since these solutions are, of course, well known,[1] only the results will be summarized. The reduced mass m_{il} and the relative momentum $\mathbf{p}_{il}^0$ are defined as

$$1/m_{il}=1/m_i+1/m_l,$$

$$\mathbf{p}_{il}=\frac{m_{il}}{m_l}\mathbf{p}_l-\frac{m_{il}}{m_i}\mathbf{p}_i. \tag{9}$$

Pairs for which the initial Lagrange coordinate R_{il}^0 is greater than the range of intermolecular force occupy aperiodic orbits. The relative momentum remains constant and equal to $\mathbf{p}_{il}^0$ until a sphere of radius R_0 with origin, say in molecule i, is penetrated. If the initial configuration allows the penetration of this sphere, the collision is completed in a time τ_c, dependent on the collision parameters, the relative momentum receives a finite increment, $\Delta\mathbf{p}^*$, and subsequently remains constant and equal to $\mathbf{p}_{il}'$. The scalar magnitude p_{il}' is equal to p_{il}^0. By conservation of total linear momentum, $\mathbf{p}_{i0}$ and $\mathbf{p}_{l0}$ experience increments $-\Delta\mathbf{p}^*$ and $+\Delta\mathbf{p}^*$, respectively. Summarizing, we have

$$\Delta\mathbf{p}^*=\mathbf{p}_{il}'-\mathbf{p}_{il}^0,\quad \Delta\mathbf{p}_l=-\Delta\mathbf{p}_i=\Delta\mathbf{p}^*,\quad \Delta\mathbf{p}^*=2p_{il}^0\cos(\chi/2)\mathbf{e},$$

$$\chi/2=\int_a^\infty\frac{bp_{il}^0dR/R^2}{[(1-b^2/R^2)p_{il}^{02}-2m_{il}V_{il}(R)]^{\frac{1}{2}}},\quad bp_{il}^0=|\mathbf{R}_{il}^0\times\mathbf{p}_{il}^0|, \tag{10}$$

where a is the greatest positive root of the equation

$$(1-b^2/a^2)p_{il}^{02}-2m_{il}V_{il}(a)=0.$$

V_{il} is the potential of the intermolecular force, $\mathbf{e}$ is a unit vector in the direction of the apse line drawn from molecule i to the orbit perihelion, and b is the impulse parameter.

For certain regions of the relative configuration space, the molecules occupy aperiodic orbits only partially traversed in the interval τ, or multiply periodic orbits with bounded $\Delta\mathbf{p}_{il}$. We now proceed to specify the several regions more precisely. To do this we select a cylindrical coordinate system in the relative Lagrange configuration space (z, b, ϵ) with origin in molecule i and z axis antiparallel to $\mathbf{p}_{il}^0$. The radial coordinate b is the impulse parameter and ϵ its azimuth. Unless the conditions,

$$(R_0^2-b^2)^{\frac{1}{2}}\leqslant z\leqslant(p_{il}^0/m_{il})\tau+(R_0^2-b^2)^{\frac{1}{2}},\quad 0\leqslant b\leqslant R_0, \tag{11}$$

are satisfied, the sphere R_0 is not penetrated in the interval τ, the momentum increment $\Delta\mathbf{p}_i$ remains zero, and the integrand, Eq. (8), vanishes. For those coordinates lying in filaments of volume,

$$(p_{il}^0/m_{il})(\tau-\tau_c)bdbd\epsilon,\quad (R_0^2-b^2)^{\frac{1}{2}}\leqslant z\leqslant(p_{il}^0/m_{il})(\tau-\tau_c)+(R_0^2-b^2)^{\frac{1}{2}}, \tag{12}$$

a complete collision is experienced in τ with momentum increments given by Eq. (10). In filaments of volume,

$$(p_{il}^0/m_{il})\tau_c bdbd\epsilon,\quad (p_{il}^0/m_{il})(\tau-\tau_c)+(R_0^2-b^2)^{\frac{1}{2}}<z\leqslant(p_{il}^0/m_{il})\tau+(R_0^2-b^2)^{\frac{1}{2}}, \tag{13}$$

partially completed collisions occur in the interval τ. In filaments of volume,

$$2(R_0^2-b^2)^{\frac{1}{2}}bdbd\epsilon,\quad -(R_0^2-b^2)^{\frac{1}{2}}\leqslant z<+(R_0^2-b^2)^{\frac{1}{2}}, \tag{14}$$

within the sphere R_0, partially completed collisions may be completed or multiply periodic orbits may be traversed in the interval τ. Possible singular behavior being excluded, the integrand of Eq. (8) remains finite for the regions specified by Eqs. (13) and (14).

Carrying out the configurational integration in Eq. (8) with the aid of Eqs. (12), (13), and (14), we obtain,

$$\nabla_{p_i}\cdot\boldsymbol{\Omega}_{li}^{(1)}=\int\cdots\int\frac{p_{il}^0}{m_{il}}\{\delta(\mathbf{p}_i'-\mathbf{p}_i)-\delta(\mathbf{p}_{i0}-\mathbf{p}_i)\}f_i^{(1)}(\mathbf{p}_{i0},\mathbf{R}_i;t)f_l^{(1)}(\mathbf{p}_{l0},\mathbf{R}_i;t)d\mathbf{p}_{i0}d\mathbf{p}_{l0}bdbd\epsilon+0(\bar{\tau}_c/\tau),$$
$$\mathbf{p}_i'=\mathbf{p}_{i0}-\Delta\mathbf{p}^*, \tag{15}$$

where $\bar{\tau}_c$ is a finite time of the order of magnitude of the mean collision duration or of τ_k, whichever is the greater. Thus if τ is selected large relative to $\bar{\tau}_c$, only completed collisions in aperiodic orbits contribute to $\nabla_{p_i}\cdot\boldsymbol{\Omega}_{li}^{(1)}$. Since incomplete collisions and motion in multiply periodic orbits correspond to regions of relative configuration space of finite volume independent of τ, their contributions may be made as small as desired.

It should be remarked that τ cannot be allowed to approach infinity, since for systems confined to a finite domain of phase space, there will exist Poincaré cycle periods within which each orbit will be traversed in the reverse sense to any desired degree of accuracy, canceling its initial contribution to $\nabla_{p_i}\cdot\boldsymbol{\Omega}_{li}^{(1)}$. The thermodynamic irreversibility implied by the non-vanishing of the right-hand side of Eq. (15) would then fail.

In order to evaluate the right-hand side of Eq. (15), it is necessary to change variables in the term involving $\delta(\mathbf{p}_i'-\mathbf{p}_i)$ from $\mathbf{p}_{i0}$, $\mathbf{p}_{l0}$ to $\mathbf{p}_i'$ and $\mathbf{p}_l'$ where

$$\mathbf{p}_i'=\mathbf{p}_{i0}-\Delta\mathbf{p}^*,\quad \mathbf{p}_l'=\mathbf{p}_{l0}+\Delta\mathbf{p}^*. \tag{16}$$

The Jacobian of this transformation is easily shown to be unity. The second term of the integral may be evaluated at once. When the common symbol $\mathbf{p}_l$ is assigned to the remaining momentum

variables of integration, $\mathbf{p}_l'$ and $\mathbf{p}_{l0}$, the two terms combine to yield,

$$\nabla_{p_i}\cdot\boldsymbol{\Omega}_{li}^{(1)}=\int_0^{2\pi}\int_0^{R_0}\int\frac{p_{il}}{m_{il}}\{f_i^{(1)}(\mathbf{p}_i+\Delta\mathbf{p}^*,\mathbf{R}_i;t)f_l^{(1)}(\mathbf{p}_l-\Delta\mathbf{p}^*,\mathbf{R}_i;t)$$
$$-f_i^{(1)}(\mathbf{p}_i,\mathbf{R}_i;t)f_l^{(1)}(\mathbf{p}_l,R_i;t)\}d\mathbf{p}_l b db d\epsilon, \quad (17)$$
$$p_{il}=|\mathbf{p}_l/m_l-\mathbf{p}_i/m_i|m_{il},$$

with the neglect of terms, $0(\bar{\tau}_c/\tau)$. Substitution of the expressions, Eq. (17), into Eq. (4) and time averaging of both sides over the interval τ gives

$$\frac{\partial\bar{f}_i^{(1)}}{\partial t}+\frac{\mathbf{p}_i}{m_i}\cdot\nabla_{R_i}\bar{f}_i^{(1)}+\mathbf{X}_i\cdot\nabla_{p_i}\bar{f}_i^{(1)}=\sum_{l=1}^{\nu}N_l\int_0^{2\pi}\int_0^{R_0}\int\frac{p_{il}}{m_{il}}\{\overline{f_i^{(1)*}f_l^{(1)*}}-\overline{f_i^{(1)}f_l^{(1)}}\}d\mathbf{p}_l b db d\epsilon,$$
$$f_i^{(1)*}=f_i^{(1)}(\mathbf{p}_i+\Delta\mathbf{p}^*,\mathbf{R}_i;t),\quad f_l^{(1)*}=f_l^{(1)}(\mathbf{p}_l-\Delta\mathbf{p}^*,\mathbf{R}_i;t), \quad (18)$$

since the second time average does not affect the left-hand side of Eq. (4), all terms of which already have only secular dependence on time.

Equation (18) becomes identical with the Maxwell-Boltzmann integro-differential equation (in this equation the symbol f_i is customarily used to denote the molecular density, $N_i\bar{f}_i^{(1)}$, of species i) only if

$$\overline{f_i^{(1)}f_l^{(1)}}=\bar{f}_i^{(1)}\bar{f}_l^{(1)}. \quad (19)$$

Equation (19) is not necessarily true, but it is true to terms of the first order for distributions departing but slightly from equilibrium, represented by ${}^0f_i^{(1)}$ and ${}^0f_l^{(1)}$, both of which are independent of time. If

$$f_i^{(1)}={}^0f_i^{(1)}+\varphi_i^{(1)},\quad f_l^{(1)}={}^0f_l^{(1)}+\varphi_l^{(1)},$$
$$\overline{f_i^{(1)}f_l^{(1)}}=\bar{f}_i^{(1)}\bar{f}_l^{(1)}={}^0f_i^{(1)}\,{}^0f_l^{(1)}+{}^0f_i^{(1)}\bar{\varphi}_l^{(1)}+{}^0f_l^{(1)}\bar{\varphi}_i^{(1)}+0(\overline{\varphi_i^{(1)}\varphi_l^{(1)}}). \quad (20)$$

Equations (18) and (20) are evidently identical with the Maxwell-Boltzmann equation to terms of the first order for small departures from statistical equilibrium. In all applications, solutions have been limited to terms of the first order. The proposed derivation of this equation from statistical mechanics is therefore complete.

Starting from Eq. (4), we should be able to develop a systematic scheme for taking into account collisions of higher order than binary and thus to obtain transport laws for gases of finite density instead of laws valid only in the limit of vanishing density. This problem is being considered. However, for this purpose, the Brownian motion approximations described in SMTI appear to offer the greatest promise.

Letters to the Editor

THIS section will accept reports of new work, provided these are terse and contain few figures, and especially few halftone cuts. The Editorial Board will not hold itself responsible for opinions expressed by the correspondents Contributions to this section should not exceed 600 words in length and must reach the office of the Managing Editor not later than the 15th of the month preceding that of the issue in which the letter is to appear. No proof will be sent to the authors. The usual publication charge ($3.00 per page) will not be made and no reprints will be furnished free.

Ultraviolet Absorption Spectrum of Nitric Oxide

H. J. BERNSTEIN* AND G. HERZBERG
Yerkes Observatory, Williams Bay, Wisconsin
November 29, 1946

Mulliken[1] has predicted a stable $^4\Pi$ state for NO which should be approximately 4.5 volts above the normal $^2\Pi$ state. One might therefore expect a weak absorption band system to occur in the spectral region λλ3500–2200A corresponding to a $^4\Pi \leftarrow {}^2\Pi$ transition. Since CO shows a somewhat similar transition ($^3\Pi \leftarrow {}^1\Sigma$) with an absorbing path of 1 meter[2] it seems not unreasonable to expect that the $^4\Pi \leftarrow {}^2\Pi$ transition of NO would be observed under comparable conditions. Experiments by Mundie,[3] however, with a path length of 6 meters, were not successful.

It was considered desirable to extend this investigation by using much longer paths of the absorbing gas. A path of 30 meters length was obtained by multiple reflection in a tube 1.5 meters long by using the method of White.[4] Nitric oxide pressures of 700, 300, 150, and 75 mm of mercury were used; corresponding to 28, 12, 6, and 3 meter-atmosphere paths, respectively.

Extreme purity of the NO was necessary. The gas was prepared by the action of sulfuric acid on potassium nitrite in the presence of potassium iodide and purified by bubbling through a 60-cm column of 90 percent H_2SO_4, a 120-cm column of 50 percent KOH, a dry ice trap, and a P_2O_5 tube. The resulting gas was then solidified in a liquid-air bath and the pure NO distilled off into the absorption tube. The purity of the gas can be judged from the fact that NO_2 absorption bands were absent from all spectra obtained with the above-mentioned path lengths (in spite of their considerable intrinsic intensity), and the HNO_2 absorption bands at λ3400 described by Melvin and Wulf[5] were observed very weakly only at the highest pressure used (700 mm i.e., a path length of 28 meter-atmospheres).

At pressures less than 150 mm the only NO absorption found down to λ2200 was the 0−1 band of the γ system. This band could be readily photographed in a few minutes with a conventional hydrogen source and a Hilger medium quartz spectrograph (which were used throughout). At higher pressures a strong continuous absorption setting in at about λ2600 made observation at shorter wave-lengths impossible. No discrete NO absorption was observed above λ2600 at 700-mm pressure, above λ2500 at 300-mm pressure, and above λ2400 at 150-mm pressure. These negative results show that either the $^4\Pi$ state has not the predicted energy or that the $^4\Pi - {}^2\Pi$ transition is much weaker than expected. This latter alternative does not appear very likely since even the $^1\Sigma \leftarrow {}^3\Sigma$ transition of O_2, which arises solely from magnetic dipole radiation, and is thus much more strictly forbidden than the $^4\Pi - {}^2\Pi$ transition of NO,[6] is readily observed under comparable conditions in an 18-meter path.[7]

The origin of the continuous absorption below λ2600 is not clear. It cannot be due to NO since its dissociation energy is 5.29 ev and therefore a continuous absorption cannot occur above λ2340A. The observed continuous absorption may be due to an impurity (perhaps HNO_2) or to N_2O_2 molecules which according to Johnston and Weimer[8] are probably present in NO at atmospheric pressure.

The absorption spectrum of liquid NO was also obtained through a 3-cm path at −152°C, with a tungsten filament as source. A strong continuous absorption starting at λ4000 and extending to shorter wave-lengths, and one at λ5600 and extending to longer wave-lengths were observed. Maximum transmission occurs around λ4600. These results agree with those obtained by Vodar.[9]

Since liquid NO is completely associated[10] the strong violet and red cut-offs are very probably due to N_2O_2 molecules.

* Division of Chemistry, National Research Council, Ottawa, Canada.
[1] R. S. Mulliken, Rev. Mod. Phys. **4**, 1 (1932).
[2] L. Gerö, G. Herzberg, and R. Schmid, Phys. Rev. **52**, 467 (1937).
[3] L. G. Mundie, M. A. Thesis, University of Saskatchewan, 1937.
[4] J. U. White, J. Opt. Soc. Am. **32**, 285 (1942).
[5] E. Melvin and O. Wulf, J. Chem. Phys. **3**, 755 (1935).
[6] G. Herzberg, Astrophys. J. **89**, 288 (1939).
[7] G. D. Liveing and J. Dewar, Proc. Roy. Soc. **46**, 222 (1889).
[8] H. L. Johnston and H. R. Weimer, J. Am. Chem. Soc. **56**, 625 (1934).
[9] B. Vodar, Comptes rendus **204**, 1467 (1937).
[10] O. K. Rice, J. Chem. Phys. **4**, 367 (1936).

Relations between Carbon-Carbon Bond Energy, Order, and Interatomic Distance

J. L. KAVANAU
University of California, Los Angeles 24, California
December 13, 1946

It is well known that smooth curves can be drawn through the points of plot of bond-energy (and energy of dissociation), bond-order, and interatomic distance for carbon-carbon bonds. Several investigators[1–4] have derived empirical equations fitting such curves.

Inspection of the curve drawn through the points plotting the bond-order, N, of C−C, C=C, and C≡C bonds against the bond-energy, E (58.6, 100, 123 kcal./mole, respectively)[5] indicate a curve of the type,

$$(N_0 - N)^p = k(E_0 - E) \qquad (1)$$

where N_0, E_0, p, and k are constants. Making use of the point (0, 0), corresponding to $E = N = 0$, k can be eliminated from (1) giving

$$[1 - (N/N_0)]^p = 1 - (E/E_0). \qquad (2)$$

The solution of Eq. (2) is facilitated by differentiating with respect to E or N and substituting for the derivative values of the slope measured from the curve. In this manner the constant p is found to be equal to 2 so that Eq. (2) becomes that of the parabola

$$[1-(N/N_0)]^2=1-(E/E_0) \tag{3}$$

with vertex at (N_0, E_0). The solution of this equation, by using the known values of E and N, gives $N_0=4$, $E_0=133$. Equation (3) becomes

$$[1-(N/4)]^2=1-(E/133) \tag{4}$$

which fits the known points with an accuracy of 0.8 percent.

The value of the constant $N_0=4$ is, perhaps, significant since theoretically this is the maximum bond-order for carbon-carbon bonds as well as being the number of carbon valence electrons. The interesting result follows that, according to Eq. (4), the maximum value of E is 133 kcal./mole, namely that of the hypothetical carbon-carbon quadruple bond.

From Eq. (4) we can calculate the carbon-carbon bond-order for benzene. Substituting the benzene value of 85.9 kcal./mole (1/6 $[Qf(\text{benzene})^5-6E_{C-H}{}^5]$) for E in Eq. (4), one obtains $N=1.62$. This is identical with the value obtained by Penney[6] through quantum-mechanical considerations and compares well with the empirical values found by others.[1, 3, 4]

A recent equation[3] by the author relates bond-order and interatomic distance of covalent bonds. For carbon-carbon bonds this type takes the form

$$D=a+b(n-\tfrac{1}{2}/n+\tfrac{1}{2})^N, \tag{5}$$

where D is the interatomic distance in A, n the principal quantum number of the valence electrons, a and b constants, and N the bond order. Eliminating N from (4) and (5) we have an equation

$$D=a+b(n-\tfrac{1}{2}/n+\tfrac{1}{2})^\gamma, \tag{6}$$

where $\gamma=4-4(1-E/133)^{\frac{1}{2}}$, relating bond-energy and interatomic distance. Substituting the numerical values[5] of n, a, and b, we have

$$D=1.015+0.875(3/5)^\gamma. \tag{7}$$

Cherton[2] has given a simple linear expression relating these same quantities. His equation has the form

$$E=(1.89-D)m, \tag{8}$$

where m is a constant of proportionality. It is most interesting to observe that for $E=0$ Cherton's equation gives the value $D=1.89$A, which is precisely the value obtained from D from (7) when $E=0$ (or from (5) when $N=0$, i.e., $a+b=1.89$A). Considering Eq. (5) we have by simultaneous solution of the three equations obtained in D_1, D_2, and D_3 by letting $N=1$, 2, 3 the identity

$$a+b\equiv\frac{D_2(D_2-D_1)+D_1(D_1-D_3)}{D_2-D_3}\equiv 1.89\text{A}, \tag{9}$$

where D_1, D_2, and D_3 are the accepted values of C−C, C=C, and C≡C bonds (1.54A, 1.33A, 1.204A, respectively[3]).

From the point of view of possible theoretical significance Eq. (7) has the advantage that it does not allow values of $D=0$ in accordance with physical considerations, whereas this is not true in the case of Cherton's equation.

In papers by Douglas Clark[1] and Fox and Martin[4] values of the energy of dissociation, E_D, are given for C−C, C=C, and C≡C bonds and the benzene carbon-carbon bond (71.8, 125.1, 161, and 105.3 kg cal., respectively). The modified form of Eq. (4)

$$[1-(N/4)]^2=1-(E_D/167) \tag{10}$$

fits the C−C, C=C, and C≡C values of E_D to within 1.5 percent. Using the benzene value of E_D in Eq. (10) we obtain a bond order of 1.62 for the benzene bond which again is identical with Penney's derivation.

[1] C. H. Douglas Clark, Nature **143**, 800 (1939).
[2] R. Cherton, Bull. Soc. Chim. Belg. **52**, 26 (1943).
[3] J. L. Kavanau, J. Chem. Phys. **12**, 467 (1944).
[4] J. J. Fox and E. A. Martin, J. Chem. Soc. **180**, 2106 (1938).
[5] L. Pauling, *The Nature of the Chemical Bond* (Cornell University Press, New York, 1940).
[6] W. G. Penney, Proc. Roy. Soc. **A158**, 306 (1937).

On the Polymerization of Unsaturated Hydrocarbons by Ionizing Radiations

WARREN M. GARRISON
Department of Chemistry, University of Wyoming, Laramie, Wyoming
December 16, 1946

It has been shown that α-particles[1, 2] polymerize acetylene to give solid polymer with a composition corresponding to $(C_2H_2)_n$. Approximately twenty acetylene molecules are removed from the gas phase per ion-pair formed. To explain these results Lind and Bardwell[3] postulated an ion cluster theory involving twenty acetylene molecules condensed about a positive ion nucleus:

$$C_2H_2\rightarrow C_2H_2{}^+ + e$$
$$C_2H_2{}^+ + 19C_2H_2\rightarrow (C_2H_2)_{20}{}^+$$
$$(C_2H_2)_{20}{}^+ + e\rightarrow (C_2H_2)_{20}.$$

Although there is some theoretical evidence for clustering, it is of interest to note that the polymerization of acetylene by ionizing radiations can be explained in terms of both an ionic and free radical mechanism either of which may be initiated by $C_2H_2{}^+$ ions.

In an ionic or Friedel-Crafts polymerization aluminum chloride, boron trifluoride, protons, and other strong acids lower the activation energy by combining with the ionic activated state in which two electrons of the unsaturated bond occupy the same orbital.[4] It has been shown, for example,[5] that in the acid polymerization of ethylene the primary process is probably:

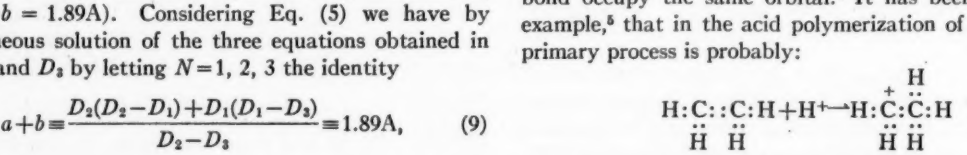

It is suggested here that in the polymerization of acetylene by ionizing radiations the $C_2H_2{}^+$ ions[6] may act as the acid catalyst by combining with the negative carbon atom of

the ionic resonance form of acetylene according to the equation:

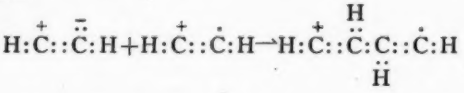

Polymer would be formed by further reaction of the positively charged carbon.

The presence of an unshared electron in $C_2H_2^+$ would permit a polymerization *via* a free radical mechanism also possible. In this case $C_2H_2^+$ would react with acetylene according to the mechanism:

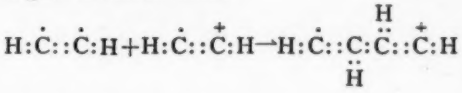

[1] Mund and Koch, Bull. Soc. Chem. **150**, 1169 (1910).
[2] Lind and Bardwell, Science **62**, 422 (1925).
[3] Lind and Bardwell, Science **62**, 593 (1926).
[4] Harman and Eyring, J. Chem. Phys. **10**, 557 (1942).
[5] Price and Meister, J. Am. Chem. Soc. **61**, 1595 (1939).
[6] Kusch, Hustrulid, and Tate, Phys. Rev. **52**, 843 (1937).